CN 059

# KINETICS AND MECHANISMS OF THE OXIDATIVE-DISSOLUTION

# OF METAL SULFIDE MINERALS FOUND IN DULUTH - GABBRO ORE

by

Michael R. Hoffmann
Steven J. Eisenreich*

Environmental Engineering Program
Department of Civil and Mineral Engineering
University of Minnesota
Minneapolis, Minnesota 55455

March 1979

Footnotes?

*To whom correspondence should be addressed

# TABLE OF CONTENTS

# Chapter 1

## Introduction

### 1.1. Composition of the Duluth-Gabbro Ore

The Duluth Gabbro Complex in northeastern Minnesota is a large body of mafic and anorthositic plutonic rocks of Late Precambian age. Primary mineral components in the feldspar-rich gabbro are plagioclase, olivine and pyroxene. Secondary minerals such as chalcopyrite, cubanite, pentlandite and pyrrhotite have potential economic and environmental significance. The chemical and mineral phase analyses of representative samples of operationally defined unmineralized and mineralized gabbro material, which were used in this study, are presented in Tables 1.1 and 1.1. Plagioclase ($NaAlSi_3O_8$/$CaAl_2Si_2O_8$) is the major feldspar mineral, chalcopyrite ($CuFeS_2$) the major copper mineral and pentlandite, the major nickel mineral. In general, gabbro ore deposits contain approximately 0.5 to 1.5 weight percent of combined copper and nickel with an average Cu to Ni ratio of 3 to 1.

### 1.2. Environmental Significance

Field studies (1) near an open-pit iron-ore mine covered by Duluth Gabbro overburden show that heavy metals and sulfate are released in significant concentrations from various seepage sites to a small stream which flows into a larger aquatic ecosystem. Potentially toxic trace metals such as Cu, Ni, Co, Cd and Zn are apparently released in aqueous solution from exposed Duluth-Gabbro ore even though the seepage effluent is buffered naturally to approximately pH 7. Leaching of mineral mining solids such as lean ore, waste rock, tailings and displaced overburden can occur through a combination of chemical, physical and biological processes. Historically, environmental concern with leaching of metal sulfides has been focused on acid mine drainage which results directly from the oxidation of iron pyrite. In general, the oxidative-dissolution of metal

sulfides depends on the availability of water, oxygen, acidity, exposed surface area, bacteria, iron content and the acid neutralizing capacity of the host mineral matrix. Release of the above metals to aquatic systems may be detrimental to the aquatic life and indirectly through the process of bioaccumulation to human health. Leachate from Duluth Gabbro mining solids is atypical because the pH and the alkalinity are unusually high. With high alkalinity and pH, in the absence of strong complexing agents, the concentrations of trace metals should be controlled at relatively low levels by their respective hydroxide and carbonate solids. However, due to the solubilizing impact of humic/fulvic material (2) present in the waters of northeastern Minnesota these metals are found primarily in the soluble phase.

1.3. Research Objectives

The primary objective of this research project was to study the detailed kinetics of the oxidative dissolution of metal sulfides and silicate minerals present in mining solids derived from the Duluth-Gabbro Complex. From a study of rate of leaching of various metals and sulfur compounds as a function of a variety of environmental parameters such a pH, T, $E_h$, $D_p$ (particle size) and catalyst concentrations and empirical rate law and a mechanism consistent with this rate law can be derived. From a knowledge of the rates of oxidative-dissolution and the primary kinetic factors affecting these rates, the relative impact of the exposure of Duluth Gabbro to the aquatic environment can be predicted. An understanding of the detailed mechanism of oxidative-dissolution and subsequent trace metal release should lead to the design of optimal control procedures to eliminate, inhibit or minimize environmental degradation.

1.4. Relevant Research

Little direct information on the oxidative dissolution of sulfidic minerals is available in the primary chemical literature. More information is available

on the microbial leaching of metal sulfides as a beneficiation technique (3). However, the majority of relevant information is available in the hydromet-allurgical literature (4,5,6). For an extensive review of the literature on metal sulfide leaching the reader is referred to an earlier paper by the principal authors (7).

Because the environmental conditions found in the mine drainage from Cu-Ni deposits, the role of microbial catalysis in the leaching of sulfidic minerals appears to be minimal. The two principal strains of sulfur metabolizing bacteria, Thiobacillus ferroxidans and Thiobaccillus thiooxidans, which are critical for microbial leaching, are acidophillic, chemolithotropic bacteria with pH optima near 2. Above pH 4, the primary mode of leaching is due to chemical oxidation by $Fe^{+3}$ and $O_2$ (8).

Under typical environmental conditions of $E_h$ (electrochemical potential) and pH the oxidation of metal sulfides to sulfate and elemental sulfur with the concomitant release of the principal metal is favored thermodynamically. Eisenreich et al., (7) have generated an equilibrium model for leaching in wasterock piles of Duluth Gabbro ore and subsequent speciation of trace metals released to aquatic systems. The model qualitatively predicts that metal sulfides will by oxidized by $O_2$ to sulfate in an aqueous environment. Subsequent mobility of the trace metals is predicted to depend highly on the nature and concentration of organic and inorganic liqands and on the nature and availability of adsorbing surfaces. The acidity which is generated upon sulfide oxidation appears to be insufficient to overcome the natural buffering capacity of silicate minerals, such as plagioclase, which undergo a unique series of weathering reactions. Examples of these reactions are given in Table 1.3.

Peters (9) has developed an extensive $E_h$-pH diagram for chalcopyrite, $CuFeS_2$, which is the predominant copper sulfide mineral in the Duluth-Gabbro complex. In a slightly acidic, oxidizing environment $CuFeS_2$ will be unstable with respect

to bornite, pyrite and $H_2S$. Further increases in oxidation potential result in the decomposition of bornite to chalcocite. Kinetically, $CuFeS_2$ is preferentially transformed to CuS, covellite, and FeS, troilite. These sulfides are oxidized in turn by $Fe^{+3}$ or $O_2$ to $Cu^{+2}$, $Fe^{+3}$, $SO_4^{-2}$ and $S^0$.

Metal sulfides such as ferrous sulfide (machinawite and pyrrhotite) and nickel sulfides (millerite and pentlandite) readily dissolve under oxic or anoxic conditions. Locker and deBruyn (10) have studied the anoxic dissolution of synthetic ZnS and CdS in acidic solution which dissolve according to the following stoichiometric equation:

$$CdS + 2H^+ + \overset{k_1}{\underset{K_{-1}}{\rightleftarrows}} Cd^{+2} + H_2S(g). \tag{1.1}$$

They showed that in a well-agitated system that the reaction rate is controlled by a heterogeneous surface reaction rather than mass transport in solution; and that in non-oxidative dissolution that the reaction products do not form a passive film that inhibits the dissolution process. The empirical rate expression obtained by these investigators is as follows:

$$(1/A) (d N_{H_2S}/dt) = k_1 [H_2SO_4] - k_{-1} [Cd^{+2}]^{0.5} {}_{H_2S}{}^{0.5}. \tag{1.2}$$

where the dissolution rate (moles/$m^2$-sec) is a function of the surface area (A in $M^2$) of the solid/liquid interface and the concentration of acid in the system. They developed a model and provide experimental evidence to show that a slow adsorption of a proton on the solid surface is the rate determining step in the reaction. Their results clearly show that the rate of non-oxidative dissolution depends on both the properties of the solid and the solution.

Pankow (11) has studied the non-oxidative dissolution of FeS (mackinawite) over the pH range 3-7. The flux, $F_s$ (moles/$cm^2$ m) from the surface of pressed FeS pellets obeyed the following empirically determined rate law:

$$F_s = \frac{V}{A}\frac{dS}{dt}t = k_1\gamma [H^+] + k_2 \tag{1.3}$$

where $k_1$ and $k_2$ are rate constants with values of 0.22

and 1.9 moles/$cm^2$-min, respectively, at $25^{\circ}$C. The $k_2$ term would predominate in the pH range of natural waters. Mechanistically, the $k_1$ term arises from direct adsorption of $H^+$ on the FeS crystal surface and the $k_2$ term arises from thermal vibrations and solvation effects which result in the dissolution of lattice constituents.

The role of oxygen in the oxidative-dissolution of FeS is apparent in the empirical rate law determined by Nelson [12].
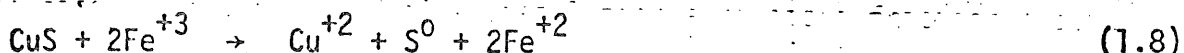
$$-d[FeS]/dt = k A_s P_{O_2} [H^+]^{0.25}. \qquad (1.4)$$

The rate of dissolution of FeS has a first-order dependence on dissolved oxygen concentration and the total available surface area; however, unlike the anoxic dissolution, the oxidative dissolution exhibits a fractional dependence on the hydrogen ion concentration. The reaction is remarkably sensitive to catalysis by Ni(II) in concentrations in excess of $10^{-5}$M. At pH 7, the rate of dissolution is accelerated ten-fold when the Ni concentration is $10^{-4}$M. Other trace metals such as Cu(II), Ag(I) and Cd(II) exhibited no catalytic or inhibitory activity. Below pH 9 the major sulfur oxidation product was elemental sulfur with significant contributions from thiosulfate and sulfate. The exclusive iron oxidation product was $\gamma$-FeOOH (lepidocrocite). In the presence of high concentrations of $Cl^-$ elemental sulfur was the exclusive sulfide oxidation product.

Under the conditions of pH7, $[O_2]$ = 4 mg/1, $[FeS]_0$ = 800 mg/1 and rapid stirring the observed oxidative dissolution rate was $10^{-4}$M$^{-1}$Min$^{-1}$. This is a significantly greater rate of oxidative-dissolution than would be predicted if the rate of either the homogeneous oxidation of Fe(II) [13] or HS$^-$ [14] at saturation values was the overall rate-determining processes. Using the rate law of Stumm and Lee [13] under the above conditions Fe(II) would be oxidized at a rate of $10^{-6}$Mmin$^{-1}$. Similarly, the rate law of Chen and Morris [14] predicts that HS$^-$ would be oxidized at a rate of $10^{-10}$ M min$^{-1}$. Both of these calculated rates are below $10^{-4}$ M min$^{-1}$. Therefore, it was concluded that the

oxidative dissolution involves direct attack of $O_2$ at the FeS surface. Furthermore, considering the results of Pankow (11) and Nelson (12) jointly, it can be concluded that kinetically FeS will preferentially dissolve via an oxidative pathway although both mechanisms should be operative simultaneously under environmental conditions.

Oxidation of the three major sulfidic minerals of economic significance in the Duluth-Gabbro complex, chlacopyrite ($CuFeS_2$).

$$CuFeS_2 + 4Fe^{+3} \rightarrow Cu^{+2} + 5Fe^{+2} + 2S^0 \qquad (1.5)$$

$$CuFeS_2 \rightarrow CuS + FeS \qquad (1.6)$$

$$4FeS + 9O_2 + 4H^+ \rightarrow 4Fe^{+3} + 4SO_4^{-2} + 2H_2O \qquad (1.7)$$

$$CuS + 2Fe^{+3} \rightarrow Cu^{+2} + S^0 + 2Fe^{+2} \qquad (1.8)$$

pentlandite $\{(Fe, Ni)_9S_8\}$,

$$18 Fe^{+3} + (Fe, Ni)_9S_8 \rightarrow 22.5Fe^{+2} + 4.5Ni^{+2} + 8S^0 \qquad (1.9)$$

$$(Fe, Ni)_9S_8 + 17.63O_2 + 6.5H^+ \rightarrow 4.5Fe^{+3} + 4.5Ni^{+2} + 8SO_4^= + 3.25 H_2O \quad (1.10)$$

and cubanite ($CuFe_2S_3$)

$$CuFe_2S_3 + 6Fe^{+3} \rightarrow Cu^{+2} + 8Fe^{+2} + 3S^0 \qquad (1.11)$$

$$CuFe_2S_3 + 6.5O_2 + 2H^+ \rightarrow Cu^{+2} + 2Fe^{+3} \ 3 SO_4^= + H_2O \qquad (1.12)$$
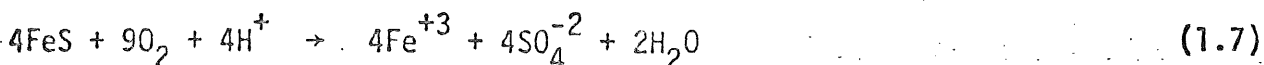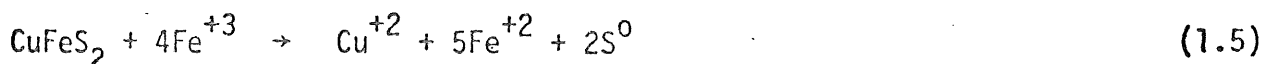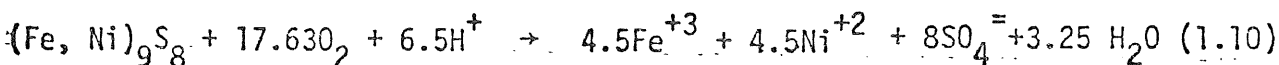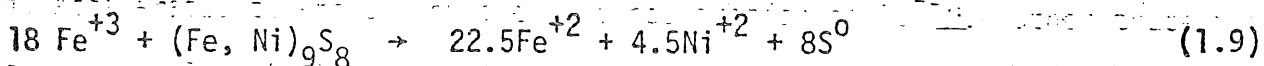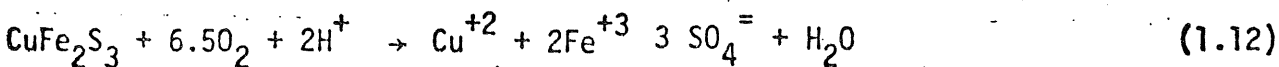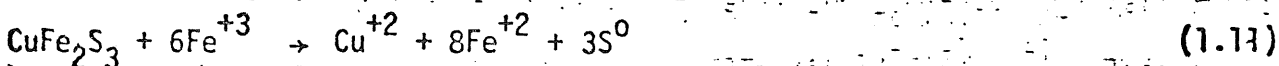
has been studied with the potential for mineral extraction as a primary goal; therefore, detailed kinetic and mechanistic information is not available, although some of the experimental results and general observations are pertinent to this

study. Kinetically, $CuFeS_2$ is the copper sulfide most resistant to oxidative dissolution (4). Madsen et al., (15) studied the large-scale (7 ton), long-term (500 days) leaching by $Fe^{+3}$ of low-grade copper sulfide ores which contained predominately chalcopyrite imbeded in feldspars (monzonite and quartz monzonite). These investigators observed parabolic release kinetics in which the extent of leaching was a direct function of total exposed surface area. They used a mixed kinetic model, in which dissolution is controlled partially by diffusion through a reacted outershell of the host rock and partially by a chemical reaction at the mineral surface, to mathematically predict the observed leaching rates. Release of Cu is initially controlled by a surface reaction, however, as the reaction proceeds a layer of reaction products builds up on the surface and diffusion of the oxidant through this reacted zone becomes rate controlling.

Wadsworth (4) reports that the oxidation of $CuFeS_2$ by $O_2$ in acidic solution followed a mixed kinetic rate law involving the sum of a parabolic and linear term

$$\frac{\Delta n^2}{k_p} + \frac{\Delta n}{k_1} = t . \tag{1.13}$$

where $\Delta n$ represents the amount of copper dissolved in solution in time t, and $k_1$ and $k_p$ are respectively the parabolic and linear rate constants. The parabolic term describes the diffusion of $O_2$ through a deposited film of product sulfur and the linear term describes a surface reaction which doesn't involve charge transfer.

Dutrizac, MacDonald and Ingraham (16) followed the rate of dissolution of synthetic cubanite by $Fe^{+3}$ oxidation at temperatures greater than $45^\circ C$. The dissolution rate was linear with an activation energy of 12 k cal/mole. At constant temperature, $k_1 = \gamma [Fe]^{0.6}$ and $[H^+]^{-0.1}$. From this evidence, it was concluded that the rate of dissolution was controlled by a chemical reation at the

sulfide surface.   Chloride ion appeared to have a catalytic effect on the rate of dissolution.

Pentlandite {$(Ni, Fe)_9S_8$} ores are readily leached in column reactors by trickling solutions of ferric sulfate (17).   Linear release rates were observed over a significant portion of the reaction where $k_1 = \gamma [Fe^{+3}]^{0.2} [H_2SO_4]^{-0.1}$.   At low flow rates the dissolution of pentlandite appears to be diffusion controlled whereas at higher flow rates the reaction appears to be chemically controlled. Formation of elemental suflfur and jarosite ($HFe_3(SO_4)_2(OH)_6$) where observed during the course of the reaction.

Other studies relevant to the potential leaching of Cu and Ni from Duluth Gabbro ore pertain to firstly, the relationship between the solubility product and the rate of metal sulfide oxidation, secondly, the role of electrochemical interactions between different metal sulfides in influencing the rate of metal leaching and thirdly, the role of organic chelating agents.   Torma and Sakaguchi (37) have shown that the rates of biooxidation of a series of synthetic metal sulfides is directly proportional to their solubility products for a given surface area.   The sulfide with the highest solubility product (i.e. NiS) is oxidized most rapidily in the following order: NiS>CoS>ZnS>CdS>CuS.

Sato (18) has observed that one metal may enhance the dissolution rate of another sulfide through electrochemical interaction.   Specifically, for two sulfides of the same metal, the one with the higher formal oxidation state is more stable than one with the lower formal oxidation state.   This appears to be consistent with the relatively high resistance of chalcopyrite to chemically induced dissolution in mixed mineral systems.   Bryner and Anderson (19) reported that the presence of $FeS_2$ accelerated the rate of Cu leaching from $CuFeS_2$. $FeS_2$, which is significantly more electropositive than chalcopyrite, should induce dissolution of $CuFeS_2$ by galvanic interactions.   However, Ichikuni (20)

reports that no galvanic effect was observed on the dissolution rate of $CuFeS_2$ in the presence of $Fe^{+3}$.

Sato (18) has proposed that the rate determining step in the dissolution of metal sulfides involves an election transfer with the formation of elemental sulfur.

$$MeS \overset{\rightarrow}{\leftarrow} Me^{+2} + S^0 + 2\bar{e} \tag{1.14}$$

The experimental potential generated by divalent metal-monosulfides measured against a reference electrode were best predicted by the half-cell reaction in equation 1.13. When $Fe^{+3}$ is the election acceptor equations 1.13 and 1.14

$$2\bar{e} + 2Fe^{+3} \overset{\rightarrow}{\leftarrow} 2Fe^{+2} \tag{1.15}$$

can be combined to give the overall equation for oxidation.

$$MeS + 2Fe^{+3} \overset{\rightarrow}{\leftarrow} Me^{+2} + 2Fe^{+2} + S^0 \tag{1.16}$$

Nelson (12) reports that leaching experiments conducted on ZnS, PbS, CuS and $FeS_2$ separately and in various combinations demonstrated that electrolytic action does substantially increase the extent and rate of oxidation of the sulfide with the lower emf, while offering considerable cathodic protection to the sulfide with the higher half-cell potential.

Chelation by naturally occurring organic macromolecules has been implicated or suggested by a number of investigators as an important pathway of weathering or solubilization of a wide variety of minerals (21, 22, 23, 24). Soil humic acids, which are heteropoly condensates with structurally indeterminate arrays of functional groups such as carboxyl, carbonyl, phenolic, amino and hydroxyl groups on the periphery of the molecule, have been shown to be effective reagents for the dissolution of a variety of metal sulfides (21). Humic acids isolated from soil exhibited a dramatic effect on the leaching of copper sulfides. Susceptibility to dissolution by humic acids was correlated with the relative bond strengths of the sulfide minerals. These minerals were susceptible to humic acid

dissolution in the following order: $Cu_2 > S > CuS > PbS > Cu_5 > FeS_4 > CuFeS_2 > ZnS$. Leaching was also accelerated by a decrease in average particle size.

Schalscha et al., (22) studied the role of the model organic acids such as salicylic, citrate, tartaric, and acetic acid on the extent of dissolution of a variety of ferrungnious oxides and silicates. The extent of leaching appears to be a function of the nature of the organic acid in terms of its complexing strength and the particle size of the oxide or silicate mineral. Gruner (25) demonstrated that water drawn through a peat bed from northeastern Minnesota attacked silicates, iron oxides and siderite but had little effect on pyrite.

From these studies, it can be concluded the concentration and nature of dissolved organic carbon in the waters of the Duluth Gabbro complex will be critical factors in the rate and extent of leaching. Field studies (1) show that dissolved organic carbon levels in groundwater near the Dunka pit range from 20 to 40 mg/l. Humic material released from peat beds surrounding the mining region may be responsible to a large extent for the observed rates of leaching in the field.

## 1.5. Weathering/Dissolution of Aluminum Silicates

Trace elements of interest in this study such as Cu, Ni, Co and Zn are present primarily as sulfides in Duluth Gabbro. The metal sulfides are disseminated as small particles in the interstices between silicate minerals (plagioclase, olivine, pyroxene) or intimately intergrown with the silicates. As a result, silicate mineral dissolution may play an important role in the release to solution of trace metals bound as sulfides. Tables 1.2 and A.8 list a detailed mineralogical analysis of the mineralized and unmineralized gabbro rock which was leached in this study. The primary minerals present in gabbro rock leached are in order of decreasing abundance (weighted mean %): plagioclase (47-64%) >clinopyroxene (7.6-26%) >olivine (11-14%) >biotite (3.3-5%). Plagioclase minerals have the general stoichiometry of (Na, Ca)

$AlSi_3O_8$ and represent a continuous solid solution feldspar series with end members albite ($NaAlSi_3O_8$) to anorthite ($CaAlSi_3O_8$). Clinoproxene and olivine have the general stoichiometry of $Ca(Fe, Mg)Si_2O_6$ and $(Fe, Mg)_2 SiO_4$, respectively. Since greater than 90% of the gabbro mass consists of silicate minerals, and the majority of silicate mineral comprised of plagioclase (a feldspar series), a discussion of the weathering/dissolution of feldspars is included.

The incongruent dissolution of aluminum silicates (weathering) can be represented by (26).

$$\text{cation - Al-silicate} + H_2CO_3^* + H_2O \rightleftharpoons HCO_3 + H_4SiO_4 + \text{cation} + \text{Al-silicate(s)} \quad (1.17)$$
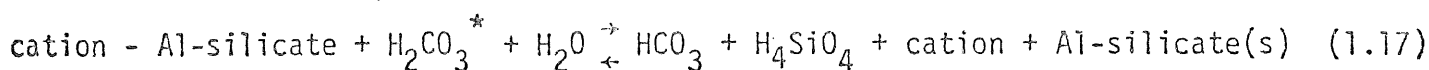
In this process, a primary silicate mineral is degraded into a secondary mineral which is often ill-defined structurally or X-ray amorphous. Aluminum is generally conserved in the reaction as it forms insoluble silicate minerals such as kaolinite ($Al_4[Si_4O_{10}](OH)_8$ or halloysite ($Al_4[Si_4O_{10}](OH)_8 2H_2O$), amorphous aluminum oxides ($AlC(OH)_3 nH_2O$) or microcrystalline Al oxides such as gibbsite ($Al_2O_3 3H_2O$). The weathering of Al silicates imparts alkalinity ($HCO_3^-$) to the water, and therefore the resulting degraded Al silicate is more acidic than the primary mineral. Silicic acid ($H_4SiO_4$) and mineral cations are released to solution, with aqueous control mechanisms being different for both. The appearance of cations ($Ca^{+2}, Mg^{+2}, Na^{+1}, K^{+1}$) and/or silicic acid to solution is offered as evidence of silicate mineral weathering, and is usually monitored in laboratory kinetic studies.

An example of the incongruent dissolution of a typical plagioclase (andesine) to give the degraded silicate kaolinite, can be represented by (26):

$$4 \, Na_{0.5}Ca_{0.5}Al_{1.5}Si_{2.5}O_8 + 6 \, H_2CO_3^* + 11 \, H_2O \rightleftharpoons 2Na^+ + 2Ca^{+2} + 4 \, H_4SiO_4 + 6 \, HCO_3^- +$$

$$3 \, Al_2Si_2O_5(OH)_4(S) \quad\quad (1.18)$$
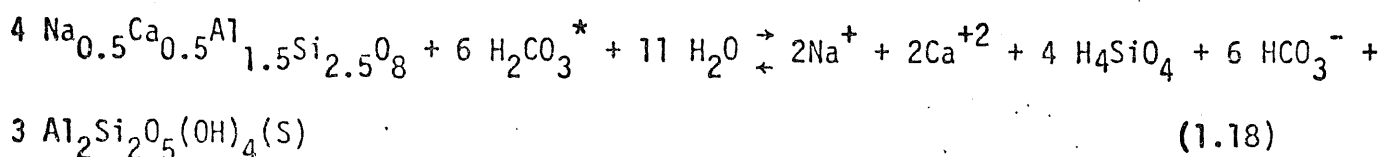
In this reaction the rate of release of the cations $Na^+$ and $Ca^{+2}$ and silicic acid can be used to determine the kinetics and possibly the mechanism of plagioclase dissolution.

In addition to the weathering of Al silicate minerals, incongruent dissolution can occur through the slower chemical process of hydrolysis. For example, the hydrolysis of anorthite, an end member of the plagioclase series, can be compared to the weathering of anorthite as represented below.

Hydrolysis

$$CaAl_2Si_2O_6(s) + 3H_2O \rightleftharpoons Ca^{+2} + 2OH^- + Al_2Si_2O_5(OH)_4(s) \qquad (1.19)$$

Weathering

$$CaAl_2Si_2O_6(s) + 2H_2CO_3 + H_2O \rightleftharpoons Ca^{+2} + 2HCO_3^- + Al_2S_2O_5(OH)_4 \qquad (1.20)$$
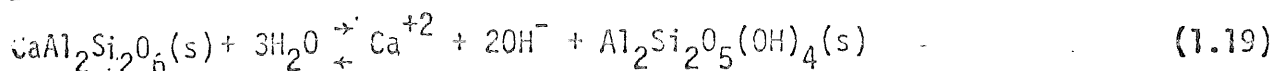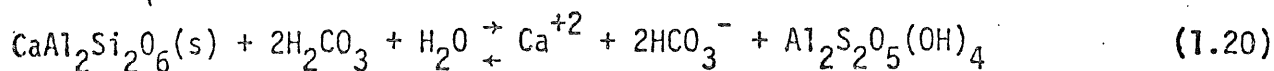
The hydrolysis of anorthite leads to the release of $Ca^{+2}$ and $OH^-$, and formation of the secondary mineral, kaolinite, but no silicic acid is released. In contrast, the weathering of anorthite releases, in addition to the above, $HCO_3^-$ and silicic acid. The rates of incongruent dissolution are slow for both reactions, but weathering processes exert a greater ultimate influence on the chemical composition of the aqueous phase.

The mechanism of aluminum silicate dissolution and the process exerting control on aqueous phase solubility on the reaction products have been studied under environmental conditions by Garrels and Howard (27), Wollast (28), Helgesen (29, 30), Luce et. al., (31), Paces (32), Petrovic (33), Busenberg and Clemency (34) Dayal (35) and Busenberg (36). Garrels and Howard (27) found that the initial interaction of feldspar with the aqueous phase consisted of a reversible ion-exchange reaction between $H^+$ from the aqueous phase and surface cations resulting in the release of a stoichiometric quantity of cation to solution, and an increase in solution pH. This was followed by the incongruent dissolution

of the feldspar surface (27, 34) leaving behind a slightly soluble product layer. Wollast (28), Helgesen (29) and others have modeled the diffusional transport of silicic acid and cations through the building product layer.

Busenberg and Clemency (34) studied the dissolution of kinetics of eight different feldspars at $25^{\circ}C$ and 1 atm of $CO_2$ partial pressure for time periods of 400-1200 hours. The incongruent dissolution of the silicate minerals could be adequately described by a four-stage process. The first stage involved an ion-exchange reaction whereby $H^+$ were exchanged with surface cations resulting in an initial rise in pH. Negligible amounts of $H_4SiO_4$ or Al were released in this stage lasting ~ 1 minute. The second stage lasting to ~ 50 hours for cations and 1.5-100 hours for silicic acid could be described by an equation of the form $C=ket^n$ where C=concentration, ke=rate constant, t=time, and n=dimensionless factor. They attributed this complex release behavior to two or more processes occurring simultaneously. The second stage was typified by a rapid release of cations and silicic acid in solution. The diffusion controlled parabolic third stage lasted up to ~ 19-21 days and could be described by an expression of the type

$$C= kpt^{1/2} + A \qquad\qquad (1.21)$$

Where kp=rate constant and A=integration constant. Parabolic release kinetics were attributed to the rate limiting process of diffusional transport of cations across a thickening product layer. Wollast (28), Busenberg and Clemency (34) and Busenberg (36) suggest that Al diffuses out of the Al silicate matrix in the first and second stages where it hydrolyzes to form an amorphous $Al(OH)_3$. Silicic acid diffusing through the secondary product layer reacts with the $Al(OH)_3$ to form an Al silicate which covers the surface. Diffusion of cations and silicic acid through the new mineral phase explain the parabolic kinetics observed in the third stage. The fourth stage lasting beyond 21 days exhibited

linear kinetics, which can be expressed as

$$C = k_1 t + B \qquad (1.22)$$

where $k_1$ = rate constant, and B = integration constant. Linear kinetics may result when the rate of formation of the secondary product layer equals the rate at which the layer is destroyed by dissolution or fragmentation (32).

Busenberg (36) has studied the products of feldspar dissolution under conditions of 1 atm partial pressure of $CO_2$ and $25^{\circ}C$. He determined that the activity of Al in the aqueous phase within the initial 4 hours was controlled by pH and the solubility of microcrystalline gibbsite ($Al_2O_3 \cdot 2H_2O$). After 100 hours, the activity of Al and $H_4SiO_4$ in solution was controlled by microcrystalline halloysite ($Al_y[Si_4O_{10}](OH)_8 \cdot 2H_2O$) a hydrolyzed form of kaolinite ($Al_4[Si_4O_{10}]-(OH)_8$. The dissolution of the secondary product layer can be represented by the equation:

$$Al_2Si_2O_5(OH)_4 \cdot 2H_2O + 6H^+ \rightleftarrows 2Al^{+3} + 3H_2O + 2H_4SiO_4 \qquad (1.23)$$
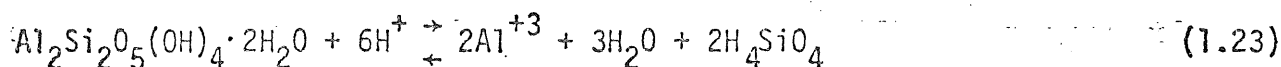
Busenberg and Clemency (34) reported that the parabolic stage rate constants ranged from $3.4 \times 10^{-14}$ to $9.3 \times 10^{-13}$ mole/cm²/sec$^{1/2}$, the linear rate constants were $(.03 - 2.5) \times 10^{-15}$ mole/cm²/sec, and the apparent diffusion coefficients (parabolic stage) were $(0.1 - 5) \times 10^{-21}$ cm²/sec. Helgeson (29) determined that the incongruent dissolution of feldspars at $25-200^{\circ}C$ exhibited parabolic constants from $10^{-10}$ to $>10^{-8}$ moles/cm² day$^{1/2}$

## 1.6. Interrelationship of Alumino-Silicate and Metal Sulfide Dissolution

The dissolution of alumino-silicate minerals (plagioclase) can effect the dissolution of base metal sulfides such as chalcopyite and pentlandite by 1) exposing additional metal sulfide surface to solution, 2) controlling solution pH through buffering reactions, 3) contributing anions ($HCO_3^-$), cations ($Ca^{+2}$, $Mg^{+2}$, $Na^+$, $K^+$) and silicic acid ($H_4SiO_4$) to solution which might

accelerate or inhibit metal sulfide dissolution or oxidation, 4) increasing ionic strength which increases the solubility of metal sulfides, and 5) sorbing released metal from metal sulfides onto primary (feldspar) or secondary product layers (amorphous $Al(OH)_3$; microcrystalline gibbsite, kaolinite, halloysite), and 6) forming insoluble metal precipitates such as metal silicates. The dissolution of silicate minerals, in general, increases with increasing acidity, increasing Pe and increasing tendency for complex formation (26).

The dissolution of silicate minerals increases with increasing surface area available to solution. Garrels and Howard (27) noted that $K^+$ release from a $K^+$ feldspar increased with increasing solution loading of -200/inch particles. Increases in solid surface area available for dissolution may be achieved by increasing loading of similar size particles or by adding equal masses of different size particles. For particles less an 1 μm in diameter or of specific surface areas greater than~3 $m^2$/g, particle surface energy may become large enough to alter surface properties. As a result, decreasing particle size may increase the solubility of particles through a thermodynamic influence of surface properties on the solubility product constant.

Solution acidity is a dominant variable in the dissolution of silicate minerals. A dilute aqueous suspension of feldspar results in an increase in pH (28) with the solution buffered at pH 7-9. Busenberg and Clemency (34) observed an increase in the pH of an acidic feldspar solution from 3.92 to 4.51.

Table 1.3 lists a series of equilibrium reactions describing the dissolution of a typical feldspar, anorthite. Reaction i represents the initial ion exchange reaction of a feldspar surface with solution where $H^+$ replace cations in surface exchangeable sites. Wollast (28) has shown that the initial reaction rate (15 mins. - 2 hrs.) depends on pH according to the expression

$$rate = k_1 (H^+)^{1/3} \qquad (1.24)$$

Under natural conditions, the rate and extent of silicate dissolution
increases from pH 8 to pH 4, and can be described by $H_4SiO_4$ diffusional transport
through a residual product layer made up of slightly soluble $Al(OH)_3$ followed by
formation of Al-silicates (equation A, Table 1.3). At pH <5, no protective
product layer is formed due to continuous dissolution of amorphous $Al(OH)_3$.
Therefore, the rate of appearance of silic acid and cations in solution at low pH
should not follow parabolic kinetics, and should not be controlled by diffusion.
Wollast (28) extrapolated the results of his experiments to the field in that
natural conditions of good drainage, and rains of high intensity and frequency,
but of short duration, should yield maximum dissolution rates. Reaction rates
increase above pH 8 due to dissolution of the slightly soluble $Al(OH)_3$ formed
on the feldspar surface. There is not agreement, however, that feldspar
dissolution is controlled by diffusional transport from pH 3-10 [33].

Dissolved oxygen exerts an indirect influence on the dissolution of
silicate minerals. As the dissolved oxygen (DO) content of the solution
increases (i.e., high Pe) there is a greater tendency for oxidation of the
metal sulfide minerals such as pyrite, pyrrohotite, chalcopyite and pentlandite.
The release of $H^+$ through the oxidation of ferrous ion and reduced sulfur species
will decrease solution pH at the surface water boundary, thereby increasing
silicate dissolution. In aqueous suspensions constituted of 95% plagioclase and
5% mineral sulfide by weight, bulk solution pH will be only slightly affected by
redox processes.

Organic and inorganic ligands may enhance the dissolution of silicate
minerals. Reaction B (Table 1.3) demonstrates the effect of organic complexation
with ligand ($Y^-$) undergoing a ligand exchange reaction with surface bound Al,
thus degrading the silicate structure. Available ligand may also bind the
released cations maintaining them in a disolved state. Organic chelation has
been observed as a factor in enhancing silicate weathering (22). Salicylate,

8-hydroxyquinoline and EDTA increased the extent of biotite dissolution by binding structural components. Plagioclase in intimate contact with ground or surface water containing naturally occurring organic ligands may enhance the dissolution of silicate and metal sulfide minerals. In addition, organic complexation of released metals may prevent their removal by sorption or precipitation.

Reaction x. (Table 1.3) demonstrates the adsorption of trace metals on the silicate surface. The mineral surface is available as the native feldspar or as secondary reaction products such as amorphous $(Al(OH)_3$, microcrystalline $Al_2O_3 \cdot 3H_2O$, kaolinite or halloysite. Thus trace metals released to solution through oxidative dissolution of the metal sulfide may be removed by adsorption on the silicate mineral surface. The relative extent and importance of adsorption as a metal removal mechanism depends on pH and total metal concentration.

## 1.7. Research Direction - Parametric Studies

From the above review it is apparent that a number of factors can control the rate and extent of metal leaching. Some of these factors include the availability of oxygen or other oxidants such as ferric ion, temperature, degree of surface saturation by water, pH, particle size, chemical or microbial catalysis, ionic strength, chelating agents, and galvanic interactions. In the following sections, laboratory research experiments will be described, that were designed to elucidate the relative importance of the above factors in controlling the rate and extent of leaching of heavy metals from Duluth Gabbro mining solids. Parametric studies were undertaken in an attempt to determine an empirical or operational rate law which can be used for predictive purposes and to elucidate a plausible mechanism for leaching consistent with observed kinetics. Kinetic and mechanistic models will be developed in subsequent chapters. Results of this research should prove to be useful in predicting the relative role of chemical leaching of Duluth Gabbro solids (mineralized, unmineralized and tailings) as a source of potential toxic metals to aquatic ecosystems in northeastern

Minnesota. A knowledge of mechanistic pathways should suggest reasonable control procedures to prevent or treat any mine drainage that results from the mining or beneficiation of Duluth Gabbro Ore.

## Chemical Composition of Gabbro: Table 1.1
### Values in Weight Percent

| Element | Unmineralized | Mineralized |
|---|---|---|
| $S^b$ | 1.1 | 3.92 |
| Ni | 0.095 | 0.36 |
| Cu | 0.24 | 1.4 |
| $Co^a$ | 0.082 | 0.039 |
| $Zn^a$ | 0.0009 | 0.012 |
| Fe | 10.4 | 17.2 |
| Ca | 2.6 | 2.3 |
| Mg | 2.0 | 1.9 |

a  Neutron Activation Analysis (University of Wisconsin)
b  Wet Chemical Analysis
c  Atomic Absorption Sepectrophotometry (all other elements)


## Mineral Analysis of Gabbro:  Table 1.2

| Mineral | Formula | Weighted Mean Volume Percent Unmineralized | Mineralized |
|---|---|---|---|
| Pentlandite | $(Fe,Ni)_9S_8$ | 0.032 | 0.34 |
| Chalcopyrite-Cubanite | $CuFeS_2-CuFe_2S_3$ | 0.13 | 1.3 |
| Pyrrhotite | $Fe_7S_8-FeS$ | 0.403 | 3.1 |
| Ilmenite | $FeTiO_3$ | 4.0 | 3.1 |
| Magnetite | $Fe_3O_4$ | | |
| Olivine | $(FeMg)_2SiO_4$ | 14 | 11 |
| Clinopyroxene | $Ca(Fe,Mg)Si_2O_6$ | 7.6 | 26 |
| Orthopyroxene | $(Fe,Mg)_2Si_2O_6$ | 2.8 | 2.3 |
| Plagioclase | $NaAlSi_3O_8-CaAl_2Si_2O_8$ | 64 | 47 |

92.97    94.14

## Table 1.3
## Silicate Dissolution, Anorthite

<u>Initial Ion Exchange</u>

    **i.** $CaAl_2Si_2O_8(s) + 2H^+ = Ca^{2+} + H_2Al_2Si_2O_8(s)$
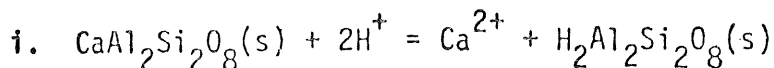
<u>Dissolution Phase for Anorthite</u>

  Inorganic Reaction

    **ii.** $CaAl_2Si_2O_8(s) + 2H^+ + H_2O = Al_2Si_2O_5(OH)_4(s) + Ca^{2+}$; $\log k = {}^+14.4^a$ (Kaolinite)

    **iii.** $Al_2Si_2O_5(OH)_4(s) + 5H_2O = 2H_4SiO_4 + Al_2O_3 \cdot 3G_2O(s)$; $\log k = -9.4^a$ (Gibbsite)

    **A.** $CaAl_2Si_2O_8(s) + 2H^+ + 6H_2O = 2H_4SiO_4 + Al_2O_3 \cdot 3G_2L(s) + Ca^{2+}$; $\log k = 5.0$
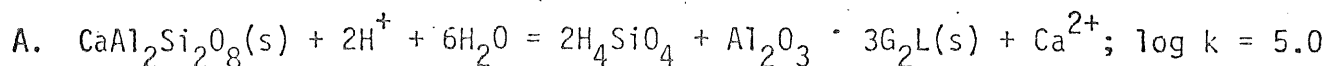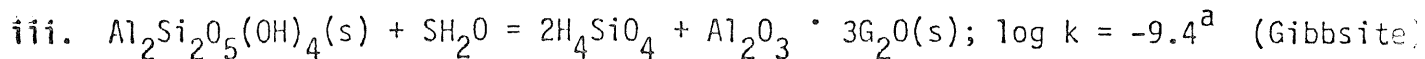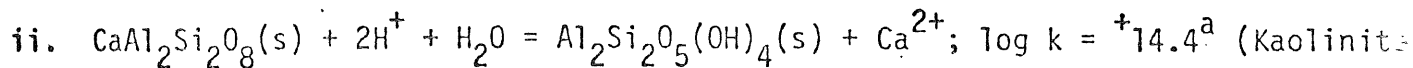
  Organic Ligand $Y^-$, effect on kaolinite dissolution

    **iv.** $Al_2Si_2O_5(OH)_4 + 2Y^- = 2AlY(aq) + 2H_4SiO_4 + H_2O^a$

    **B.** $CaAl_2Si_2O_8(s) + 8H^+ + 2Y_+^- = Ca^{2+} + 2AlY(aq) + 2H_4SiO_4$

<u>Additional Reactions</u>

    **v.** $Al_2O_3 \cdot 3H_2O(s) = 2Al^{3+} + 6OH$      $\log k = 68.0^a$

    **vi.** $Al_2O_3 \cdot 3H_2O(s) + OH^- = Al(OH)_4^-$      $\log k = -1.0^a$

    **vii.** $SiO_2$ (amorph) $+ H_2O = H_4SiO_4$      $\log k = -2.7^a$

    **viii.** $H_4SiO_4 = SiO(OH)_3^- + H^+$      $pk = 9.46^a$

    **ix.** $(-SiOH) = (-SiO^-) + H^+$      $pk\ int = 6.8 \pm 0.2^{a,b}$

    **x.** $Me^{ni} + N (-SiOH) = Me(OSi-) + NH^{+c}$

        (similar to reaction of $Me^{n+}$ with $(OH^-)$)
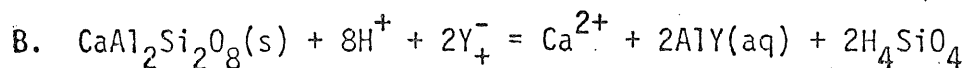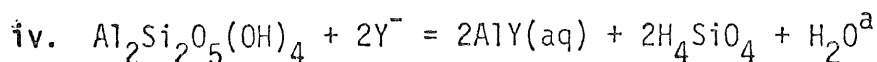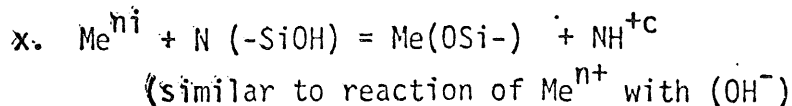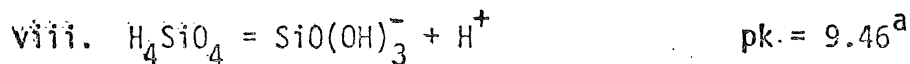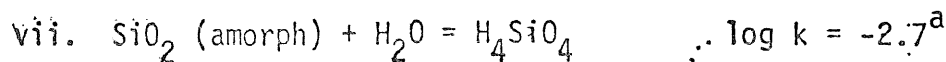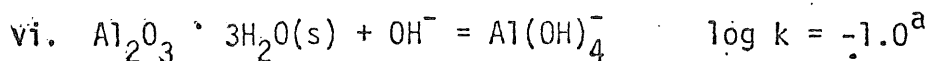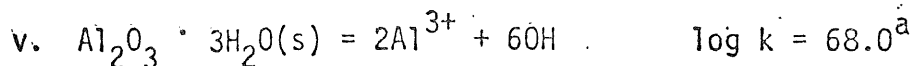
a. Reference 26; 25°C, 1atm.
b. o.1 <u>M</u> $NaClO_4$, Schindler & Kamber (1968) in Stumm & Morgan (26)
c. Dugger (1964) in Stumm & Morgan (26)

# Chapter 2

## Experimental Procedure

### 2.1. Sample Preparation

Duluth Gabbro rock was obtained as sample composites from mineralized and unmineralized areas of the Dunka Pit mine. The two samples were ground at the Mineral Resources Research Center at the University of Minnesota. The grinding process consisted of subjecting the rock sequentially to jaw crusheers of 2.54 cm and 1.27 cm capacity and gyro crusher. The sample was then split into 1.8kg portions using a basic splitter and submitted to Bond Ball Mill grinding dry at 70 rpm. The resulting sample was sieved through a Tyler screen shaker for 5 minutes of grinding and 15 minutes of shaking. The minus 200 mesh portion was retained for use in laboratory leaching experiments, and stored in polyethylene containers.

In initial experiments, representative portions of the bulk Gabbro sample were selected by the coning and quartering method. In later experiments, samples to be leached were obtained by removing the desired quantity from the well-mixed bulk material.

### 2.2 Apparatus

The experimental apparatus used in the batch leaching studies consisted of six, 4-1 Pyrex beakers in which the lips had been removed, and the assembly covered by a fitted Plexiglass top. Six air diffusers were connected to a manifold by Tygen tubing with a diffuser inserted into each beaker through the protective cover, and sealed with an aluminum-foil covered rubber stopper. The gabbro suspension in the reaction flask was mixed continuously with a laboratory stirrer consisting of a teflon shaft and blade protruding through the top of the Plexiglass cover. Samples were withdrawn by pipette through a stoppered sampling port. All reactors were maintained in a constant temperature room at $20.0 \pm 1^{0}C$.

The beakers, mixing shafts and gas diffusers were prepared for each experiment by washing with 3 portions of distilled water, 3 portions of 0.1 N $HNO_3$ and 3 additional portions of distilled water. Distilled water (3500 ml) was measured into each reaction flask and the air bubbled the solution for 24 hours prior to each experiment, except when disolved oxygen was being varied.

## 2.3 Procedure

Gabbro samples (-200 mesh) were weighed on a Sartorius Analytical Balance and poured into the reaction flasks, initiating the experiment. Samples were withdrawn at periods exceeding 1000 hours at the time intervals of 0.5, 6, 24 and 48 hours and 1, 2, 3, 4 and 5 weeks. The 150 ml sample was withdrawn through the sampling port from a point in the reaction flask two thirds depth of the liquid. With the exception of the particle size experiment, no water was replaced to the reaction flask because representative amounts of solid and liquid were taken for analysis. The samples were placed into washed, pre-weighed 250 ml polyethylene bottles, re-weighed and the weight of the sample recorded. The samples were filtered immediately through acid-washed, $0.4\mu$ Nuclepore filters placed in a Millipore Filtration Apparatus. The filtered sample was acidified to pH1 with concentrated $HNO_3$.

In some experiments, the quantity of metal precipitated or adsorbed to the leached particle surface was determined. The untreated Gabbro suspensions obtained from the reaction flask were filtered through $0.4\mu m$ Nuclepore membrane filters and the particulate-laden filter was re-suspended in 100 mls of 0.01N $HNO_3$ for 60 seconds. The sample was re-filtered and the filtrate saved for chemical analysis.

The metals studied in the leaching experiments were Cu, Ni, Fe, Ca and Mg, and were determined by Atomic Absorption Spectrophotometry (AAS) in the flame

(Varian Model 175 AA) or flameless mode (PE Model 360 AAS with $D_2$ background corrector and HGA 2100 graphite furnace). Analyses were performed according to the general instructions of the manufacturer with minor modifications to account for the high salt matrix encountered. Quantification was achieved by comparison to standards or by standard addition. Reproducibility measurements indicated a variation of <10%. Sulfate was determined by the recommended procedure in Standard Methods (37) with modification to smaller sample volumes. Soluble reactive silica determined in some experiments was analyzed for by the method of Strickland and Parsons (38). Spectrophotometric measurements were performed with a Beckman Model 26 UV-VIS Spectrophotometer.

Dissolved oxygen measurements were made with a YSI Model 54 D.O. Meter, with a Model 5739 D.O. probe. Dissolved oxygen of reaction solutions was adjusted using various combinations of $O_2$, $N_2$ and compressed air. Solution pH was determined with a Corning Model 10 pH meter and a microelectrode, or an Orion Digital pH meter (Model 701A). pH was maintained in controlled experiments by daily or hourly additions of HCL or NaOH.

# Chapter 3

## Experimental Results - Metal Sulfide Dissolution Kinetics

### 3.1 Background

Previous investigations, which were reviewed in Chapter one, on the dissolution kinetics of the slightly soluble metal sulfides have shown that the critical factors are available reactive surface area, pH, dissolved oxygen concentration and the presence of active catalysts. In order to formulate a reasonable kinetic expression which adequately describes the process of oxidative-dissolution of metal sulfides, each important parameter must be varied independently of the other parameters in order to ascertain the relative impact of that particular variable on the dissolution of the metal sulfides.

The study of reaction kinetics in heterogeneous systems is a difficult problem even for simple systems which involve only two phases (i.e. one liquid and one solid phase). In simple homogeneous systems the rate of reaction is most often controlled by formation of an "activated complex" to use the terminology of transition state theory (39). However in hetergeneous systems, mass transport or diffusion limitations to reaction rate become important. In a hetereogeneous system as complex as the Duluth Gabbro ore, which according to Table 1.2 involves at least a minimum of nine solid phases, one liquid phase and one gaseous phase, the problem of resolving the detailed kinetics and mechanism of dissolution is immense if not impossible. In order to simplify the presentation of experimental results the problem of metal sulfide dissolution will be separated from the problem of silicate mineral dissolution, although these two processes are not mutually exclusive. In the discussion of results presented in Chapter 5 the two problems will be interfaced in a unifying manner.

The primary metal sulfides identified by x-ray diffraction analysis were in their relative order of abundance pyrrhotite ($FeS$), chalcopyrite ($CuFeS_2$), pentlandite ($(Fe,Ni)_9S_8$) and cubanite ($CuFe_2S_3$). From an environmental and

economic standpoint the rate of appearance of Cu and Ni in solution is of primary importance. X-ray analysis also shows that ore samples which are ground to a finely divided state (i.e., <74μ in particle diameter, Dp) contain distinct fractions of metal sulfide independent of the original silicate matrix. Assuming that the metal sulfides are found in discrete inclusions and are liberated totally from the surrounding silicate (plagioclase) matrix by grinding to a Dp <0.74μ , the problem of metal sulfide dissolution can be separated from the problem of silicate dissolution (weathering) as a fist approximation. Silicate dissolution kinetics are presented separately in Chapter four.

3.2. Preliminary Experiments and Kinetic Analysis

Well-mixed batch reactors described in section 2.2 were used for all kinetic runs. Preliminary experiments were run with powdered Gabbro material with a Dp <74μ suspended in doubly-distilled water by mechanical stirring. The goal of these initial experiments was to determine optimal conditions for following the rate of release of Cu, Ni and Fe into aqueous solution. During each kinetic run aliquots of the solid-liquid slurry were extracted while the system was well-mixed. Ideally the solid to liquid ratio was maintained constant during each experiment. A liquot were taken at pre-established time intervals during the course of each experiment. Total time of reaction was generally around 1000 hours.

Initial experiments in unbuffered, pH uncontrolled systems were designed to determine the impact of increasing solids to volume ratio in a search for optimal experimental conditions for subsequent studies. The effect of increasing total specific surface area or loading on the relase of Cu, Ni and Fe was studied at mass loadings of 2, 10, 50 and 100 grams of Dp <74μ of unmineralized Gabbro material. Increasing the Gabbro loading at constant volume increases the total specific surface area of sulfide minerals for reaction with oxygen,

on one hand, but on the other hand, an increase in total specific surface area of the silicate minerals, which have charged surface silanol groups, increases the possibility of adsorptive interactions with charged aquated and hydrolyzed metals in solution.

The overall impact of increased loading on total metal release is illustrated in Figure 3.1. As the loading increases the pH of the slurry rises in response to the incongruent dissolution of plagioclase which releases $HCO_3^-$ to solution according to equation 3.1

$$4\ Na_{0.5}Ca_{0.5}Al_{1.5}Si_{2.5}O_8 + 6H_2CO_3^* + 11H_2O = 2Na^+ + 2Ca^{+2} + 4H_4SiO_4 + 6HCO_3^- + 3Al_2SiO_5(OH)_4(s) \quad (3.1)$$
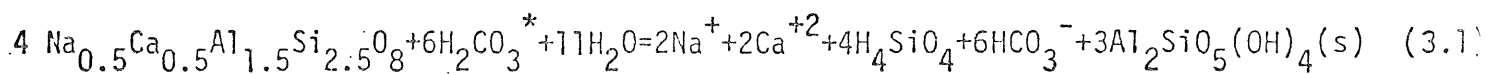
This effect is shown more clearly in Figure 3.2. The release of bicarbonate to solution accounts for the unique buffering capacity exhibited by the Gabbro material in equilibrium with water. After 2,800 hours the Gabbro $H_2O$ air system can be assumed to have reached equilibrium with respect to pH. This assumption is verified by the results presented in Figure 3.3 which show that the pH stablizes at a constant value after approximately 500 hours for different Gabbro loadings. The buffering capacity of the Gabbro ore appears to be a direct function of the total specific surface area and the total bicarbonate released to the system. For example, for a reactor system dominated by bicarbonate buffer exposed to the atmosphere equations 3.2 and 3.3 can be combined to show the approximate dependence of the sytem pH on the bicarbonate concentration if all other equilibrium are ignored.

$$H_2CO_3^* = K_H PCO_2 = 10^{-5}M \quad (3.2)$$

$$[H^+][HCO_3^-] = K_1\ [H_2CO_3^*] = 10^{-6.3} \times 10^{-5} \quad (3.3)$$

$$pH = 11.3 + \log\ [HCO_3^-] \quad (3.4)$$

If the $[HCO_3^-]$ in solution at equilibrium is 30 mg/l (log $HCO_3^-$ = -3.3) the pH would be 8.0. From the results shown in Figure 3.2, it can be seen that the

equilibrium pH approaches 8.0 given sufficient time and high Gabbro loadings.

Referring to Figure 3.1 again, the greatest total release, which is the sum of the solution phase metal and the adsorbed phase metal, for Ni and Fe occurs at relatively low loading rates and consequently relatively low pH. Copper, on the other hand, shows a greater total release at higher pH although the majority of released metal was found in the adsorbed phase. In general as the pH rises the released metals are found predominately in the adsorbed phase. This is consistent with the known surface characteristics of $\alpha$-quartz and other silicate minerals in aqueous solution.

In general, at lower pH FeS and $(Ni,Fe)_9S_8$ would be expected to dissolve more readily independent of any surface oxidation. However, $CuFeS_2$ dissolution is relatively insensitive to increasing acidity while surface oxidation plays a more important role. It is well-known that oxidation of $HS^-$ increases with increasing pH (14, 40) and by analogy the oxidation of $CuFeS_2$ may also increase with increasing pH. A summary of the effect of loading on metal release is present in Table 3.1.

Using raw data presented in Table A. 1 (Appendix A) concentration versus time profiles on Cu and Ni can be constructed as shown in Figure 3.4. At mass loadings $\leq 10$ g $l^{-1}$, the concentration of Ni as a function of time appears to be linear. This linear or apparent zero-order rate of dissolution of Ni was observed consistently over a wide variety of conditions. The rate of appearance of Cu with time was more complex and showed a greater sensitivity to pH. In order to observe Cu release rates, it was necessary to keep to solution pH below 6; whereas Ni release rates were less sensitive to pH and maintained apparent linearity. Initial release of Cu at lower pH could be described as parabolic with a later linear stage of release. The fate of Cu in solution is more sensitive to pH because of the formation of $Cu(OH)_2$ and $CuC^-_3(s)$ at pH 6 and electrostatic and chemical interactions with surface $-SiOH^-$ groups. For this reason, it
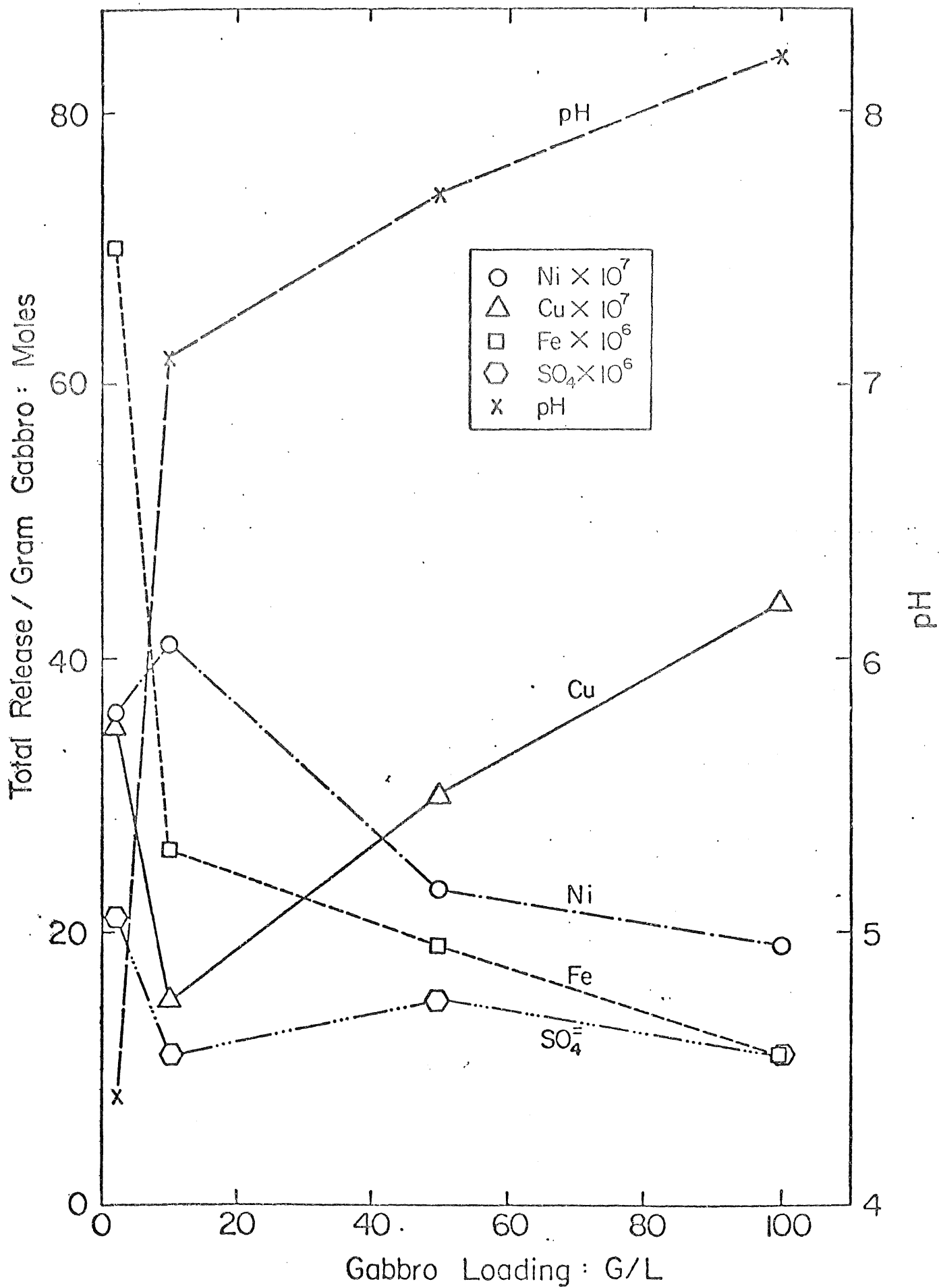
## Table 3.1

### Total Release: Effect of loading on unmineralized gabbro
Ad: Adsorbed & Precipitated, Sol: In solution, Tot: Total Release
All values in moles $* 10^6$ per gram gabbro

Time: 750 Hrs

| g $\frac{\text{Gabbro}}{\text{Liter}}$ | pH | $Ni_{Ad}$ | $Ni_{Sol}$ | $Ni_{Tot}$ | $Cu_{Ad}$ | $Cu_{Sol}$ | $Cu_{Tot}$ | $Fe_{Ad}$ | $Fe_{Sol}$ | $Fe_{Tot}$ | $Ca_{Ad}$ | $Ca_{Sol}$ | $Ca_{Tot}$ | $Mg_{Ad}$ | $Mg_{Sol}$ | $Mg_{Tot}$ | $SO_{Tot}$ |
|---|---|---|---|---|---|---|---|---|---|---|---|---|---|---|---|---|---|
| 2 | 4.4 | 0.083 | 3.6 | 3.6 | 0.24 | 0.24 | 3.5 | 7.0 | 63 | 7.0 | 6.6 | 32 | .38 | 2.6 | 19 | 19 | 21 |
| 10 | 7.1 | 3.7 | 0.44 | 4.1 | 1.5 | <0.01 | 1.5 | 26 | 0.027 | 26 | N.D. | 13 | N.D. | N.D. | 6.1 | N.D. | 11 |
| 50 | 7.7 | 2.2 | 0.035 | 2.3 | 3.0 | 0.01 | 3.0 | 19 | 0.01 | 19 | 58 | 7.6 | 65 | 13 | 3.3 | 16 | 15 |
| 100 | 8.2 | 1.8 | 0.02 | 1.9 | 4.4 | 0.01 | 4.4 | 11 | 0.01 | 11 | N.D. | 5.6 | N.D. | N.D. | 2.7 | N.D. | 11 |
| 2* | 5.2 | 0.12 | 2.2 | 2.3 | 0.22 | 0.28 | 0.50 | 9.9 | 59 | 69 | 5.5 | 24 | 29 | 3.6 | 16 | 20 | 18 |
| 50* | 7.7 | 1.8 | 0.01 | 1.8 | 2.2 | 0.01 | 2.2 | 20 | 0.01 | 20 | 56 | 6.0 | 62 | 16 | 3.5 | 19 | 4.4 |

* Nitrogen Diffusion
ND: Not Determined
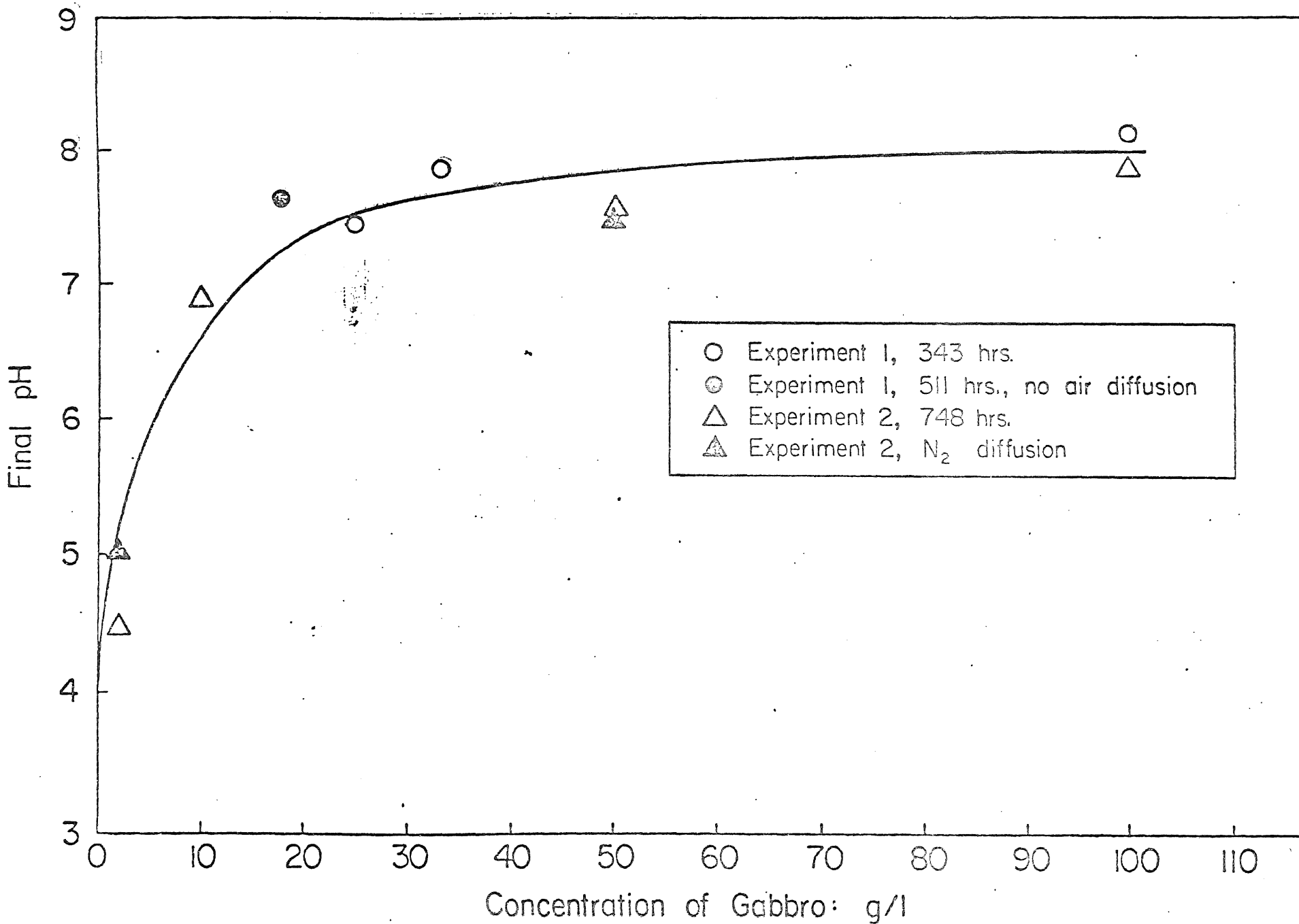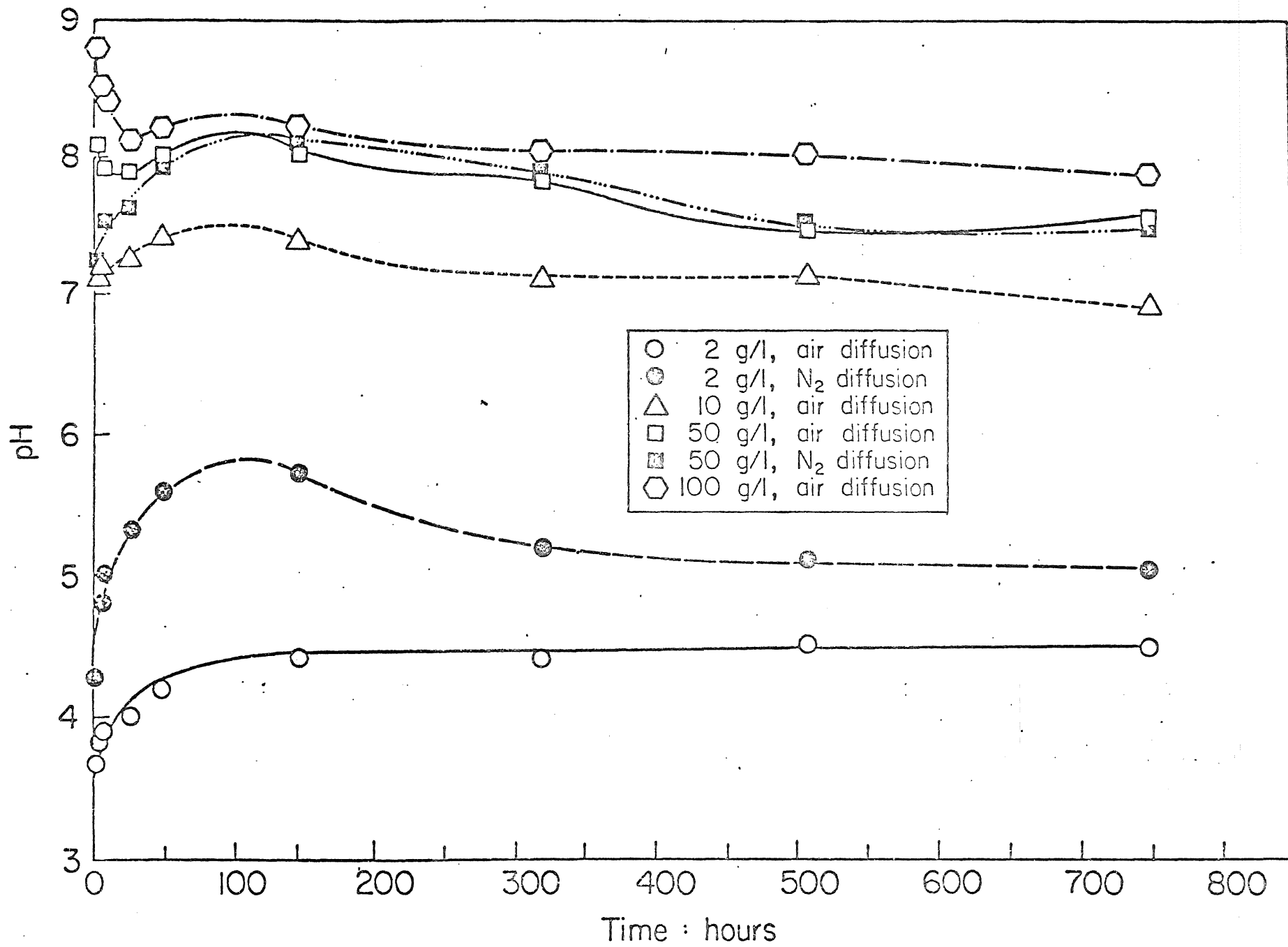
was decided to follow the appearance of Ni with time as a measure of the intrinsic rate of oxidative dissolution of metal sulfides.

The rate of oxidative-dissolution can be expressed mathematically in the following way:

$$-d[(Fe,Ni)_9S_8]/dt = kA_s^l[O_2]^m[H^+]^n \qquad (3.5)$$

assuming that the kinetics of dissolution have a similar dependence on active surface area as oxygen concentration and hydrogen ion concentration. Superscripts $l$, $m$, $n$ are the reaction orders for $A_s$, $[O_2]$ and $[H^+]$, respectively. Under constant conditions any catalytic factors would be accounted for by $k$, the overall rate constant. From the stoichiometry for the oxidative-dissolution of pentlandite by oxygen

$$(Fe,Ni)_9S_8 + 17.63O_2 + 6.5H^+ \rightarrow 4.5Fe^{+3} + 4.5Ni^{+2} + 8SO_4^= + 3.25H_2O \qquad (3.6)$$
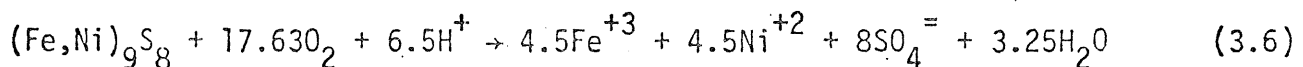
The rate of disappearance of pentlandite will be related to the rate of appearance of $Ni^{+2}$ in solution by equation 3.7.

$$-d[(Fe,Ni)_9S_8]/dt = (1/4.5)d[Ni^{+2}]/dt \qquad (3.7)$$

and substituting into equation 3.5 gives

$$(1/4.5)d[Ni^{+2}]/dt = kA_s^l[O_2]^m[H^+]^n \qquad (3.8)$$

Under conditions of constant $O_2$, pH and $A_s$ equation 3.8 can be rewritten as a pseudo zero-order reaction

$$d[Ni^{+2}]/dt = k^l \qquad (3.9)$$

where

$$k^l = 4.5kA_s^l[O_2]^m[H^+]^n \qquad (3.10)$$

Equation 3.10 predicts that a plot of $[Ni^{+2}]$ versus time should be linear with a slope equal to $k^l$ as is actually observed in all kinetic runs when all other variables are held constant. The pseudo zero-order rate constant, $k^l$, will have units of ug $l^{-1}$ hr$^{-1}$.

The rate of dissolution of $(Fe,Ni)_9S_8$ can be also expressed as a flux when the total reaction volume V and active surface area, $A_s$, are considered. In general, for a heterogeneous reaction of a solid surface with a surface area $A_s$ ($cm^2$) dissolving in a solvent system of volume V ($Cm^3$) the flux ($moles/cm^2sec$) of material escaping from the surface into solution can be written in terms of the rate of the bulk concentration value, $Ni^{+2}$ ($moles/cm^3$) as follows:

$$\frac{d[Ni^{+2}]}{dt} = \frac{A_sF}{V} \tag{3.11}$$

or

$$F(\frac{moles}{cm^2-sec}) = \frac{V}{A_s}(d[Ni^{+2}]/dt) \tag{3.12}$$

Since $A_s$ was not determined experimentally but is a function of the actual surface area, $A(cm^2/g)$, the mass of Gabbro, m, can be substituted for $A_s$ assuming that

$$A_s = mA \tag{3.13}$$

Substituting this expression into equation 2.12 allows an "operational" surface flux to be calculated according to equation 3.14.

$$AF = F^1(\frac{moles}{g-sec}) = \frac{V}{m}\frac{d[Ni^{+2}]}{dt} \tag{3.14}$$

In subsequent sections results of a parametric study on the factors controlling the absolute value of $k^1$ or $F^1$ will be presented sequentially starting with particle size, followed by pH, dissolved oxygen, ionic strength and chelating agents.

## 3.3. Effect of Particle Size, Dp.

In general, finely divided solids have a greater solubility than large crystals. This phenomenon is commonly known as the Kelvin effect (26). The free energy change, $\Delta G$, involved in subdividing a coarse solid suspended in aqueous solution into a finely divided one of molar surface area, $S$, is given by

$$\Delta G = 2/3 \bar{\gamma} S \qquad (3.15)$$

where $\bar{\gamma}$ is the surface tension of the solid-liquid interface. This change in

free energy can be considered in the overall free energy change for dissolution.

$$\Delta G^1 = \Delta G_0 + \Delta G_s \qquad (3.16)$$

which yields

$$\log k_{so(S)} = \log k_{so(S=0)} + \frac{2/3 \bar{\gamma} S}{2.3RT} \qquad (3.17)$$

Equation 3.17 shows that the thermodynamic behavior of a solid is a function

of the surface area. If the rate of oxidative-dissolution were dependent on a

pre-equilibrium dissociation of the sulfide mineral followed by a rate determining

oxidation of $Fe^{+\Delta}$ or $HS^-$ in solution, then a shift in the equilibrium constant

due to a change in solid surface area would become significant. At $25^\circ C$ with $\bar{\gamma}$

= 400 ergs/cm$^2$ and S = $10^4$ m$^2$/mole the effect on log $k_{so}$ is approximately 0.5.

Alternatively, if the rate of oxidative-dissolution is a function of the

number of reactive sites on the surface, then increasing the total available

surface area should increase the reaction rate. To test this hypothesis, the effect

of four discrete particle size fractions at a fixed mass loading on the reaction

rate was studied. The four size fractions examined were

$Dp \leq 74\mu$, $74\mu < Dp \leq 420 \mu$, $420\mu < Dp \leq 840\mu$, and $840\mu < Dp \leq 2380$ .

The approximate surface area of the $Dp \leq 74$ fraction was determined using a

sub-sieve sizer. The areas of the other fractions were estimated using this

approximate value, finer sieving analysis and mathematical extrapolation. The

areas as determined by the above methods were 1700, 190, 62 and 25 cm$^2$/g.

Elemental analyses for Ni, Cu, Fe, Ca and Mg found in each discrete particle

size function are presented in Table 3.2

As particle size was reduced the rate of dissolution increased. This

effect is shown clearly in Figure 3.5. Using kinetic data presented in Table

A.3 it is possible to determine the sensitivity of k to changes in As where

## Table 3.2a

### Effect of Particle Size

COMPOSITION: All Values in mg $(\text{g gabbro})^{-1}$

| Diameter (mm) | Ni | Cu | Fe | Ca | Mg |
|---|---|---|---|---|---|
| d≤0.074 | 3.55 | 14.1 | 172. | 22.7 | 19.2 |
| 0.074 d≤0.42 | 1.82 | 8.25 | 155. | 17.6 | 18.2 |
| 0.42 d≤0.84 | 4.52 | 12.8 | 259. | 29.3 | 37.9 |
| 0.84 d<2.38 | 4.08 | 23.5 | 460. | 47.3 | 80.2 |

## Table 3.2b

Total Release: Effect of particle size: Mineralized Gabbro
Ad: Adsorbed & Precipitated, Sol: In solution, Tot: Total Release
All values in moles $* 10^6$ per gram gabbro

Time: 890 Hrs.

| S.A. $cm^2 l^{-1}$ | pH | $Ni_{Ad}$ | $Ni_{Sol}$ | $Ni_{Tot}$ | $Cu_{Ad}$ | $Cu_{Sol}$ | $Cu_{Tot}$ | $Fe_{Ad}$ | $Fe_{Sol}$ | $Fe_{Tot}$ | $Ca_{Ad}$ | $Ca_{Sol}$ | $Ca_{Tot}$ | $Mg_{Ad}$ | $Mg_{Sol}$ | $Mg_{Tot}$ | $SO_{Tot}$ |
|---|---|---|---|---|---|---|---|---|---|---|---|---|---|---|---|---|---|
| 4900 | 6.0 | 0.09 | 6.3 | 6.4 | 0.08 | 0.33 | 0.41 | 0.47 | 0.27 | 0.74 | 2.2 | 9.1 | 11 | 0.57 | 6.1 | 6.7 | 30 |
| 540 | 6.4 | 0.08* | 2.2 | 2.3 | 0.05* | 0.03 | 0.3* | 0.3* | 0.02 | 0.32 | 2* | 6.3 | 8.3 | 0.4* | 2.8 | 3.2 | 19 |
| 180 | 6.5 | 0.05 | 1.2 | 1.2 | 0.02 | 0 | 0.17 | 0.17 | 0.03 | 0.19 | 1.4 | 4.7 | 6.1 | 0.08 | 2.2 | 2.2 | 17 |
| 72 | 6.2 | 0.04 | 0.76 | 0.80 | 0.02 | <0.01 | 0.36 | 0.37 | 0.06 | 0.42 | 1.9 | 4.0 | 5.8 | 0.42 | 1.2 | 1.6 | 15 |

## Table 3.3

Total Release: Effect of pH on unmineralized Gabbro
Ad: Adsorbed & Precipitated, sol.: In solution, Tot: Total Release
All values in moles $* 10^6$ per gram gabbro

| pH | $Ni_{Ad}$ | $Ni_{Sol}$ | $Ni_{Tot}$ | $Cu_{Ad}$ | $Cu_{Sol}$ | $Cu_{Tot}$ | $Fe_{Ad}$ | $Fe_{Sol}$ | $Fe_{Tot}$ | $Ca_{Ad}$ | $Ca_{Sol}$ | $Ca_{Tot}$ | $Mg_{Ad}$ | $Mg_{Sol}$ | $Mg_{Tot}$ | $SO_{Tot}$ |
|---|---|---|---|---|---|---|---|---|---|---|---|---|---|---|---|---|
| 6.9 | 0.33 | 2.6 | 3.0 | 0.17 | 0.02 | 0.19 | 1.9 | 0.03 | 1.9 | 10 | 18 | 29 | 0.88 | 8.6 | 9.5 | 14 |
| 4.7 | 0 | 4.7 | 4.7 | 0.03 | 1.2 | 1.2 | 1.8 | 35 | 37 | 1.1 | 23 | 24 | 0.08 | 15 | 15 | 20 |
| 4.3 | <0.01 | 3.2 | 3.2 | 0.05 | 1.5 | 1.5 | 2.7 | 71 | 74 | 1.5 | 46 | 48 | 0.49 | 23 | 23 | 19 |
| 4.0 | <0.01 | 2.7 | 2.7 | 0.03 | 1.1 | 1.2 | 1.9 | 100 | 100 | 0.91 | 64 | 65 | 0.35 | 37 | 37 | 18 |
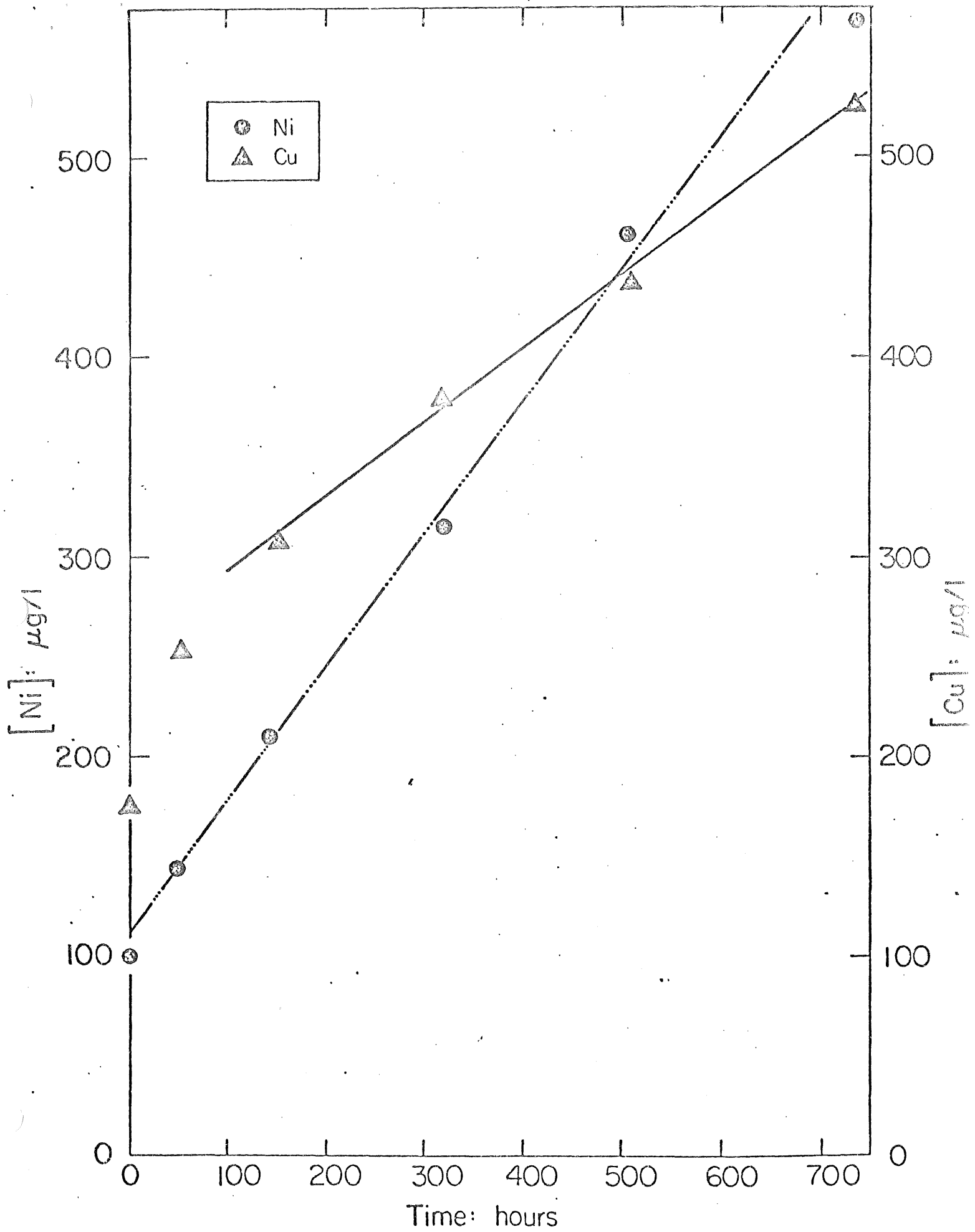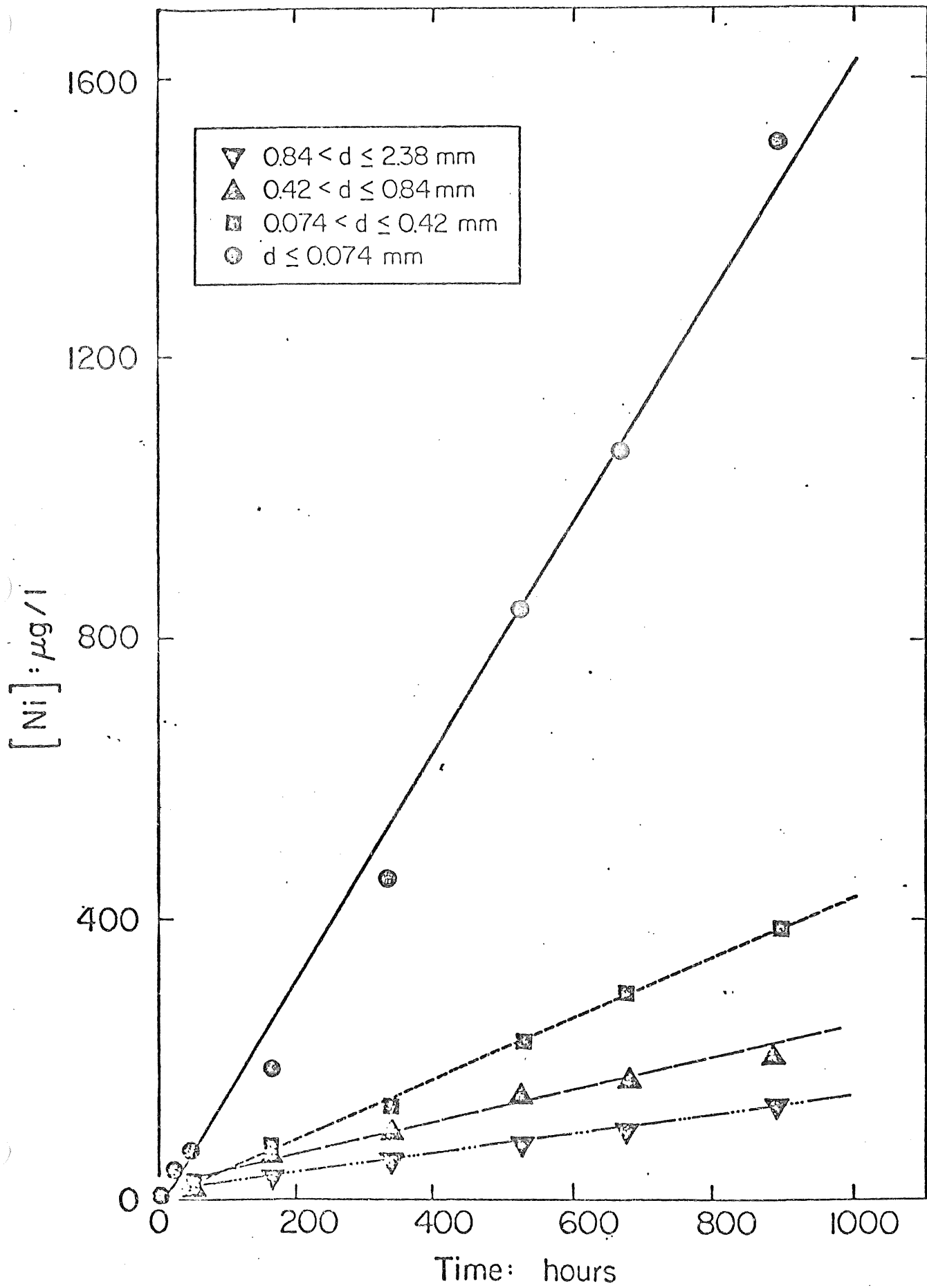
$$k^1 = k\, A_s^{\ 1} \qquad\qquad (3.18)$$

Taking the logarithm of both sides of this equation yields

$$\log k^1 = \log k + 1\ \log As \qquad\qquad (3.19)$$

which is a linear equation with a slope equal to the reaction order, 1, for the surface area. Equation 3.19 is plotted in Figure 3.6 with data taken from Table 3.10. From this linear relationship the reaction order in $A_s$ was determined to be 0.4. From data presented in Table 3.3 it can be seen that total metal release for all metals studied increases with a decrease in particle size although this effect is most promounced for the metals which are thought to originate from sulfidic minerals. Copper and Ni appear predominately in solution whereas the majority of iron is found in the adsorbed state, most likely as FeOOH.

As total specific surface area is increased within the same particle size fraction the apparent dissolution rate remains unaffected as shown in Figure 3.7. This result indicates that metal solubility as defined by the solubility product relationship may control the rate of appearance of Ni in solution. Decreasing the particle size would have the net effect of increasing the solid solubility as predicted by equation 3.17.

If the rate of dissolution were controlled by a chemical reaction on the sulfide surface then increasing the total reactive surface area should result in a demonstrable increase in reaction rate.

Further evidence for a solution phase rate limiting step in the dissolution of pentlandite is presented in Figures 3.8 and 3.9 which show the time dependent changes in pH and sulfate, respectively. pH remained relatively constant in the larger particle size fractions; however, in the lowest size fraction the pH was progressively lowered as the reaction proceeded. This indicates that significant oxidation of $HS^-$ and $Fe^{+2}$ is occurring with a concomitant release of $H^+$ to solution.

Table 3.10

## Nickel Kinetics - Summary of Data

$$[Ni] = kt+b$$
$k$ in mole sec$^{-1}$ (g gabbro)$^{-1}$
$b$ in mole (g gabbro)$^{-1}$
$t$ in seconds

| Reactor | $r^2$ | $b*10^9$ | $k*10^{13}$ | Description |
|---|---|---|---|---|
| 2-1 | 0.8814 | 890 | 24 | 2 g$l^{-1}$ unmineralized gabbro, air diffusion |
| 2-2 | 0.9914 | 17 | 16 | 10 g$l^{-1}$ unmineralized gabbro, air diffusion |
| 2-3 | 0.9687 | -1.4 | 3.2 | 50 g$l^{-1}$ unmineralized gabbro, air diffusion |
| 2-4 | 0.8531 | 0.081 | 0.79 | 100 g$l^{-1}$ unmineralized gabbro, air diffusion |
| 2-5 | 0.8911 | 450 | 17 | 2 g$l^{-1}$ unmineralized gabbro, $N_2$ diffusion |
| 2-6 | 0.4274 | 2.5 | -0.15 | 50 g$l^{-1}$ unmineralized gabbro, $N_2$ diffusion |
| 3-1 | 0.9938 | 3.1 | 30 | 2.86 g$l^{-1}$ unmineralized gabbro, PH 6.9 |
| 3-2 | 0.9853 | 270 | 37 | 2.86 g$l^{-1}$ unmineralized gabbro, PH 4.6 |
| 3-3 | 0.9424 | 360 | 27 | 2.86 g$l^{-1}$ unmineralized gabbro, PH 3.9 |
| 3-4 | 0.8723 | 400 | 18 | 2.86 g$l^{-1}$ unmineralized gabbro, PH 3.5 |
| 4-1 | 0.9972 | 53 | 21 | 2.86 g$l^{-1}$ -200 mesh mineralized gabbro |
| 4-2 | 0.9759 | 25 | 4.9 | 2.86 g$l^{-1}$ +200 - -40 mesh mineralized gabbro |
| 4-3 | 0.9710 | 15 | 5.1 | 2.86 g$l^{-1}$ +40 - -20 mesh mineralized gabbro |
| 4-4 | 0.8935 | 23 | 3.5 | 2.86 g$l^{-1}$ +20 - -8 mesh mineralized gabbro |
| 5-1 | 0.8903 | -1.0 | 4.8 | 2.86 g$l^{-1}$ mineralized gabbro, D.O.=1 mg$l^{-1}$ |
| 5-2 | 0.9879 | 58 | 11 | 2.86 g$l^{-1}$ mineralized gabbro, D.O.=5 mg$l^{-1}$ |
| 5-3 | 0.9779 | 180 | 22 | 2.86 g$l^{-1}$ mineralized gabbro, D.O.=9.3 mg$l^{-1}$ |
| 5-4 | 0.8929 | 170 | 21 | 2.86 g$l^{-1}$ mineralized gabbro, D.O.=44 mg$l^{-1}$ |
| 6-1 | 0.9858 | 39 | 12 | 5.71 g$l^{-1}$ mineralized gabbro, PH 5 |
| 6-2 | 0.9963 | 21 | 9.4 | 5.71 g$l^{-1}$ mineralized gabbro, PH 6 |
| 6-3 | 0.9814 | 20 | 5.8 | 5.71 g$l^{-1}$ mineralized gabbro, PH 7 |
| 6-4 | 0.9964 | 10 | 5.1 | 5.71 g$l^{-1}$ mineralized gabbro, PH 8 |
| 7-3 | 0.9475 | 1.3 | 11 | 5.71 g$l^{-1}$ mineralized gabbro, $\mu$=0.005 |
| 7-4 | 0.9830 | 4.4 | 12 | 5.71 g$l^{-1}$ mineralized gabbro, $\mu$=0.05 |
| 8-1a | 0.9230 | 20 | 1.2 | |
| 8-1b | 0.6944 | 80 | 3.1 | |
| 8-2a | 0.9780 | 2.4 | 0.31 | |
| 8-2b | 0.9192 | 5.7 | 0.42 | |
| 8-3a | 0.5324 | 0.43 | 0.0098 | |
| 8-3b | 0.6554 | 3.4 | -0.015 | |

Table 3.10 Continued

| Reactor | $r^2$ | $b*10^9$ | $k*10^{13}$ | Description |
|---|---|---|---|---|
| 3-5 | 0.9970 | 77 | 40 | 2.86 $gl^{-1}$ unmineralized gabbro, $1.29 \times 10^{-3}$ citrate |
| 3-6 | 0.9977 | 55 | 91 | 2.86 $gl^{-1}$ unmineralized gabbro, $1.29 \times 10^{-4}$ citrate |
| 4-5 | 0.8706 | 250 | 39 | 2.86 $gl^{-1}$ unmineralized gabbro, $1.29 \times 10^{-3}$ citrate |
| 4-6 | 0.9989 | 160 | 110 | 2.86 $gl^{-1}$ unmineralized gabbro, $1.29 \times 10^{-4}$ citrate |
| 5-5 | 0.9478 | 200 | 50 | 2.86 $gl^{-1}$ unmineralized gabbro, $1.29 \times 10^{-3}$ citrate, pH7 |
| 5-6 | 0.9868 | 240 | 56 | 2.86 $gl^{-1}$ unmineralized gabbro, $1.29 \times 10^{-}$ citrate, pH7 |
| 7-1 | 0.8120 | 0.50 | 1.4 | 5.71 $gl^{-1}$ mineralized gabbro, bog water |
| 7-2 | 0.9544 | 0.72 | 2.0 | 5.71 $gl^{-1}$ mineralized gabbro, ground water |
| 7-5 | 0.9862 | 0.94 | 2.6 | 5.71 $gl^{-1}$ mineralized gabbro, $1.29 \times 10^{-4}$ phthallic, pH7 |
| 7-6 | 0.8382 | 0.24 | 0.66 | 5.71 $gl^{-1}$ mineralized gabbro, $1.29 \times 10^{-}$ phthallic, pH7 |
| 8-4a | 0.7509 | 2.0 | 0.025 | |
| 8-4b | 0.9893 | 2.3 | 0.03k | |
| 8-5a | 0.0028 | 1.4 | -0.00021 | |
| 8-5b | 0.9881 | 1.5 | 0.043 | |

$$\log k' = \log k + l \log A_s$$
$$l = 0.4$$

Legend (within figure):
- O $d \leq 0.074$ mm
- △ $0.074 < d \leq 0.42$ mm
- ☐ $0.42 < d \leq 0.84$ mm
- ⬡ $0.84 < d \leq 2.38$ mm

Y-axis: pH (7.0, 6.5, 6.0, 5.5, 5.0)

X-axis: Time: hours (0, 200, 400, 600, 800)
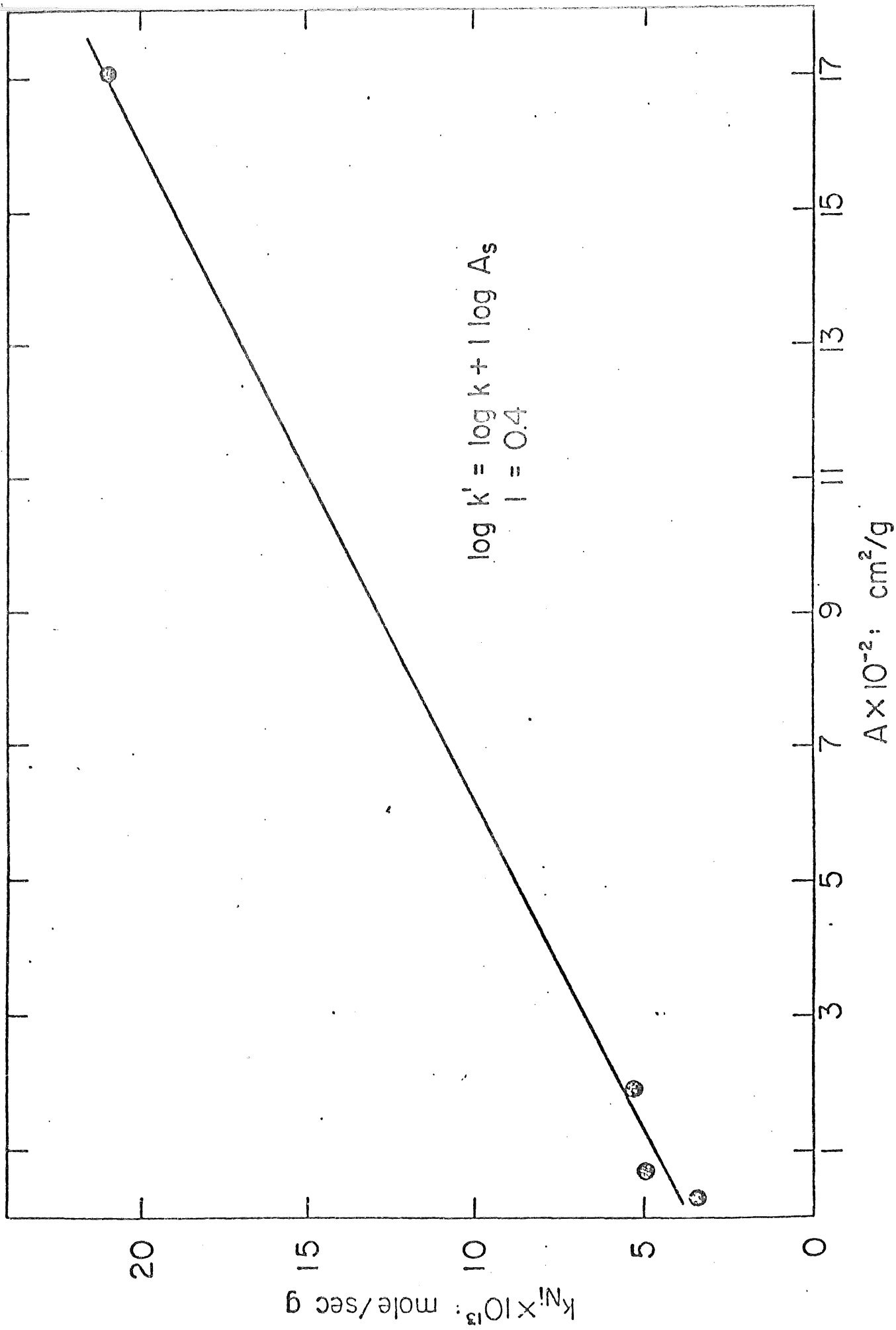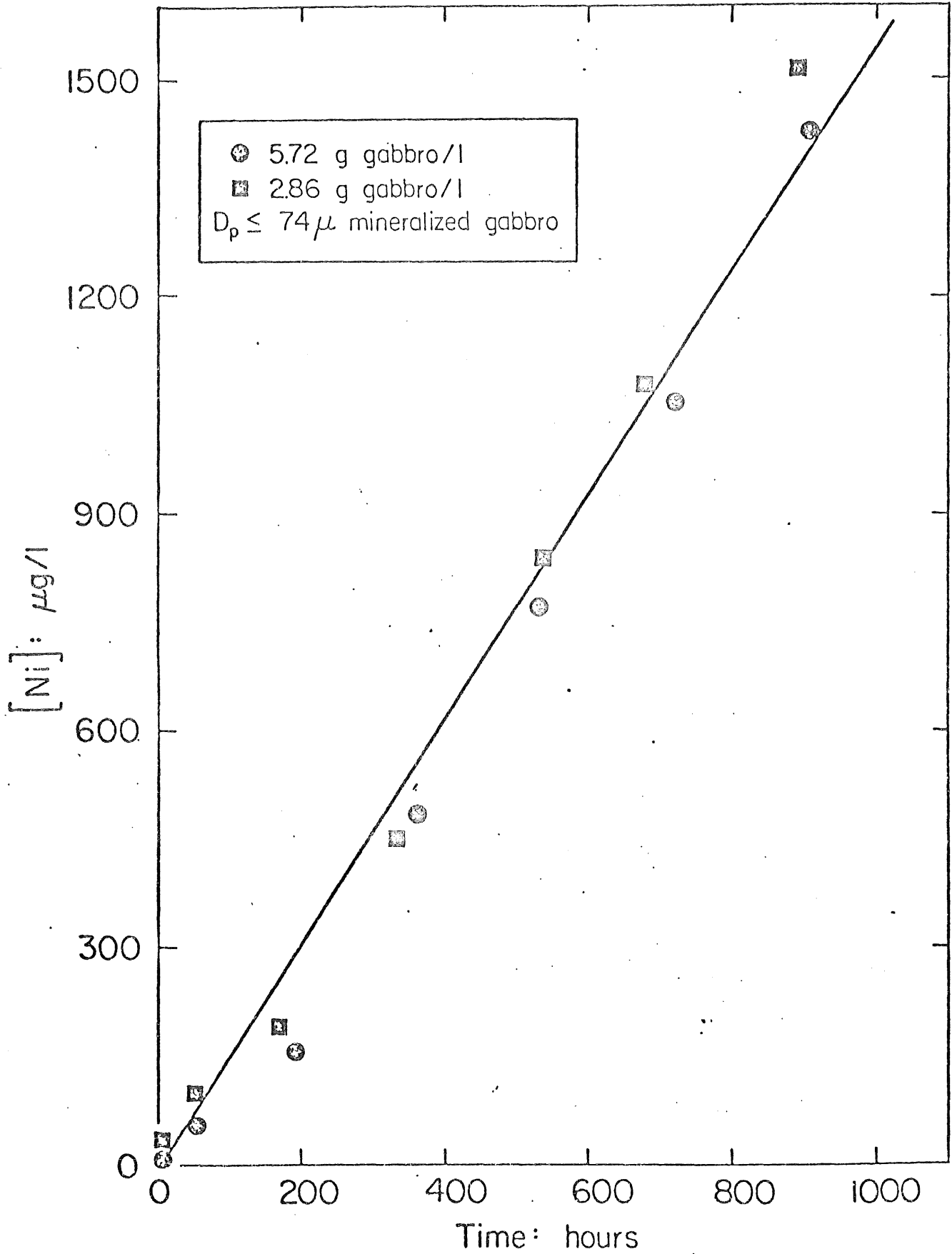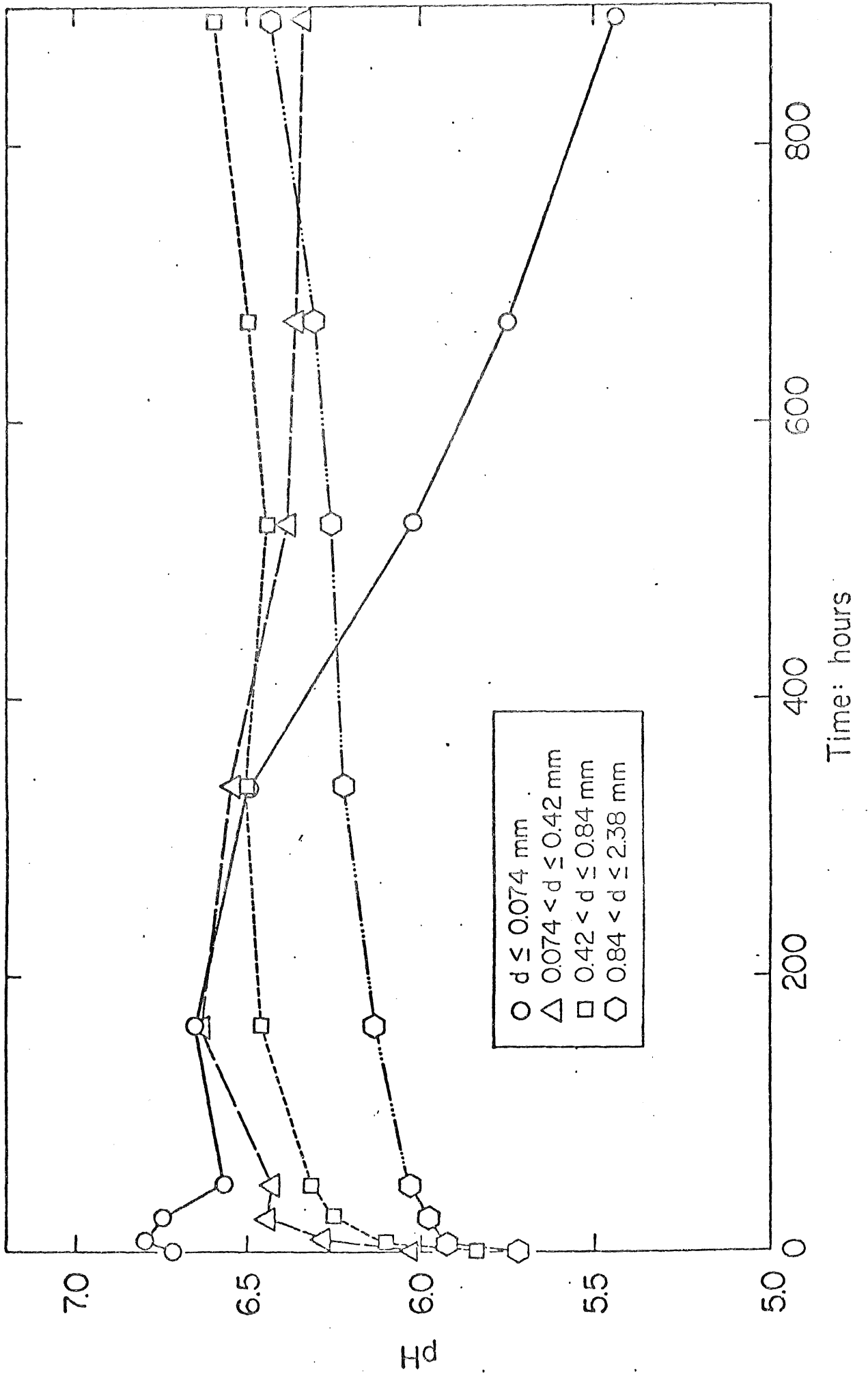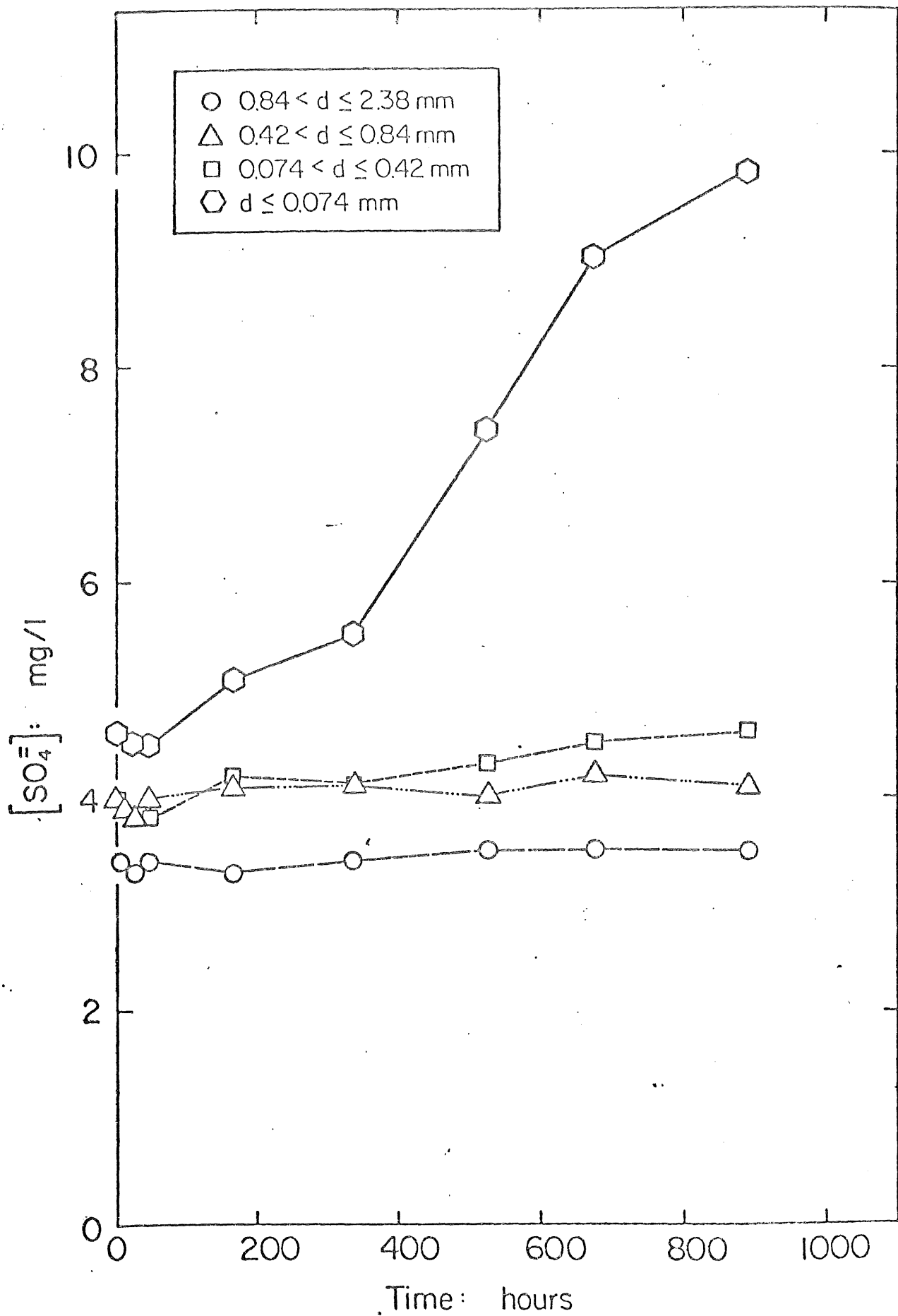
This idea is corroborated by the $SO_4^=$ vs. time profile in Figure 3.9. Significant increases of sulfate with time occurred only in the lowest particle size fraction indicating that a pre-equilibrium dissolution of pentlandite may be rate controlling. Oxidation of $Fe^{+2}$ to $Fe^{+3}$ and subsequent hydrolysis to $Fe(OH)_3$ or formation of jarosite, $KFe_3(SO_4)_2(OH)_6$ will result in the release of either 3 or 6 moles of H+ released per mole of $Fe^{+2}$ oxidized.

$$Fe^{+2} + 1/4O_2 + H^+ \to Fe^{+3} + 1/2H_2O \tag{3.18}$$

$$Fe+3 + 3H_2O \to Fe(OH)_3 + 3H^+ \tag{3.19}$$

$$K^+ + 2Fe^{+3} + 2SO_4^= + 6H_2O \to KFe_2(SO_4)_2(OH)_6 + 6H^+ \tag{3.20}$$
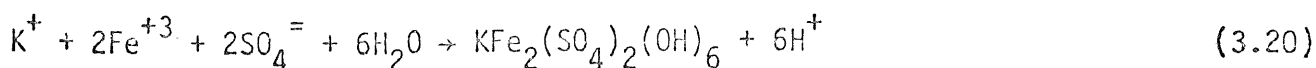
Regardless of the mechanistic implications, the kinetic results show that empirically equation 3.9 can be rewritten to take surface area into account in the following fashion

$$-d\ [(Fe_1Ni)_9S_8] = d\ [Ni(II)] = 4.5k_sA_s^{0.4} \tag{3.21}$$

where

$$k_s = k[O_2]^m[H^+]^n \tag{3.22}$$

## 3.4. Effect of Dissolved Oxygen Concentration

The oxidation of FeS, $CuFeS_2$ and $(Fe, Ni)_9S_8$ by oxygen to a variety of products is favored thermodynamically under experimental conditions used in this study. However, the stoichiometries presented in equations 1.4 through 1.11 are incomplete. Oxidized sulfur is found in a variety of metastable oxidation states. These states include elemental sulfur, $S^0$, polysulfide, $S_n^{-2}$, dithionite, $S_2O_4^{-2}$, thiosulfate, $S_2O_3^{-2}$, trithionate, $S_3O_6^{-2}$, tetrathionate, $S_4O_6^{-2}$, sulfite, $S_2O_6^{-2}$, and dithronate, $S_2O_6^{-2}$; although under the conditions of these experiments sulfate, $SO_4^=$, is the predicted end-product of oxidation. For example, in the oxidation of pyrrhotite

$$FeS + MO_2 \to products \tag{3.23}$$

the stoichiometric coefficient, M, can vary from 0.75 when sulfur is the exclusive oxidation product to 2.25 when sulfide is oxidized to sulfate. For a given set of experimental conditions where the reaction variables are held constant, the value of M should remain constant in the absence of any autocatalytic influences which may arise during the course of the reaction. Experimentally, the reaction order of oxygen, M, can be determined by studying the variation of $k^1$ with $[O_2]$ when all other variables are held constant.

Variable $[O_2]$ concentrations were achieved by differential mixing of $N_2$ and $O_2$ gas through four different reactors. Concentrations of oxygen of 1, 5, 9.3 and 44 mg/l were obtained and held constant throughout the reaction by gas diffusion through a fritted glass dispersion tube with continuous mechanical stirring.

The apparent Ni release rates increased as a direct function of increasing $[O_2]$ until 9.3 mg/l as shown in Figure 3.10. Above 10 mg/l in $[O_2]$ the reaction rate shows no further increase. This result suggests that the rate may be limited by the number of reactive surface available for direct attack by oxygen. Once these reactive sites were fully saturated there would be no further rate increases with increasing $[O_2]$ in solution. The dependence of $k^1$ on $[O_2]$ can be ascertained from the following linear relationship

$$k^1 = k [O_2]^m \tag{3.24}$$

$$\log k^1 = \log k + m\log[O_2] \tag{3.25}$$

which is plotted for the kinetic data presented in Table A.4 in Figure 3.11. From this graphical relationship it can be seen that the reaction order in $[O_2]$ is 0.8 which is fairly close to one. This suggests that at low $[O_2]$ the reaction order is one and at high concentration it should be zero. This saturation effect is seen in Figure 3.11.
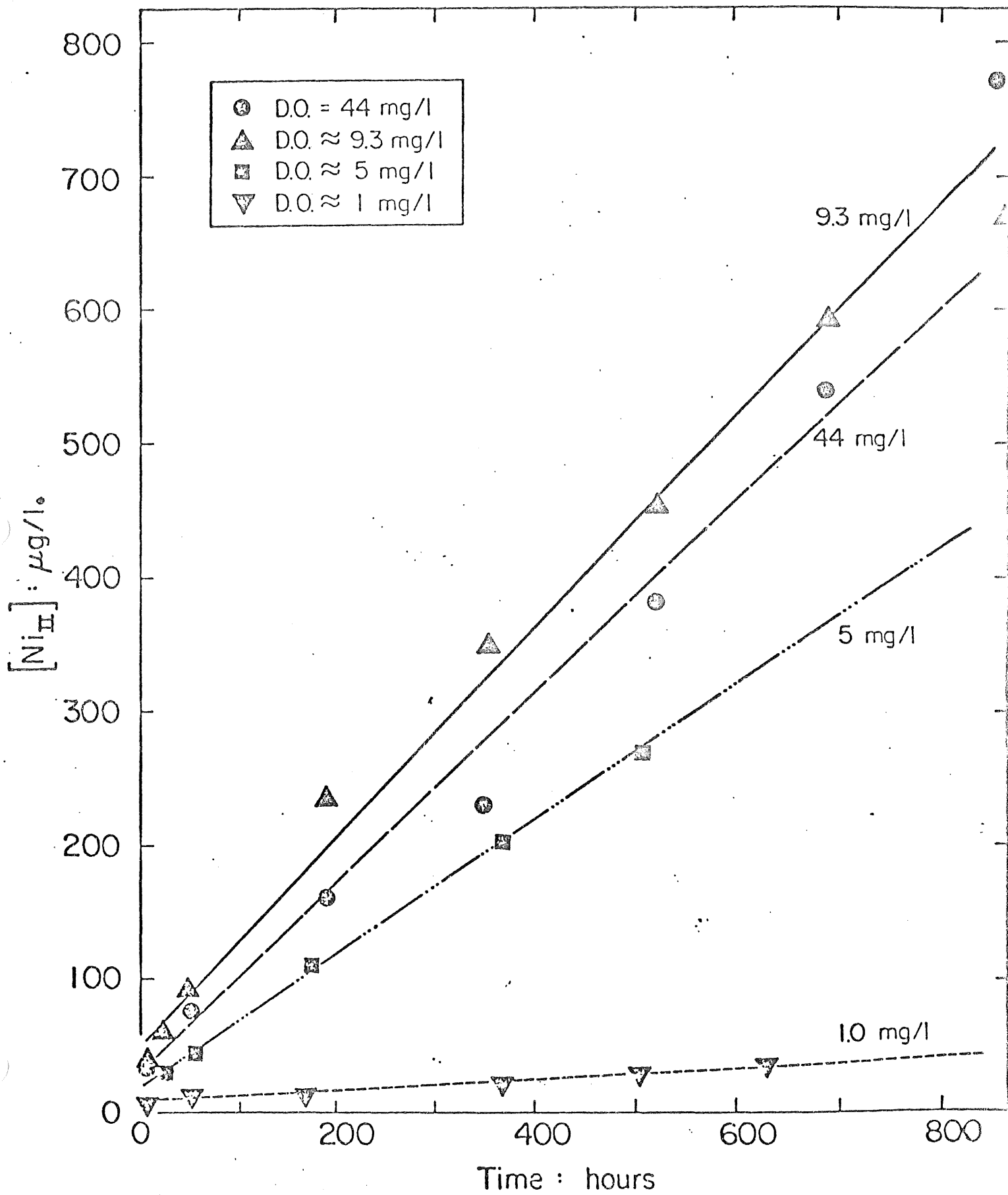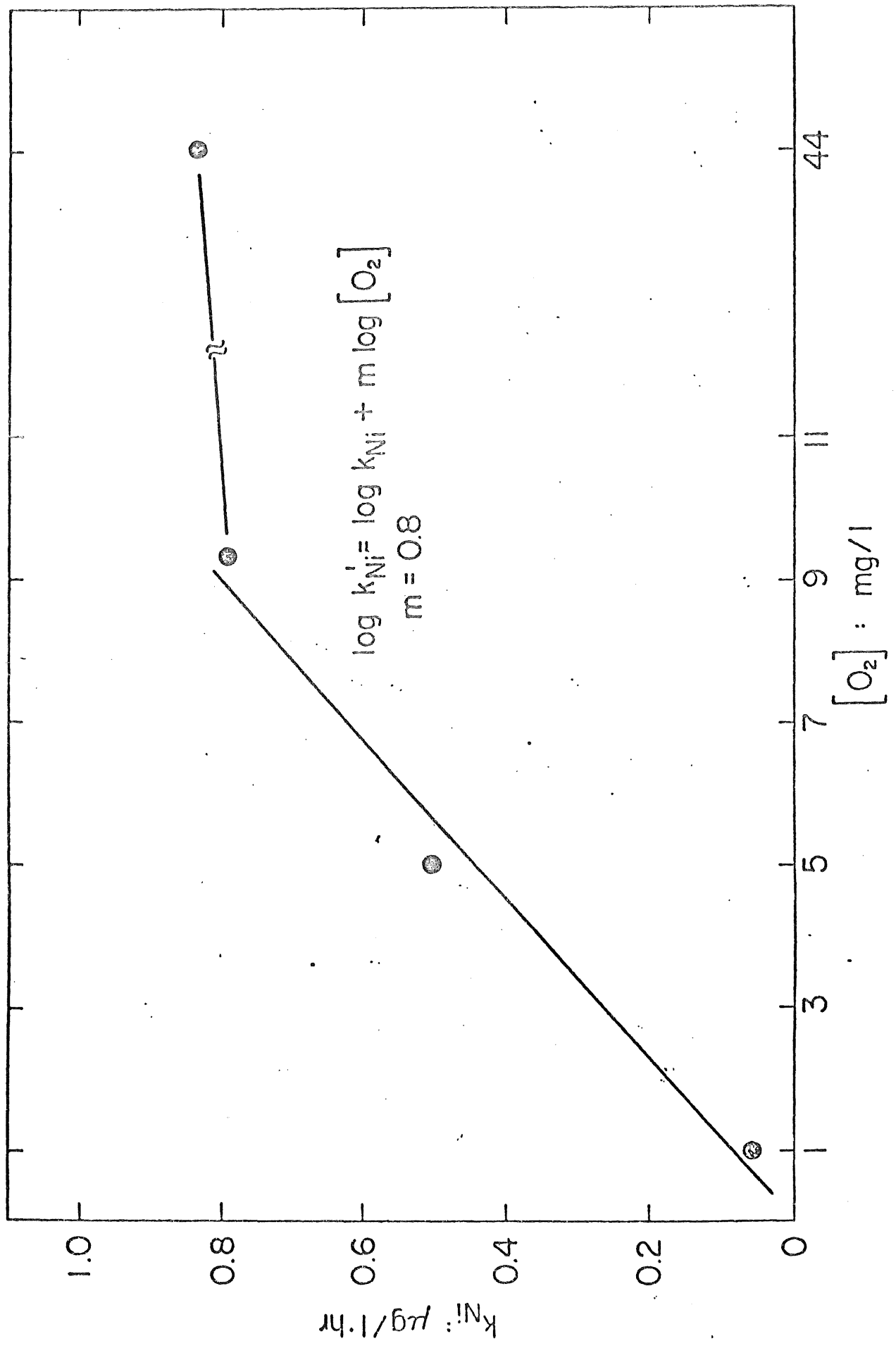
Combining this information with that contained in equation 3.21 allows the empirical rate law to be written as

$$\frac{d\,[Ni(II)]}{dt} = k^{11}As^{0.4}[O_2]^{0.8} \qquad (3.26)$$

where

$$k^{11} = 4.5k[H^+]^n \qquad (3.27)$$

Significant release of Cu with time during the $O_2$ variation experiments did not occur until the oxygen concentration exceeded 5.0 mg/l. Unfortunately during the course of these experiments the pH was not maintained absolutely constant. Initially, the pH at each $[O_2]$ was stable but as the reactions proceeded, especially when $[O_2]$ >9.0 mg/l the pH dropped as the buffering capacity of the Gabbro was exceeded. The change in pH during the later portion of each experiment may explain the Cu release rates observed in Figure 3.12. Even if oxidation proceeds at an appreciable rate, Cu oxidation products would be expected to accumulate as $Cu_2CO_3(OH)_2$ and $Cu(OH)_2$ in a reacted zone on the surface of $CuFeS_2$. When pH drops below 6, release of Cu to the aqueous solution will occur.

These interrelationships are illustrated more clearly in the data presented in Table 3.4. Nonetheless, the pronounced dependence of the dissolution rate and extent of metal release on the dissolved oxygen concentration implies that sulfide oxygen plays an important role in the leaching process. Saturation of the rate of release of Ni at higher $[O_2]$ suggests a surface controlled reaction which is limited by the number of available reaction sites.

Although the reaction rate is not significantly increased when the $[O_2]$ exceeds 10 mg/l, the extent of and rate of $SO_4^=$ formation (Figure 3.31) is increased at higher concentrations. This would be expected to occur if the initial sulfide oxidation product was a metastable intermediate such as $S^o$, $S_2O_3^=$ or $S_4O_6^=$. Given sufficient time these metastable sulfur products will be oxidized completely to sulfate.

# Table 3.4

### Total Release: Effect of pH; Mineralized Gabbro
### Ad: Adsorbed & Precipitated, Sol: In solution, Tot: Total Release
### All Values in Moles $* 10^6$ per gram gabbro

| PH | $Ni_{Ad}$ | $Ni_{Sol}$ | $Ni_{Tot}$ | $Cu_{Ad}$ | $Cu_{Sol}$ | $Cu_{Tot}$ | $Fe_{Ad}$ | $Fe_{Sol}$ | $Fe_{Tot}$ | $Ca_{Ad}$ | $Ca_{Sol}$ | $Ca_{Tot}$ | $Mg_{Ad}$ | $Mg_{Sol}$ | $Mg_{Tot}$ | $SO_{Tot}$ |
|---|---|---|---|---|---|---|---|---|---|---|---|---|---|---|---|---|
| 5.0 | 0.04 | 2.3 | 2.3 | 0.10 | 0.55 | 0.65 | 0.65 | 1.8 | 2.4 | 0.57 | 10 | 11 | 0.24 | 8.3 | 8.5 | 31 |
| 6.0 | 0.16 | 2.8 | 2.9 | 0.20 | 0.13 | 0.34 | 0.66 | 0.10 | 0.77 | 2.9 | 10 | 13 | 0.41 | 7.4 | 7.8 | 13 |
| 7.0 | 0.19 | 1.0 | 1.2 | 0.56 | 0.06 | 0.61 | 1.1 | 0.39 | 1.5 | 6.5 | 7.8 | 14 | 0.71 | 5.7 | 6.5 | 16 |
| 8.0 | 0.21 | 0.09 | 0.30 | 0.67 | 0.01 | 0.68 | 1.3 | 0.07 | 1.4 | 8.4 | 6.9 | 15 | 1.1 | 4.7 | 5.8 | 15 |

# Table 3.5

### Total Release: Effect of Dissolved Oxygen on Mineralized Gabbro
### Ad: Adsorbed & Precipitated, Sol: In solution, Tot: Total Release
### All values in moles $* 10^6$ per gram gabbro

| D.O. MG/L | PH | $Ni_{Ad}$ | $Ni_{Sol}$ | $Ni_{Tot}$ | $Cu_{Ad}$ | $Cu_{Sol}$ | $Cu_{Tot}$ | $Fe_{Ad}$ | $Fe_{Sol}$ | $Fe_{Tot}$ | $Ca_{Ad}$ | $Ca_{Sol}$ | $Ca_{Tot}$ | $Mg_{Ad}$ | $Mg_{Sol}$ | $Mg_{Tot}$ | $SO_{Tot}$ |
|---|---|---|---|---|---|---|---|---|---|---|---|---|---|---|---|---|---|
| 1 | 7.9 | 0.21 | 0.11 | 0.32 | 0.32 | <0.01 | 0.32 | 1.9 | 0.07 | 2.0 | 15 | 10 | 25 | 4.6 | 6.0 | 11 | 22 |
| 5 | 7.0 | 0.19 | 0.27 | 0.47 | 0.35 | 0.02 | 0.36 | 1.4 | 0.04 | 1.5 | 9.1 | 10 | 19 | 1.7 | 6.9 | 8.5 | 16 |
| 9.3 | 6.0 | 0.30 | 2.9 | 3.2 | 0.29 | 0.17 | 0.45 | 0.90 | 0.05 | 0.95 | 10 | 14 | 24 | 1.1 | 5.6 | 6.7 | 22 |
| 44 | 5.3 | 0.06 | 3.0 | 3.1 | 0.11 | 1.9 | 2.0 | 0.57 | 3.4 | 3.9 | 5.5 | 22 | 27 | 0.70 | 7.7 | 8.4 | 39 |
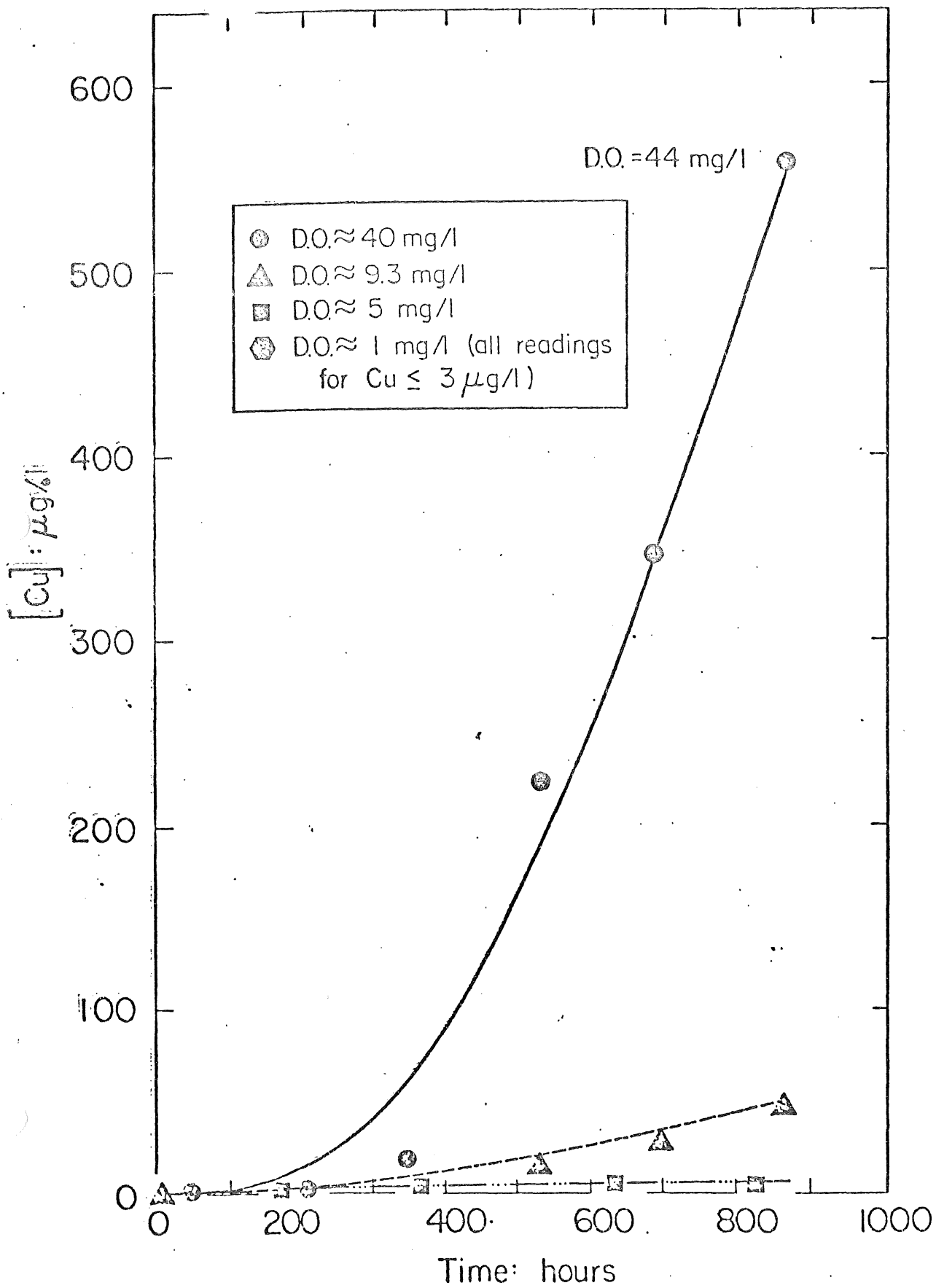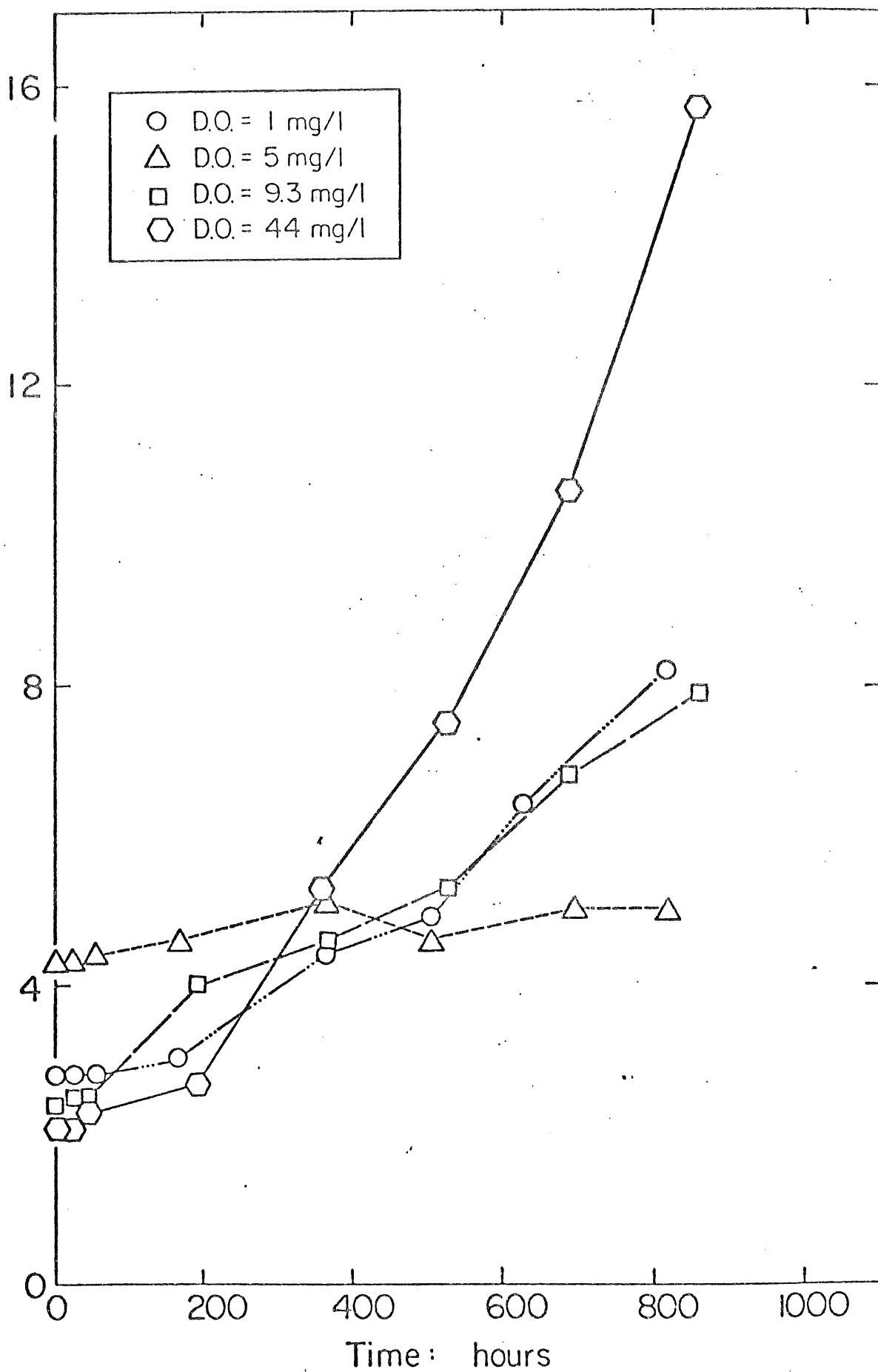
## 3.5. Effect of pH

From the results of previous studies (12, 16), on the oxidative-dissolution of metal sulfides, the role of pH is relatively unclear. At most there seems to be a reciprocal dependence of dissolution rate on the hydrogen ion concentration.

In order to determine the impact of pH on the observed rate constant for Ni release, four different reactors were run with pH maintained constant by the addition of acid or base. Mass loadings and $[O_2]$ were maintained constant in each reactor at 5.71 $gl^{-1}$ of $\leq$ 74μ mineralized Gabbro and 9.3 mg/l, respectively. Results of this controlled pH variation are presented graphically in Figure 3.14 and in tabular form in Table A.5. From the trends observed in Figure 3.14 it is apparent that the Ni release rate increases as the pH drops from 8 to 5 although the most significant change occurs between pH 8 and 6.

The observed rate constant, $k^1$, depends on the $[H^+]$ with all other variables held constant in the following way

$$k^1 = k_H [H^+]^n \tag{3.28}$$

$$\log k^1 = \log k_H + n \log[H^+] \tag{3.29}$$

where

$$k_H = k A_s^{0.4}[O_2]^{0.8} \tag{3.30}$$

The reaction order, n, was determined to be 0.2 from a least-squares fit of the linear relationship presented in equation 3.29. The pH dependency and reaction order is illustrated in Figure 3.15. A similar pH dependency on Cu release kinetics is illustrated in Figure 3.16. Copper release rates are accelerated as pH drops from 8 to 5. The net impact of pH is summarized in Table 3.5.

The increase in dissolution rate with a decrease in pH suggests that a surface controlled reaction which is dependent on protonation before the rate determining step. This could be visualized as a step involving protonation of

k: μg/l·hr

pH

pH | k
5 | 1.12
6 | 0.76
7 | 0.46
8 | 0.23

$n = 0.2$

$k' = k [H^+]^{0.2}$

$\log k' = \log k + 0.2 [H^+]$

% Total Metal vs pH

Legend: Fe △, Cu ○, Ni ⬡, Ca □, Mg ◇
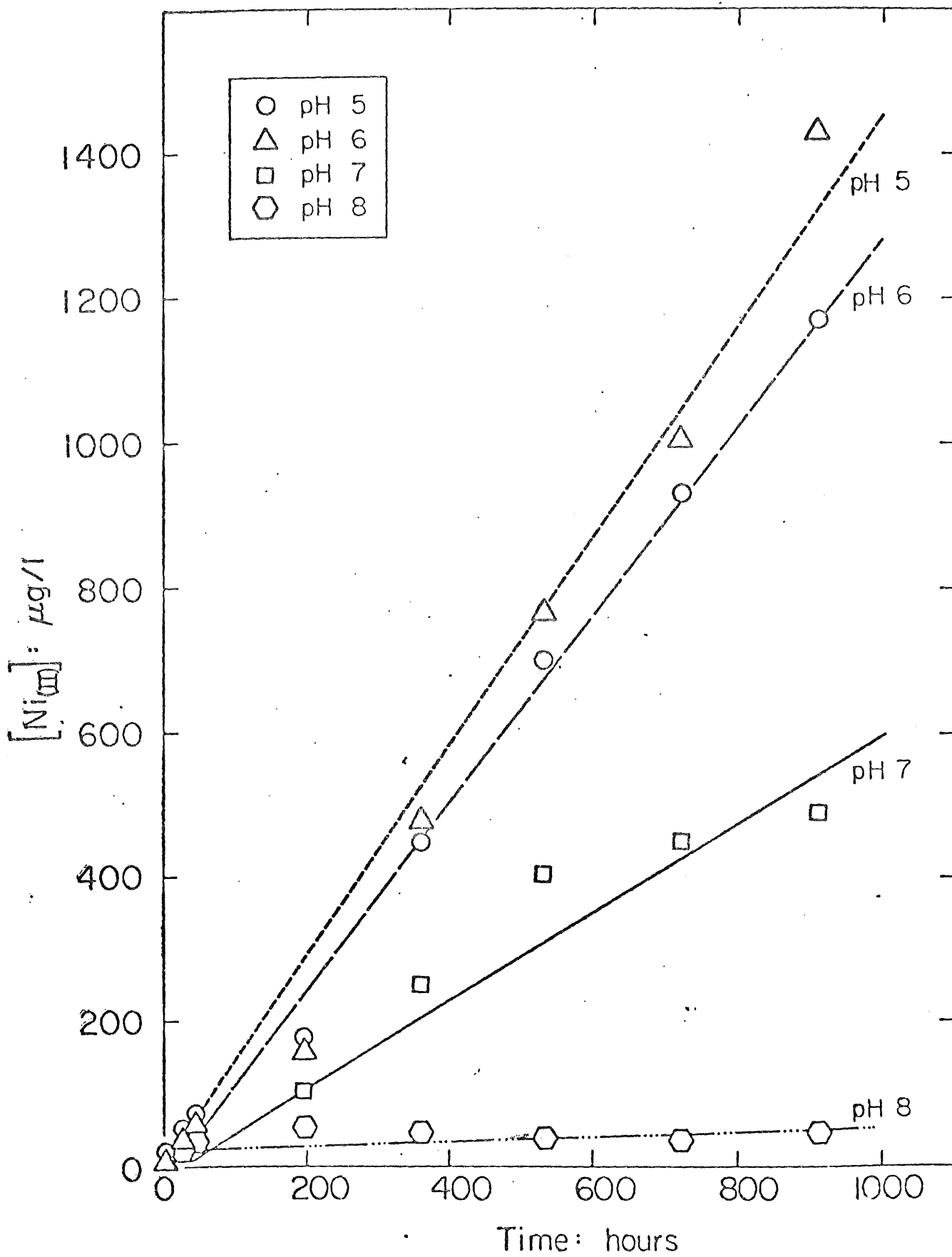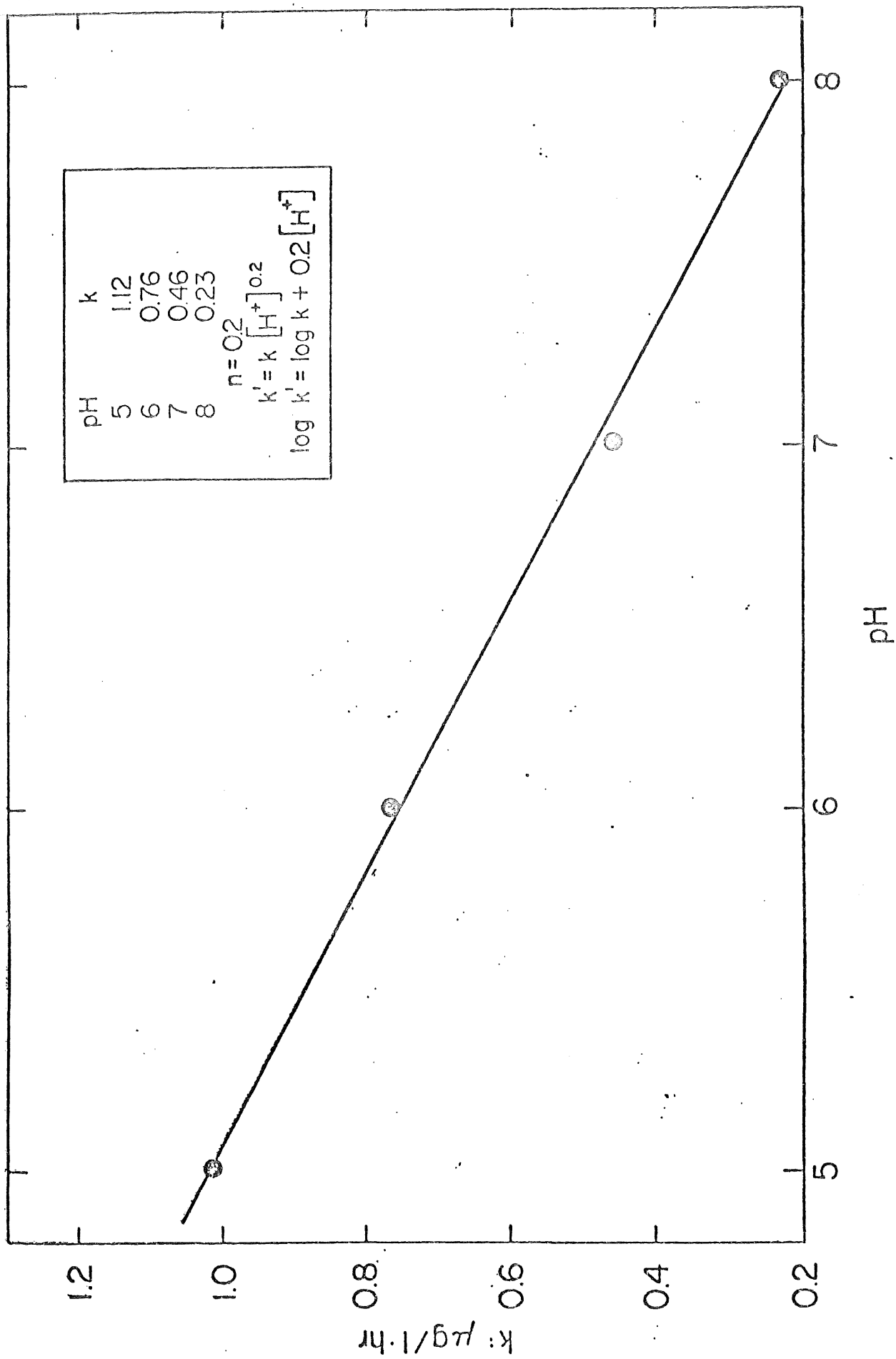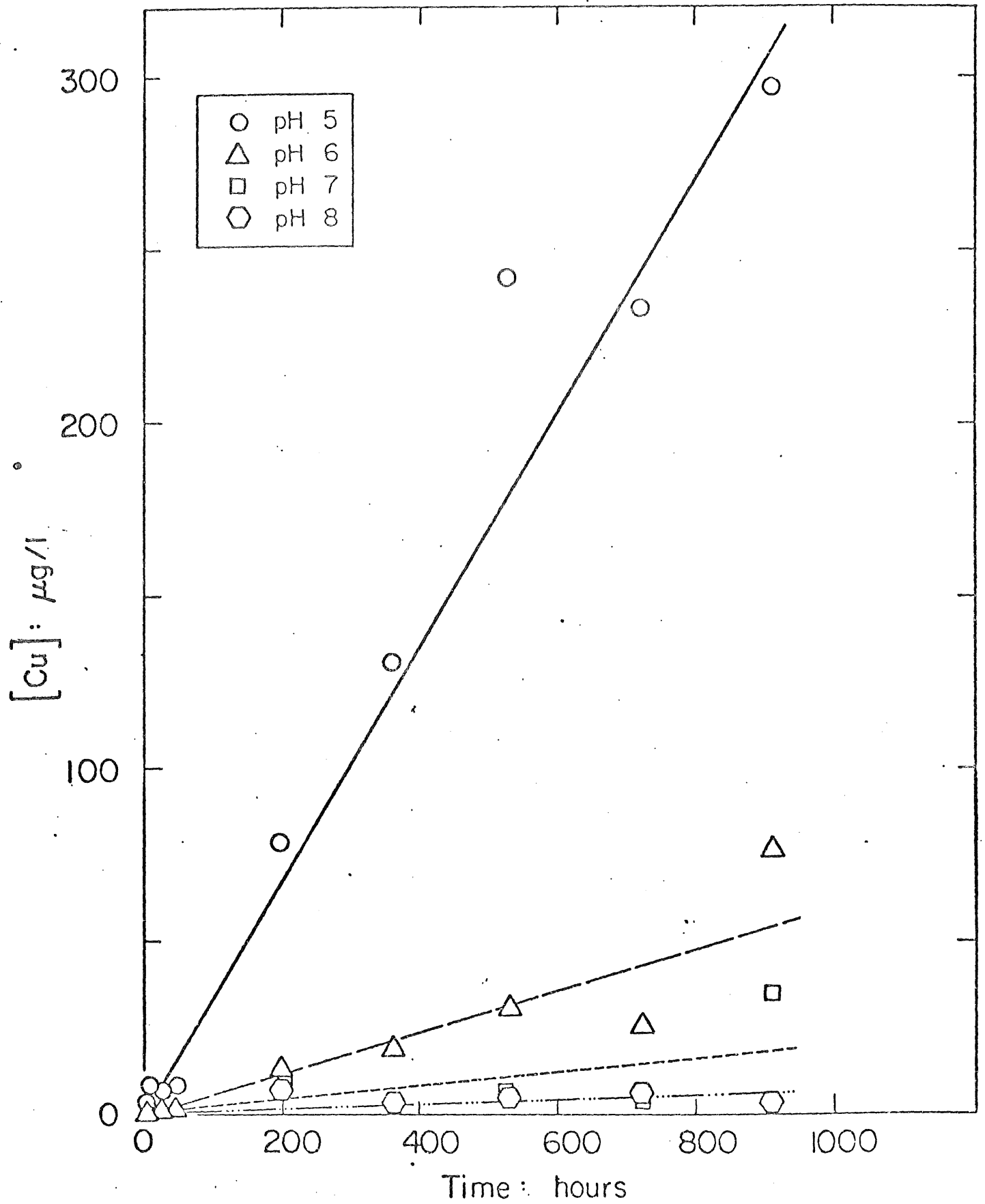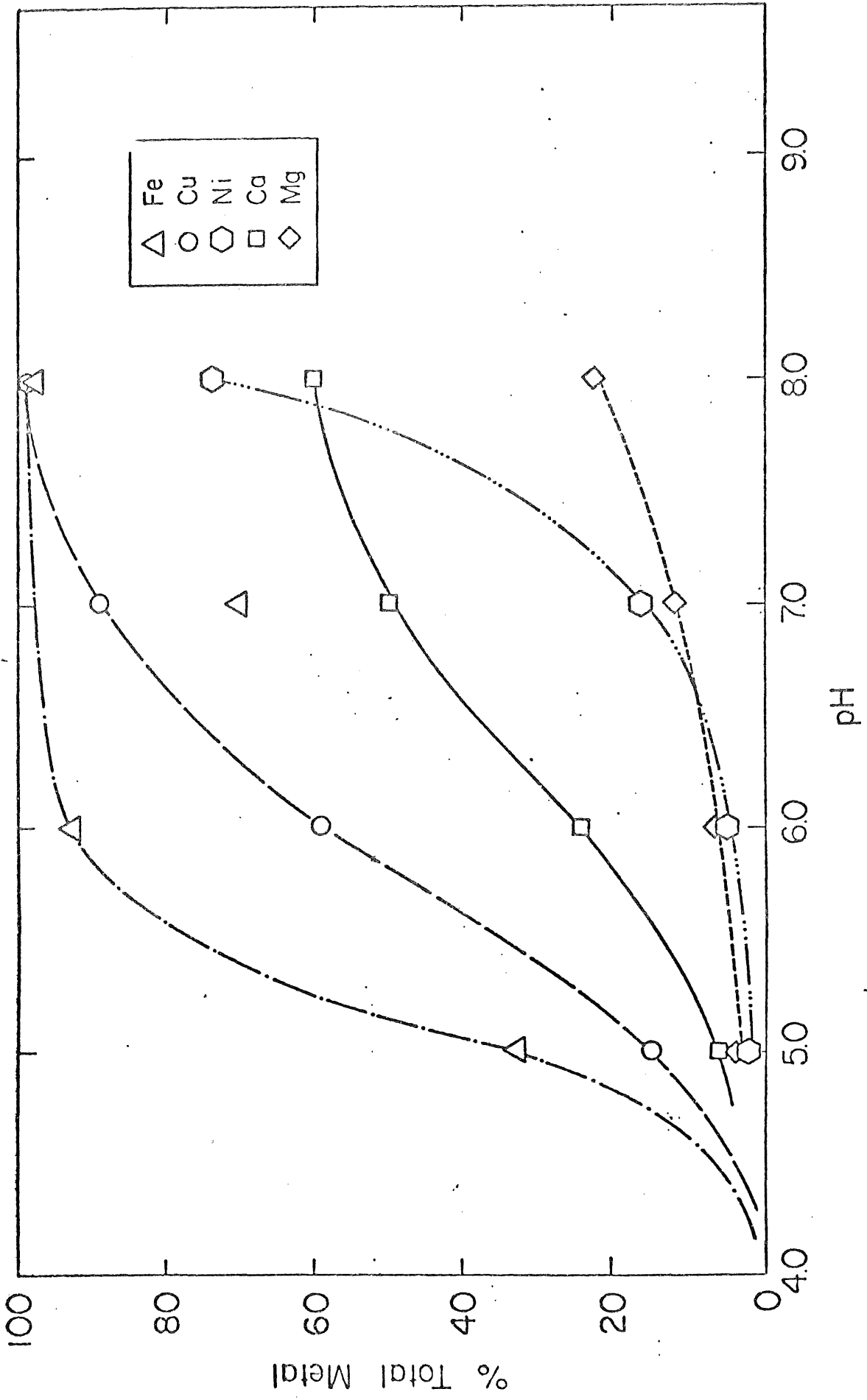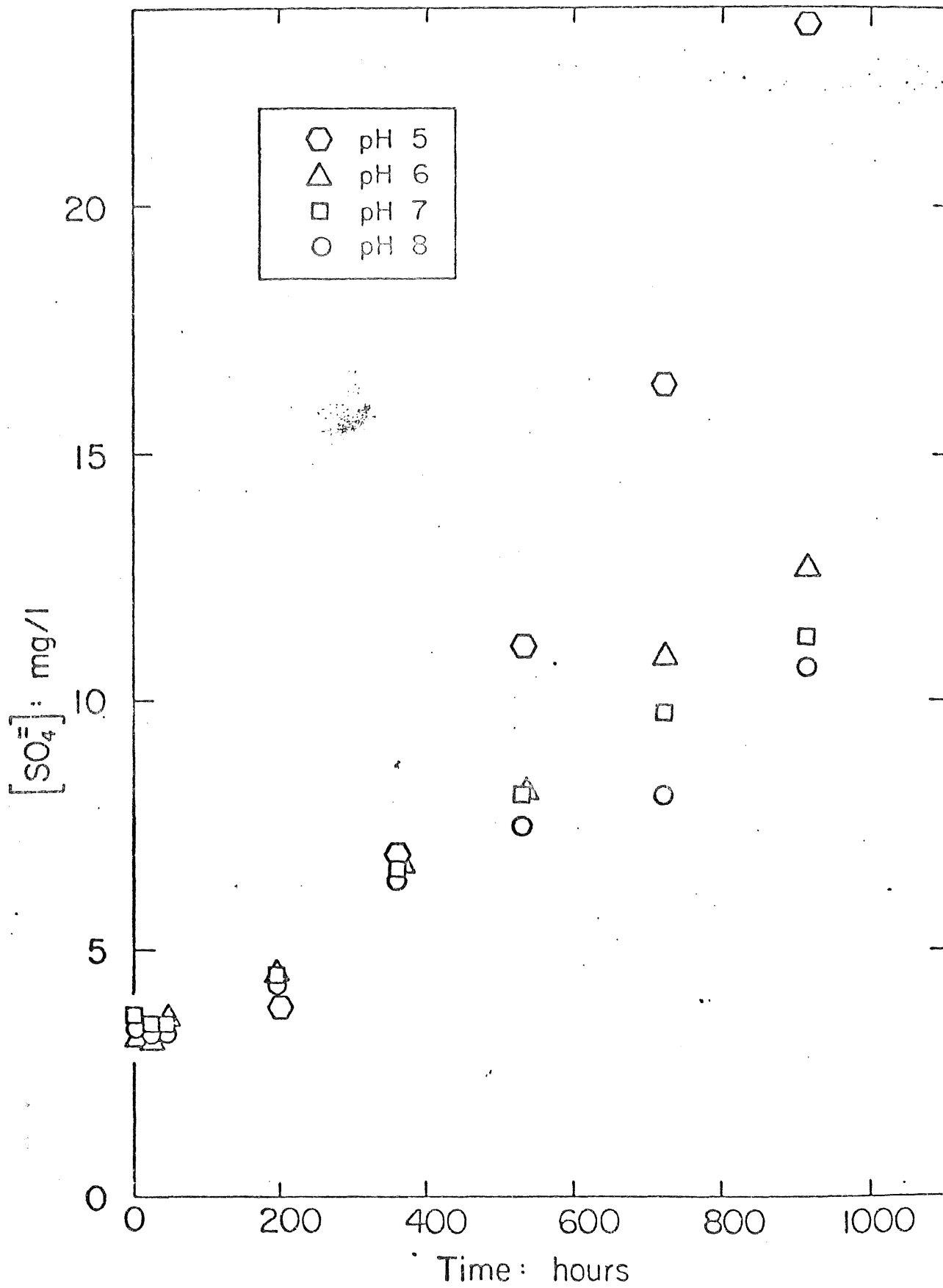
surface sulfide groups from +S to +SH or +SH$_2$. Pankow (11) has shown that the rate of anoxic dissolution of FeS depends directly on the [H$^+$] to the first-order. Without further experimental information, it would be difficult to conclude that reaction rate is controlled exclusively by a surface reaction that involves a proton in the transition state. The observed pH dependency would also be consistent with a solution phase reaction which depends on a pre-equilibrium dissolutionof the metal sulfide. However, the rate of oxidation of HS$^-$ has been shown to decrease with a decrease in pH (14, 40).

This is also true for the oxidation rate of Fe$^{+2}$ by O$_2$ which depends on [OH$^-$]$^3$ (13). Although unlikely in this pH range, Fe$^{+3}$ could serve as the principal oxidant.

In addition to increasing the rate of oxidative dissolution with a decrease in pH, the solution phase mobility of Cu and Fe, in particular, is enhanced and to a lesser extent the mobility of Ni is also enhanced. As the pH drops from 8 to 5 the dominant solid and adsorbed phases become less important. This effect can be seen in Figure 3.17 which was calculated with the aid of REDEQL2 (41) using the maximum observed concentrations at the lowest pH. This effect is also illustrated by the data in Table 3.5.

Additional evidence for increased surface reactivity with an increase in [H$^+$] is given in Figure 3.18 which shows that the sulfate concentration increases more rapidly at low pH. This trend is opposite the known solution phase kinetics of sulfide oxidation (14, 40) and suggests that increased protonation of reactive surface sites accelerates electron transfer on the surface.

3.6. Effect of Ionic Strength

Changes in ionic strength are expected to affect the rate of homogeneous reactions when charged species are reacting. In heterogeneous system such as

metal sulfide $-H_2O-O_2$ system ionic strength would be expected to affect the solubility product. For example considering the dissolution of FeS

$$FeS \overset{K_{so}}{\underset{\leftarrow}{\rightarrow}} Fe^{+2} + S^{-2} \tag{3.31}$$

the solubility product can be written as

$$K_{so} = [Fe^{+2}] [HS^-] f_{Fe} f_s \tag{3.32}$$

By using the extended Debye-Huckel law, equation 3.32 can be rewritten as

$$\log K_{so} = \log {}^c K_{so} - (Z_{Fe}^2 + Z_s^2) \left( \frac{0.5 \ I}{1 + I} \right) \tag{3.33}$$

Equation 3.33 illustrates that the solubility increases with increasing ionic strength and that the effect is especially pronounced for solids containing multivalent ions.

To experimentally determine the effect of ionic strength, three reactors loaded with 5.71 g/l of Gabbro each were run under normal conditions except that one reactor contained 0.005 $\underline{M}$ NaCl antoher reactor contained 0.05 $\underline{M}$ NaCl and the third reactor was used as a control. The pH in each reactor was maintained constant at 7.0 with the controlled addition of acid or base. The effect of ionic strength on the rate of release of Ni is shown in Figure 3.19. A slight enhancement in the rate of release of Ni is observed as the ionic strenght is increased to 0.05 $\underline{M}$ NaCl. The pseudo zero-order rate constant for nickel release, $k_{Ni}$, is plotted as a function of ionic strenght, $\mu$, in Figure 3.20. As predicted by equation 3.33, the solubility of pentlandite increases with an increase in $\mu$. A summary of experimental results is presented in Table 3.6. In general total metal release for all metals is enhanced by an increase in ionic strength although the most pronounced effect was observed for the metal sulfides. Surprisingly, the sulfate concentrations remained relatively unaltered with changes in ionic strenth.

Legend inside plot:

⊛ No NaCl: K = $5.8 \times 10^{-13}$ M/sec (g gabbro)

△ $5 \times 10^{-3}$ M NaCl: K = $11 \times 10^{-13}$ M/sec (g gabbro)

▣ $5 \times 10^{-3}$ M NaCl: K = $12 \times 10^{-13}$ M/sec (g gabbro)

Y-axis: $[Ni] : \mu g/l$

X-axis: Time: hours

Table 3.6.

Total Release:  Effect of Ionic Strength
Ad:  Adsorbed & Precipitated, Sol:  In Solution, Tot:  Total Release
All Values in Moles $* 10^6$ per gram gabbro

| M | PH | $Ni_{Ad}$ | $Ni_{Sol}$ | $Ni_{Tot}$ | $Cu_{Ad}$ | $Cu_{Sol}$ | $Cu_{Tot}$ | $Fe_{Ad}$ | $Fe_{Sol}$ | $Fe_{Tot}$ | $Ca_{Ad}$ | $Ca_{Sol}$ | $Ca_{Tot}$ | $Mg_{Ad}$ | $Mg_{Sol}$ | $Mg_{Tot}$ | $SO_{Tot}$ |
|---|---|---|---|---|---|---|---|---|---|---|---|---|---|---|---|---|---|
| 0[a] | 7.0 | 0.19 | 1.0 | 1.2 | 0.56 | 0.06 | 0.61 | 1.1 | 0.39 | 1.5 | 6.5 | 7.8 | 14 | 0.71 | 5.7 | 6.5 | 16 |
| 0.005[b] | 7.0 | 0.67 | 1.4 | 2.1 | 0.50 | 0.01 | 0.51 | 2.7 | 0.04 | 2.7 | 9.8 | 9.0 | 19 | 1.2 | 7.0 | 8.2 | 19 |
| 0.05[b] | 7.0 | 0.42 | 2.6 | 3.0 | 0.94 | 0.01 | 0.95 | 4.1 | 0.05 | 4.2 | 6.7 | 11 | 18 | 0.97 | 7.0 | 8.0 | 21 |

a:t = 910 hrs.
b:t = 1030 hrs.

Table 3.7

Total Release:  Effect of Citrate on Unmineralized Gabbro
Ad:  Adsorbed & Precipitated, Sol:  In Solution, Tot:  Total Release
All Values in Moles $* 10^6$ per gram gabbro

| [CIT]:M | PH | $Ni_{Ad}$ | $Ni_{Sol}$ | $Ni_{Tot}$ | $Cu_{Ad}$ | $Cu_{Sol}$ | $Cu_{Tot}$ | $Fe_{Ad}$ | $Fe_{Sol}$ | $Fe_{Tot}$ | $Ca_{Ad}$ | $Ca_{Sol}$ | $Ca_{Tot}$ | $Mg_{Ad}$ | $Mg_{Sol}$ | $Mg_{Tot}$ | $SO_{Tot}$ |
|---|---|---|---|---|---|---|---|---|---|---|---|---|---|---|---|---|---|
| 1.3E-4 | 7.0 | 0.64 | 1.6 | 2.2 | 0.28 | 0.20 | 0.48 | 2.1 | 3.5 | 5.6 | 15 | 20 | 35 | 1.9 | 11 | 13 | 14 |
| 1.3E-3 | 7.0 | 0.09 | 5.3 | 5.4 | 0.16 | 0.95 | 1.1 | 4.8 | 130 | 140 | 18 | 19 | 37 | 5.4 | 38 | 44 | 43 |
| 1.3E-4 | 7.5 | 0.50 | 0.55 | 1.1 | 0.23 | 0.03 | 0.26 | 2.3 | 1.9 | 4.1 | 13 | 33 | 46 | 0.66 | 8.4 | 9.1 | 13 |
| 1.3E-3 | 8.2 | 0.28 | 4.8 | 5.1 | 0.12 | 0.86 | 0.98 | 4.4 | 23.0 | 39.0 | 13 | 29 | 41 | 1.9 | 12 | 14 | 11 |
| 1.3E-4 | 7.7 | 0.18 | 0.33 | 0.52 | 0.22 | 0.03 | 0.25 | 0.12 | 2.2 | 2.3 | 4.7 | 7.1 | 12 | 0.47 | 8.0 | 8.5 | 15 |
| 1.3E-3 | 8.3 | 0.22 | 0.02 | 0.24 | 0.36 | 0.12 | 0.47 | 2.5 | 9.0 | 12 | 6.5 | 6.9 | 13 | 1.9 | 9.9 | 12 | 11 |
| 0 | 6.9 | 0.33 | 2.6 | 3.1 | 0.17 | 0.02 | 0.19 | 1.9 | 0.03 | 1.9 | 10 | 18 | 29 | 0.88 | 8.6 | 9.5 | 14 |
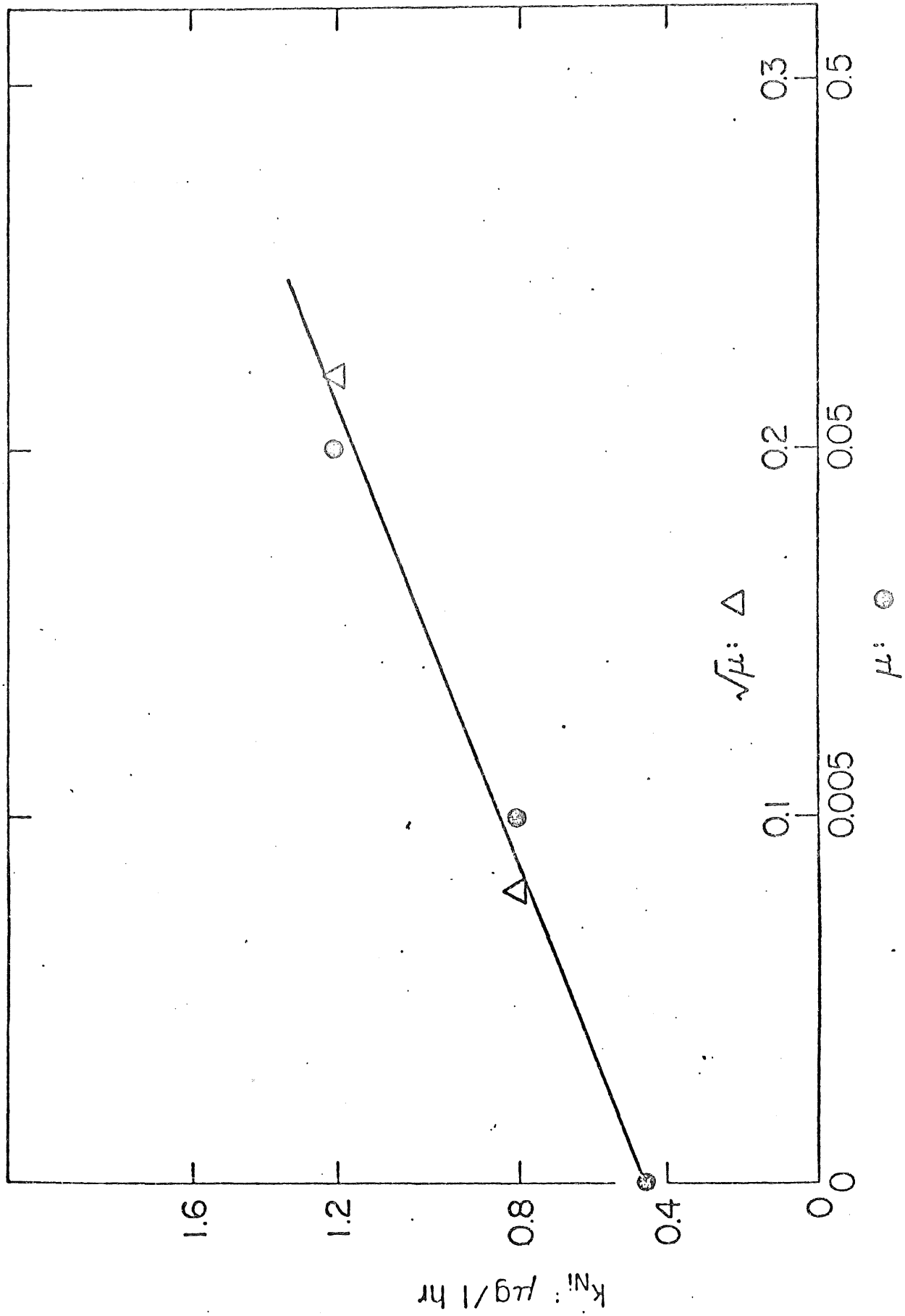
## 3.7.  Effect or Organic Ligands and Natural Waters

High concentrations of dissolved organic carbon have been observed in the natural waters surrounding the Erie Mining Company's Dunka Pit (1).  Complexation capacity measurements show that a strong affinity exists between the dissolved components in the natural waters and added metals such as Cu, Pb, Cd and Zn. Most likely, organometallic complexes (2) are formed between the naturally-occurring organic material and the trace transition metals in the aqueous phase.  Complexation should enhance the solubility and transport of metals such as Cu, Ni and Fe. Concentrations of these metals are normally controlled by their sulfide, hydroxide and carbonate solids.

The effect of synthetic and natural organic ligands on the weathering of silicate and sulfide minerals is well-documented (21-24).  In general, the rate and extent of metal dissolution is enhanced in the presence of moderately strong chelating agents.  This rate enhancement may arise from either a shifting of the equilibrium dissolution or from a surface catalytic influence.  For example, if the rate of dissolution is limited by diffusion through a layer of reaction products on the surface of the sulfide mineral, chelation of a particular metal may accelerate the normally slow diffusion through the reacted zone.  The other possibility is that an organometallic complex acts as a catalyst for the activation of molecular oxygen to a more reactive state and as a consequence accelerate the surface oxidation (40).

If the rate of dissolution is controlled by a solution phase oxidation of either $Fe^{+2}$ or $HS^-$ then shifting of the pre-equilibrium dissolution step will increase the apparent rate of oxidation.  Using FeS as an example the following sequence of reactions can be hypothesized.

$$H^+ + FeS \xrightleftharpoons{K_{so}} Fe^{+2} + HS^- \tag{3.32}$$

$$Fe^{+2} + Y^{-2} \xrightleftharpoons{B} FeY \tag{3.33}$$

$$HS^- + O_2 \xrightarrow{k \text{ (slow)}} HSO_2^- \tag{3.34}$$

$$HSO_2^- + O_2 \xrightarrow{fast} HSO_4^- \tag{3.35}$$

Since equation 3.34 represents the slow rate determining step in the reaction sequence, the rate of oxidative dissolution can be written as

$$\frac{-d\,[FeS]}{dt} = k\,[HS^-][O_2] \tag{3.36}$$

From the equilibrium expressions written in equations 3.32 and 3.33

$$[HS^-] = [H^+]\,K_{so}/[Fe^{+2}] \tag{3.37}$$

$$[Fe^{+2}] = [FeY]/B[Y^{-2}] \tag{3.38}$$

Substitution of these expressions into equation 3.34 yeilds

$$\frac{-d[FeS]}{dt} = \frac{kK_{so}B[Y^{-2}][O_2][H^+]}{[FeY]} \tag{3.39}$$

Equation 3.37 predicts that the rate of oxidative dissolution will be directly proportional to the ligand concentration, $[Y^{-2}]$. A similar rate expression should result if the complex FeY were an active catalyst for the surface oxidation of FeS.

To experimentally determine the impact of organic ligands on the rates of oxidative dissolution, two synthetic chelates, citrate and phthalate, and natural water plus peat bog organics were used in conventional leaching experiments according to procedures previously described. Experiments with citric acid, which is a highly soluble tri-carboxylic acid $\{HO_2CCH_2C(OH)(CO_2H)CH_2CO_2H\}$ with pk's of 3.13, 4.76 and 6.40 for the successive dissociation of the carboxylate protons,

Legend:
△ No Citrate: $k = 3.8 \times 10^{-12}$ mole/sec (g gabbro)
○ $1.29 \times 10^{-4}$ $\underline{M}$ Citrate: $k = 4.3 \times 10^{-12}$ mole/sec (g gabbro)
□ $1.29 \times 10^{-3}$ $\underline{M}$ Citrate: $k = 8.3 \times 10^{-12}$ mole/sec (g gabbro)
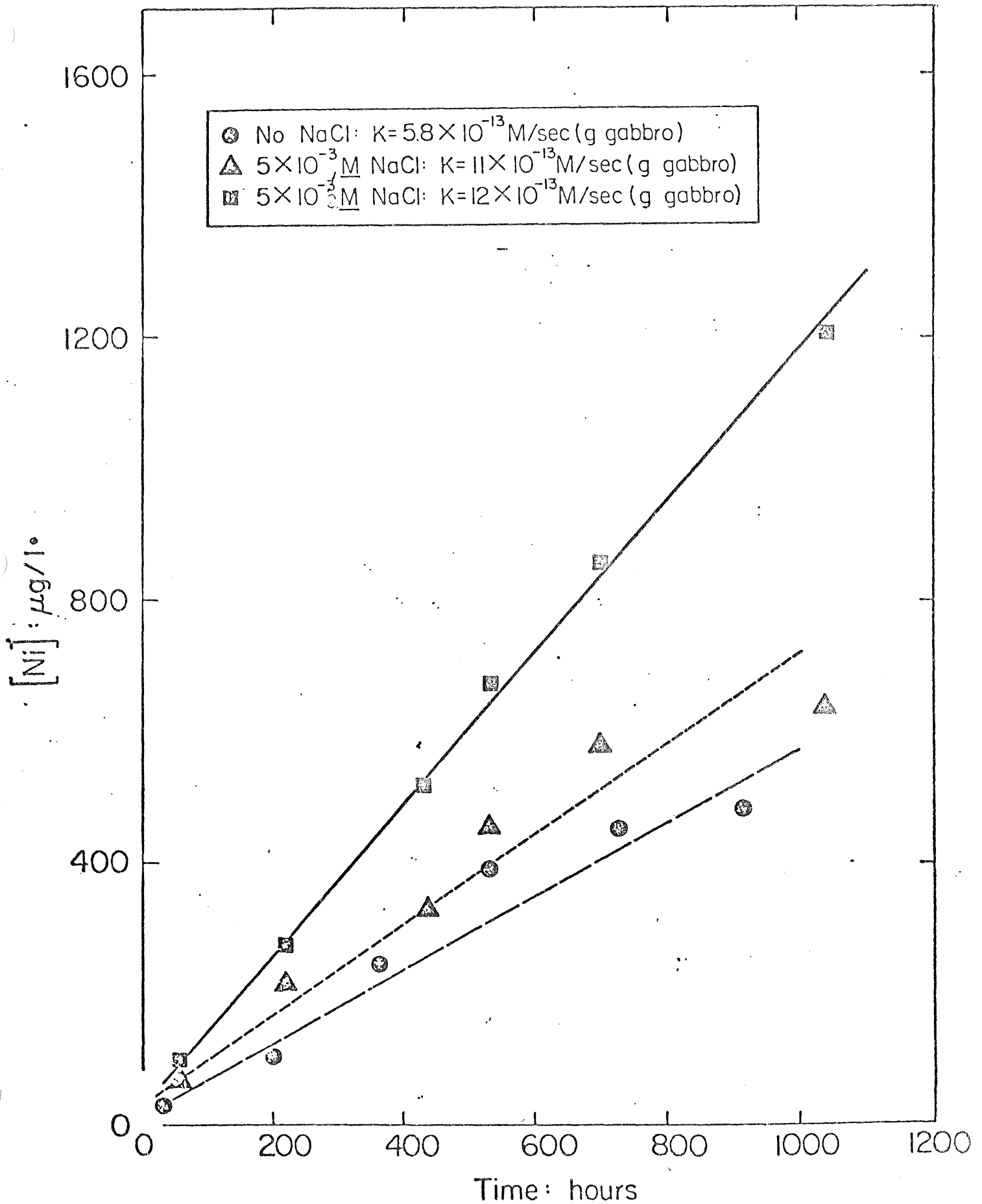
Y-axis: $[Ni]$: $\mu g/l$

X-axis: Time: hours
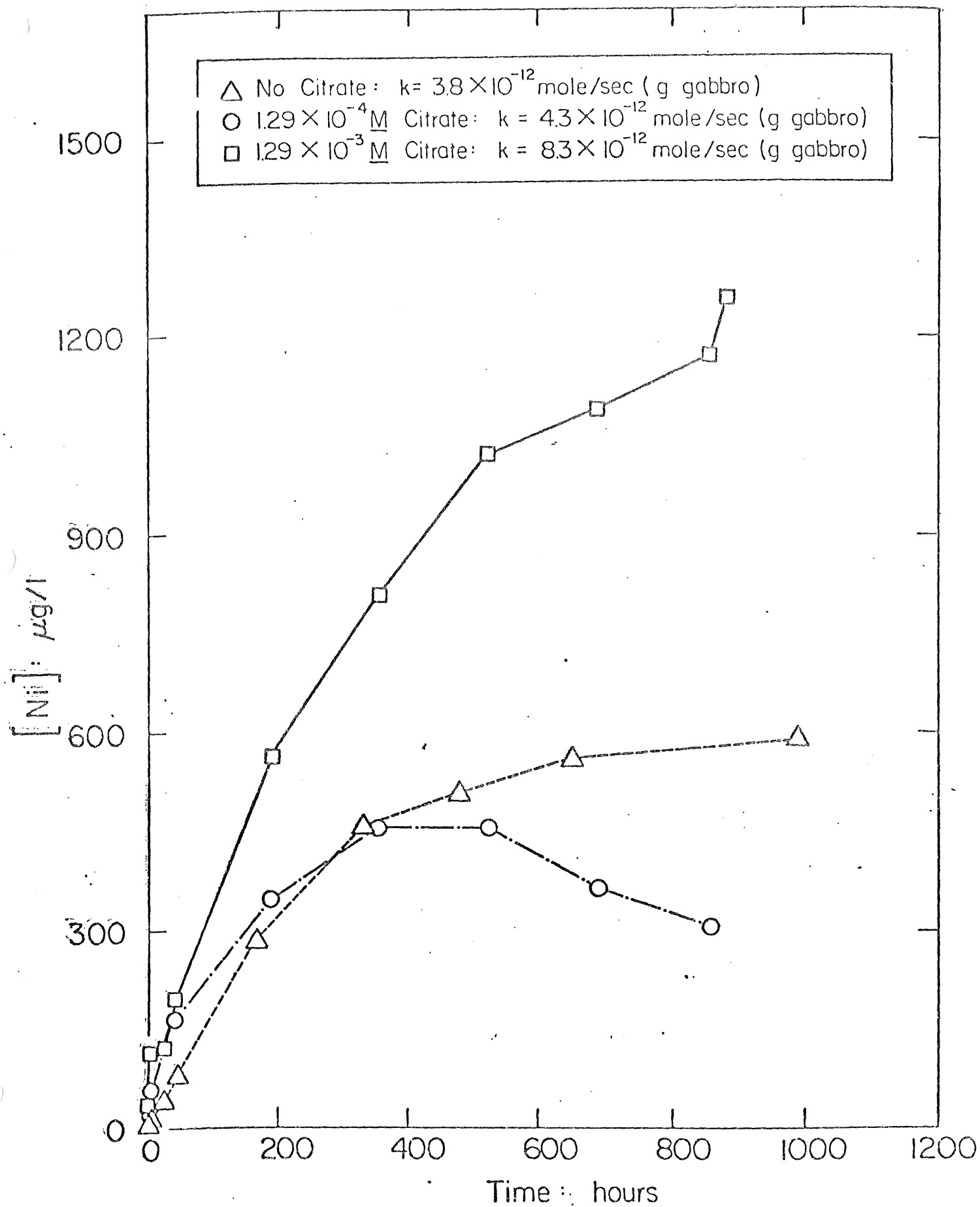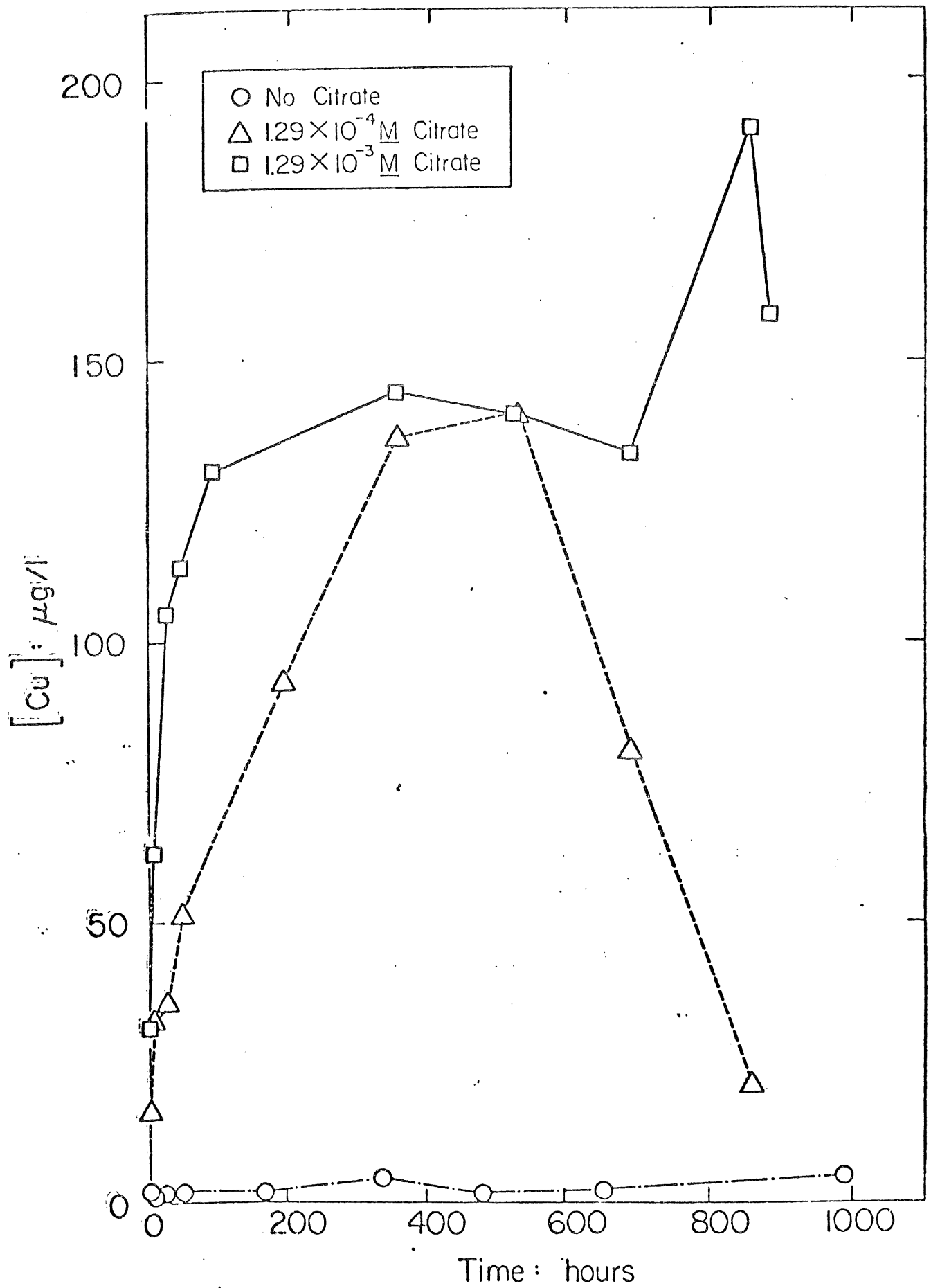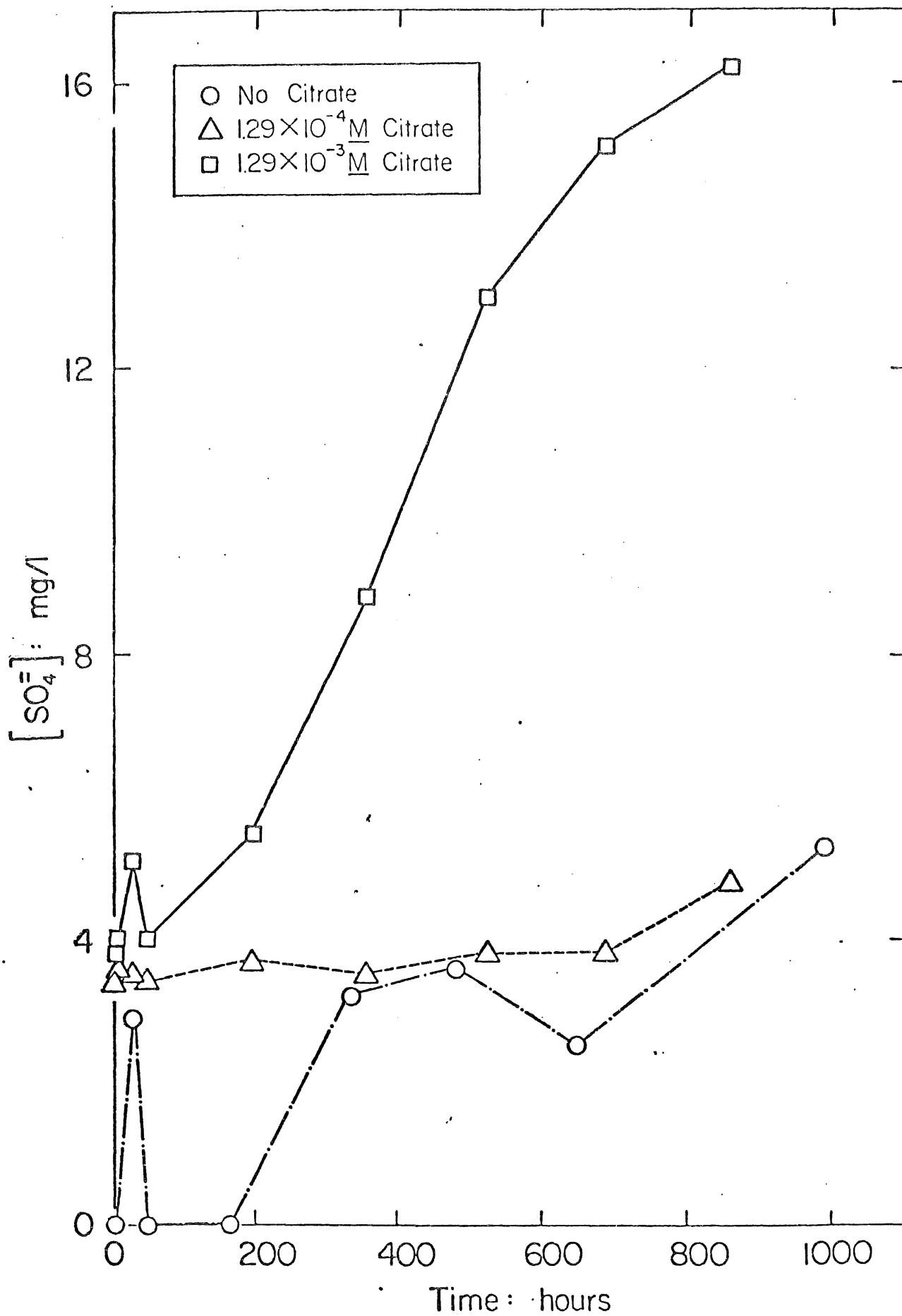
## Table 3.8

**Total Release: Effect of Phthallic Acid**
Ad: Adsorbed & Precipitated, Sol: In Solution, Tot: Total Release
All Values in Moles $* 10^6$ per gram gabbro

| thallic id | PH | $Ni_{Ad}$ | $Ni_{Sol}$ | $Ni_{Tot}$ | $Cu_{Ad}$ | $Cu_{Sol}$ | $Cu_{Tot}$ | $Fe_{Ad}$ | $Fe_{Sol}$ | $Fe_{Tot}$ | $Ca_{Ad}$ | $Ca_{Sol}$ | $Ca_{Tot}$ | $Mg_{Ad}$ | $Mg_{So}$ | $Mg_{Tot}$ | $SO_{Tot}$ |
|---|---|---|---|---|---|---|---|---|---|---|---|---|---|---|---|---|---|
| | 7.0 | 0.19 | 1.0 | 1.2 | 0.56 | 0.06 | 0.61 | 1.1 | 0.39 | 1.5 | 6.5 | 7.8 | 14 | 0.71 | 5.7 | 6.5 | 16 |
| 3E-4[b] | 7.0 | 0.36 | 0.92 | 1.3 | 0.04 | 0.01 | 0.05 | 1.4 | 0.23 | 1.6 | 7.2 | 8.5 | 16 | 0.62 | 7.0 | 7.6 | 16 |
| 3E-3[b] | 7.0 | 0.60 | 0.49 | 1.1 | 0.39 | 0.03 | 0.42 | 2.3 | 0.61 | 2.9 | 9.0 | 13.5 | 22 | 2.7 | 6.2 | 8.9 | 11 |

a. 912 hrs.
b. 1034 hrs.

## Table 3.9

**Total Release: Effect of Natural Waters**
Ad: Adsorbed & Precipitated, Sol: In Solution, Tot: Total Release
All Values in Moles $* 10^6$ per gram gabbro

| Water | PH | $Ni_{Ad}$ | $Ni_{Sol}$ | $Ni_{Tot}$ | $Cu_{Ad}$ | $Cu_{Sol}$ | $Cu_{Tot}$ | $Fe_{Ad}$ | $Fe_{Sol}$ | $Fe_{Tot}$ | $Ca_{Ad}$ | $Ca_{Sol}$ | $Ca_{Tot}$ | $Mg_{Ad}$ | $Mg_{Sol}$ | $Mg_{Tot}$ | $SO_{Tot}$ |
|---|---|---|---|---|---|---|---|---|---|---|---|---|---|---|---|---|---|
| Megapure | 8.0 | 0.21 | 0.09 | 0.30 | 0.67 | 0.01 | 0.68 | 1.3 | 0.07 | 1.4 | 8.4 | 6.9 | 15 | 1.1 | 4.7 | 5.8 | 15 |
| BOG | | 0.21 | 0.09 | 0.30 | 0.62 | 0.05 | 0.67 | 5.0 | 0.24 | 5.2 | 18 | -1.6 | 16 | 5.3 | -8.5 | -3.2 | 4.3 |
| Ground | | 0.37 | 0.07 | 0.44 | 1.3 | 0 | 1.3 | 9.9 | 0.01 | 9.9 | 34 | -10 | 24 | 8.5 | -3.5 | 5 | 6.6 |

a:t = 912 hrs.
b:t = 1034 hrs.

were run at concentrations of $1.3 \times 10^{-4}$ M and $1.3 \times 10^{-3}$ M at a mass loading of 2.86 g/l of mineralized Gabbro adjusted to pH 7. At pH 7, which was maintained constant during the course of the reaction with the addition of acid or base, the citric acid added to the system is essentially non-protonated and would be expected to behave as a moderately strong chelate. Phthalic acid, an aryldicarboxylic acid, with successive pk's of 2.95 and 5.4, is a relatively weak bidentate ligand, which is commonly thought to be representative of the functionality found in aquatic humates (32). Reactions with phthalic acid added at concentrations of $1.3 \times 10^{-4}$ M and $1.3 \times 10^{-3}$ M were run with mineralized Gabbro loadings of 5.71 g/l at pH 8. At this pH the phthalic acid will be totally deprotonated and should exhibit weak to moderate chelating ability. Natural organic material present in bog water and ground water was tested with Gabbro loadings of 5.71 g/l adjusted to pH 8. All other conditions were identical to those used in previous experiments.

Results of these experiments are summarized in Tables 3.7-3.9, A.2, A.3, A.7 and A.8 and graphically depicted in Figures 3.21-3.27. The presence of citrate had a noticeable impact on rate and extent of mineral dissolution in addition to enhancing the solution phase mobility of the metals. However during the later stages of the reactions a sudden drop in the concentration of metals in solutions occurred. This occurrence was also observed by Schalscha et. al., (22) in their studies of silicate dissolution by organic chelates. Rapid dissolution of the silicate matrix may result in the solution being supersaturated in dissolved silica as $SiO_2$ or $H_4SiO_4$. At some point the soluble silica precipitates as amorphous, opaline silica is a discontinuous fashion resulting in a sweep-floc removal of dissolved metals as coprecipitates or adsorbed species.

The effect of increasing citrate concentrations on the rate of appearance of Ni is illustrated in Figure 3.21. In these experiments linear dissolution
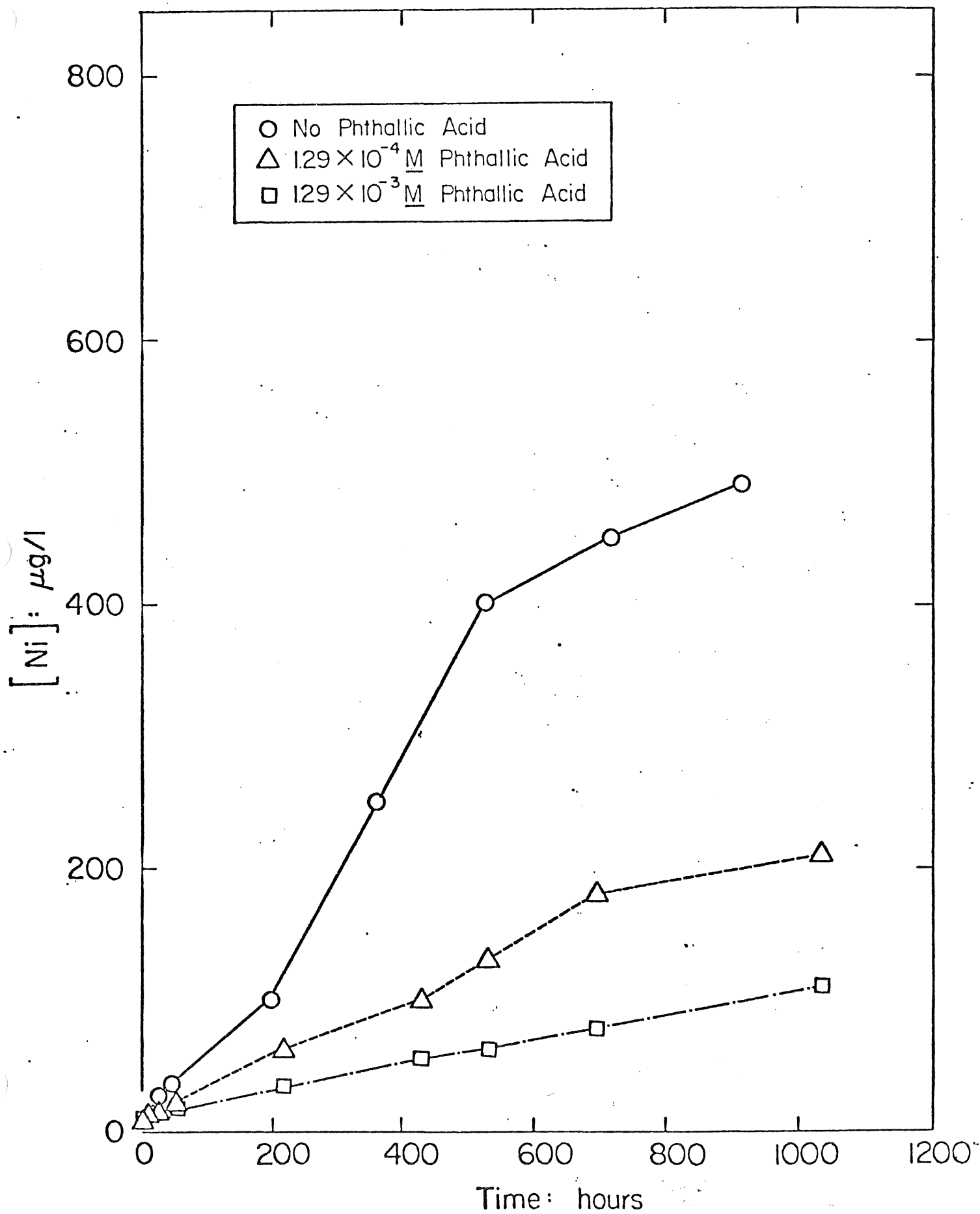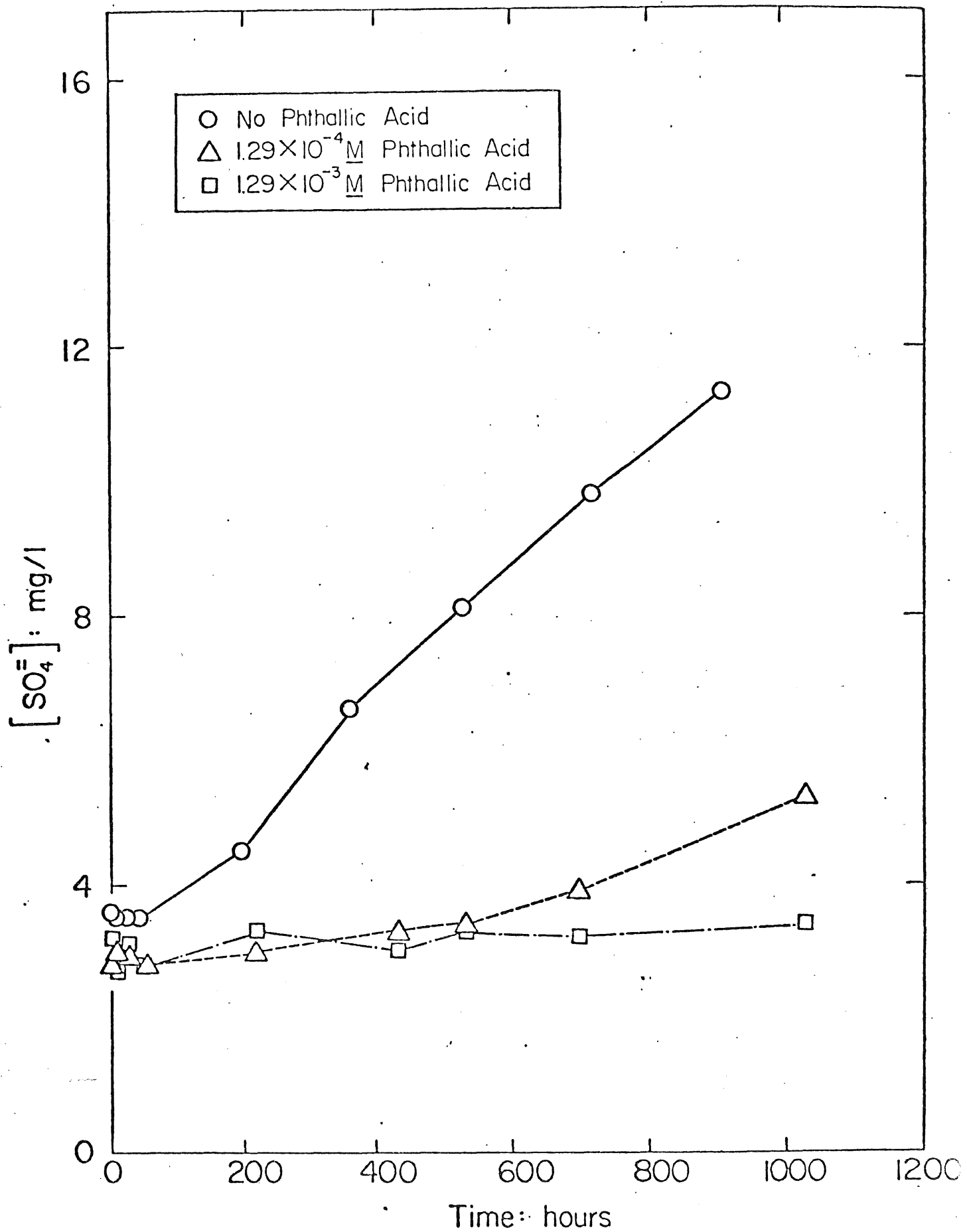
kinetics were only observed for the first 100-200 hours. During later stages release appeared to be parabolic. Comparing the linear stages of Ni release shows that as the concentration of citrate increases tenfold the pseudo zero-order rate constant, $k^1$, approximately doubles. Similar trends are observed when these experiments are run in duplicate. From these results $k^1 \sim k_0 [citrate]^{0.3}$. Similar rate enhancements are shown for Cu release in Figure 3.22, although in later stages a sudden drop in concentration occurs due to the precipitation of silica. Support for the mechanism postulated in equations 3.32 to 3.35 is obtained from the results presented in Figure 3.23 which shows a dramatic increase in the rate of appearance of $SO_4^=$ as compared to the system with no citrate. This result would be predicted if equation 3.34 were rate limiting and equation 3.37 representative of the rate of dissolution.

The effect of phthallic acid on the apparent dissolution rates was dramatically different than citrate. This effect is predicted to some extent by equation 3.37 since B (phthalate) < B (citrate) with all other factors held constant. The effect of phthalate can be seen in Figures 3.24 and 3.25. Increasing concentrations of phthalate have an inhibitory effect on the rate of release of Ni and the rate of appearance of sulfate. Chen and Morris (33) have shown that the rate of autoxidation of sulfide in aqueous solutions is inhibited by a number of organic reagents. A similar inhibition in Ni release rate is observed when bog and ground water from the Dunka Pit region is used, (see Figures 3.26 and 3.27) although bog water does enhance the rate and extent of Cu release. This suggests a specificity of the complexing agents present in bog water for Cu. Preferentially binding of Cu over Ni for the same ligand is predicted thermo-dynamically.
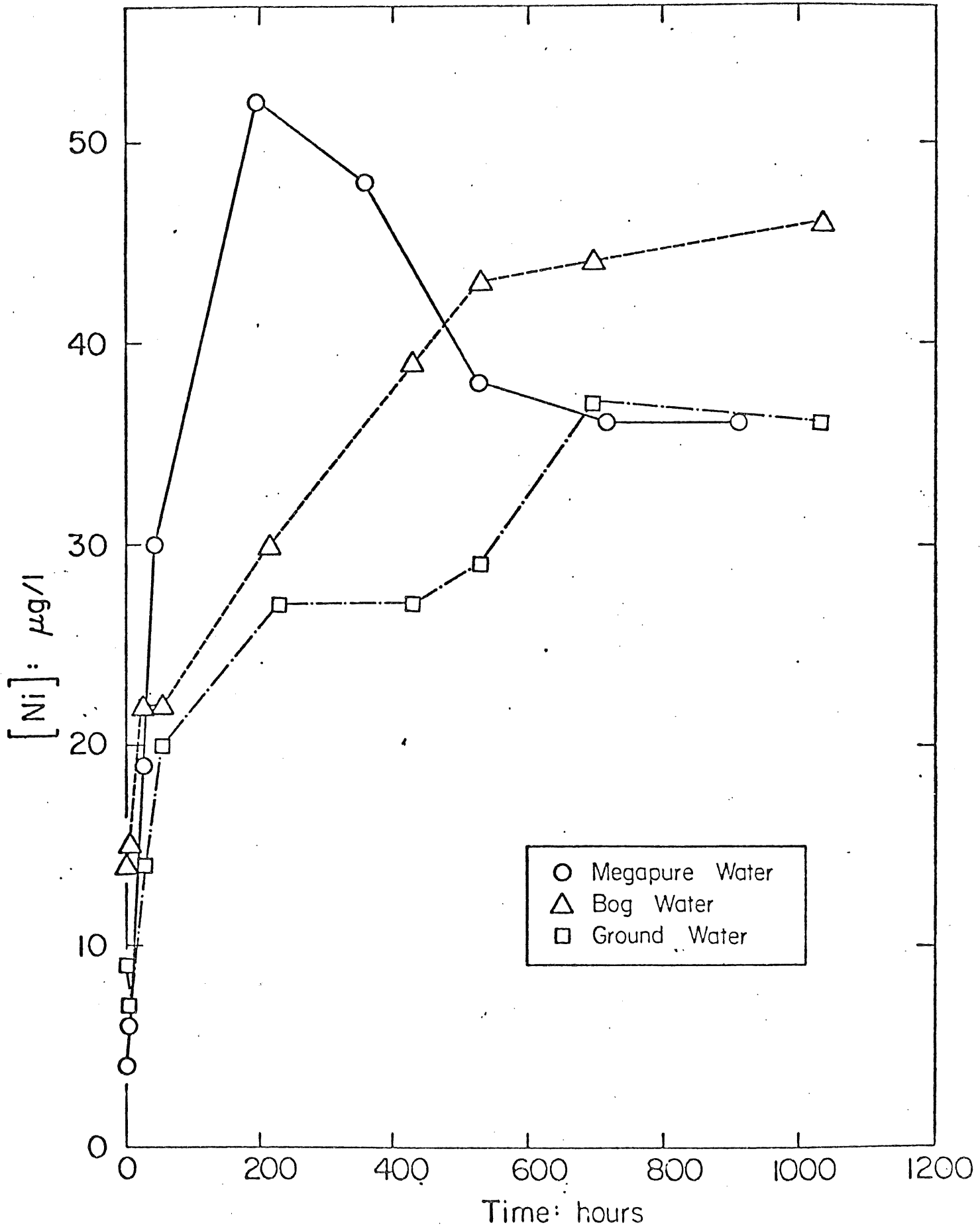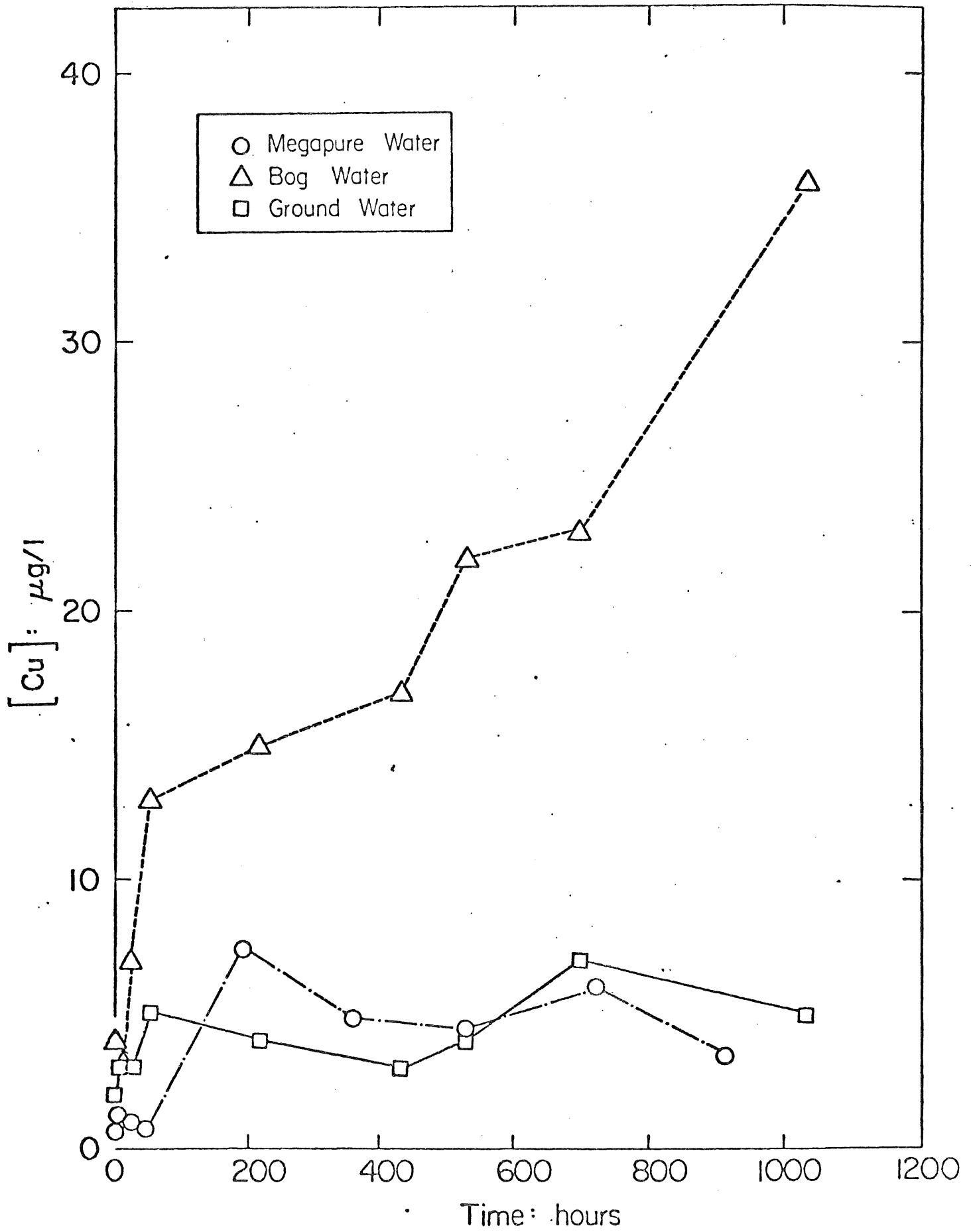
## Chapter 4

## Results:  Silicate Dissolution

4.1

The dissolution of the alumino-silicate minerals (primarily plagio-
clase) in continuous mix batch reactors was investigated as a function of
particle surface area, solution pH, dissolved oxygen concentration, organic
ligand concentration, and ionic strength.  Results are presented in terms
of a time-dependent chemical release as affected by the above dependent
variables.  Experiments were performed under natural conditions of constant
temperature (20°C) and atmospheric pressure.  Therefore, the dissolution
rates and constants may be extrapolated to environmental conditions.

4.2

### Kinetic Treatment

The incongruent dissolution of alumino-silicate minerals in aqueous
solution under natural conditions has been described by a sequential four-
stage process in which $H^+$ initially replaces surface cations followed by
stages which were represented by the expressions (Busenberg and Clemency,
1976):

$$C = k_e t^n \qquad \text{2nd stage; competing processes} \quad (4.1)$$

$$C = k_p t^{1/2} + A \qquad \text{3rd stage; parabolic kinetics} \quad (4.2)$$

$$C = k_l t + B \qquad \text{4th stage; linear kinetics} \quad (4.3)$$

The above expressions are derived from the general equation $C = kt^n$ where

$$C = \text{concentration} \qquad\qquad (4.4)$$

$$k = \text{overall rate constant}$$

$$t = \text{time}$$

$$n - \text{integer between p and 1.}$$

A single power law of the above type was used to describe the release (surface

flux) of $Ca^{+2}$ and $Mg^{+2}$ in continuous-mix batch reactors from alumino-silicates in Duluth Gabbro. The limited number of data points makes the four-stage delineation impractical. A power law equation of the type ($C = kt^n$) was used as an estimation of the release kinetics over the time span of the experiment to $\sim$ 1000 hours.

4.3

Effect of Particle Surface Area

The effect of particle surface area on $Ca^{+2}$ and $Mg^{+2}$ release with time was investigated in two separate experiments. Initially 2, 10, 50 and 100 g/l suspensions of unmineralized gabbro (-200 mesh) were subjected to the mineral batch leaching procedure for periods up to 750 hours. The observed concentrations of $Ca^{+2}$ and $Mg^{+2}$ increased with time at each mass loading, and increased in separate reactors with increased loading (Figure 4.1). The results are not unambiguous as the pH of the solution also increased with increased gabbro loading and may have resulted in changes in the dissolution mechanism.

The rates of $Ca^{+2}$ and $Mg^{+2}$ release decreased non-linearly with increased loading as shown below:

| Loading | $k_{Ca}{+2}$ | $k_{mg}{+2}$ |
|---|---|---|
| 2 g.l$^{-1}$ | 2.4 | 2.9 |
| 10 " | .51 | .009 |
| 50 " | .06 | .06 |
| 100 " | .009 | .03 |

$k_{Ca}{+2}$ (mole . sec$^{-1}$ . g$^{-1}$) x $10^5$;

$k_{Mg}{+2}$ (mole . sec$^{-1}$ . g$^{-1}$) x $10^6$

The rate of $Ca^{+2}$ release varied from (.009-2.4) x $10^{-5}$ mole . sec$^{-1}$ . g$^{-1}$ while $Mg^{+2}$ rates varied from (.009-2.9) x $10^{-6}$ moles . sec$^{-1}$ . g$^{-1}$.

Interpretation of the release behavior was complicated by the concurrent pH variations observed at increased loading.

To determine the effect of particle size on $Ca^{+2}$ and $Mg^{+2}$ release, four discrete size fractions at a fixed mass loading (2.86 g.$1^{-1}$) were leached for $\sim$ 890 hours. The four size fractions examined were $D_p \leq 74$ µm, 74 µm < $D_p \leq 420$ µm, 420 < $D_p \leq 840$ µm, and 840 µm < $D_p \leq 2380$ µm. Particle surface areas were estimated to be 1700, 190, 62 and 25 $cm^2$/g (Section 3). Elemental analyses (Table 3.2) show that Ca and Mg are enriched in the 840 µm $D_p \leq 2380$ m particle size fraction, and decrease by factors of $\sim$ 2 and 4, respectively, in the smallest size fraction.

The concentrations of $Ca^{+2}$ and $Mg^{+2}$ and the dissolution rate of the silicate matrix increase with decreasing particle size (Figure 4.2). The cation release behavior is characterized by a rapid initial release, presumably due to the replacement of surface cations by $H^+$ and a subsequent buildup of the secondary product layer. After $\sim$ 50 hours, the concentrations of $Ca^{+2}$ (Figure 4.2) and $Mg^{+2}$ tend to plateau to a constant value except for the < 74 µm particles, which continue to release $Ca^{+2}$ at a linear rate. In these experiments, final pH varied from 6.0 to 6.5, and was not a major factor in the concentrations observed.

To determine the sensititivy of $k_{As}$ to changes in the particle surface area, an equation of the following type was developed (Section 3):

$$\log k' = \log k + \ell \log A_s \tag{4.5}$$

where   k  = rate constant

A$_s$ = surface area

$\ell$ = reaction order

Equation 4.2 is a linear function, and if log k' is plotted versus log A$_s$,

the reaction order, $\ell$, can be determined for the dependence of $A_s$ on dissolution rate. The $k_{As}$ values are plotted in Figure 4.3 while equation 4.2 is plotted in Figure 4.4 with k values obtained from Table   . The reaction order, $\ell$, for the effect of particle surface area, determined as the slope of the line in Figure 4.3 was $\sim$ 2.0 for the release of $Ca^{+2}$ and 0.5 for the release of $Mg^{+2}$ for $A_s \leq 200$ $cm^2 \cdot g^{-1}$. A discontinuity in the log $k_{As}$-log $A_s$ plots was observed for both $Ca^{+2}$ and $Mg^{+2}$ for particles $<$ 740 $\mu m$ in particle size. In the case of $Ca^{+2}$, release rates became smaller than expected, while $Mg^{+2}$ release rates increased. The increase in $Mg^{+2}$ release rate may result from its enhanced concentration in the smallest size particle. The surface area loading for which particle size effects on release rates were greatest appears to be $\sim$ 200 $cm^2 \cdot g^{-1}$ gabbro. The differences in reaction rates and orders describing $Ca^{+2}$ and $Mg^{+2}$ release may be dependent on surface concentration, bulk solid concentration, diffusional transport through the secondary product layer and aqueous chemical removal processes. The data in Table 1.2 describing the mineralogical composition of the gabbro suggests that $Ca^{+2}$ is largely derived from plagioclase and clinopyroxene while $Mg^{+2}$ has olivine and clinopyroxine as its origin. The surface exchangeable $Ca^{+2}$ is likely in higher concentration than $Mg^{+2}$.

At the conclusion of the experiment, from 60-90% of the $Ca^{+2}$ released and > 90% of the $Mg^{+2}$ released appeared in solution as soluble cation (Table 3.3). However, as the $A_s$ available for dissolution decreased, the percentage of surface-associated $Ca^{+2}$ (sorbed/precipitated) increased. The discontinuities observed in the $k_{Ca^{+2}}$ and $k_{Mg^{+2}}$ may be related to the tendency for formation of secondary precipitates.

4-a

| log $A_s$ | log $k_{Ca^{+2}}$ | log $k_{Mg^{+2}}$ |
|-----------|-------------------|-------------------|
| 3.23 | −4.62 | −5.53 |
| 2.28 | −5.29 | −7.07 |
| 1.8 | −6.24 | −7.21 |
| 1.4 | −7.02 | −7.51 |

log k: moles/sec g

$Ca^{+2}$

I = 2.0

$Mg^{+2}$

I = 0.5

−5

−6

−7

1.0   2.0   3.0

log $A_s \times 10^{-2}$: $cm^2/g$
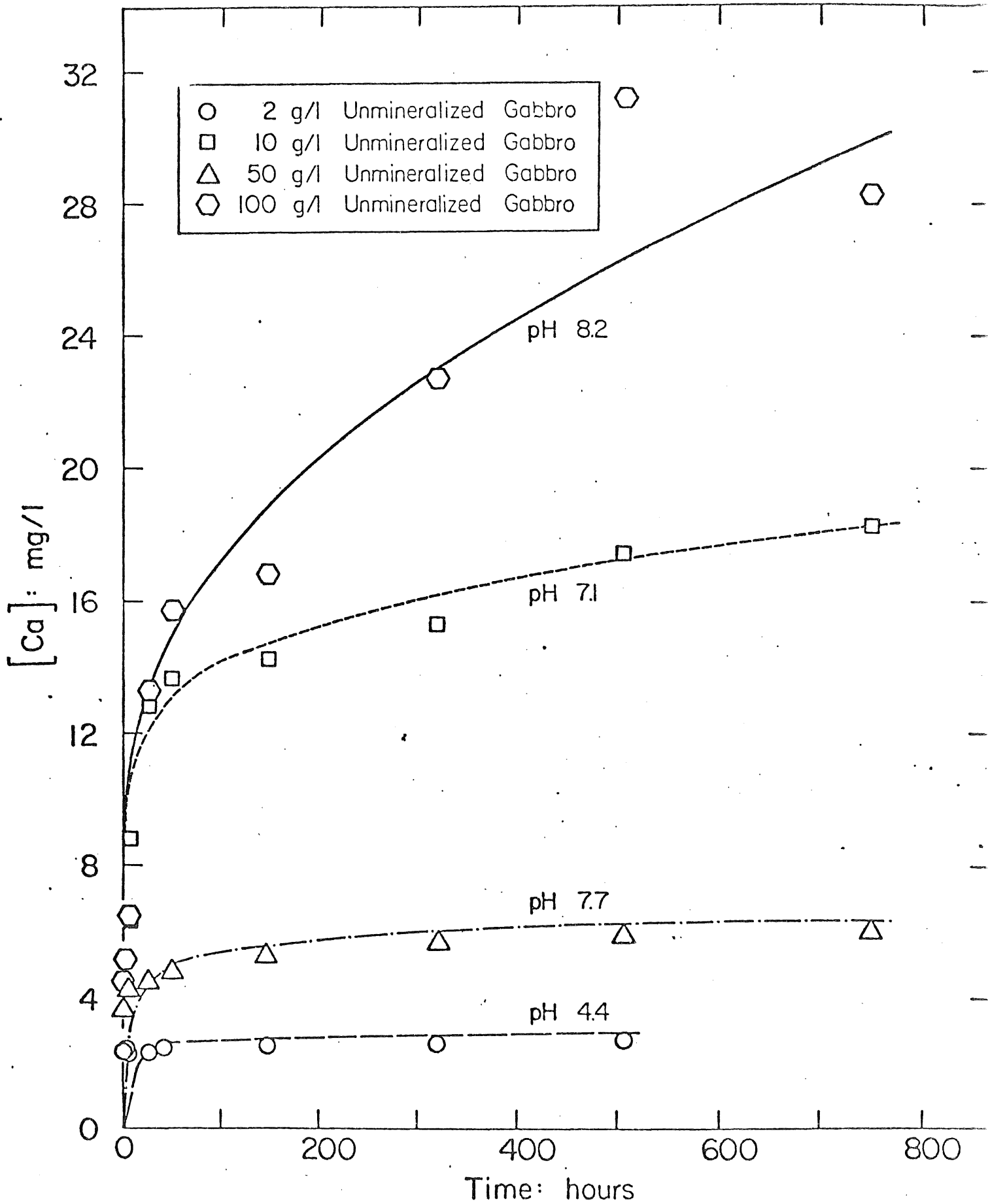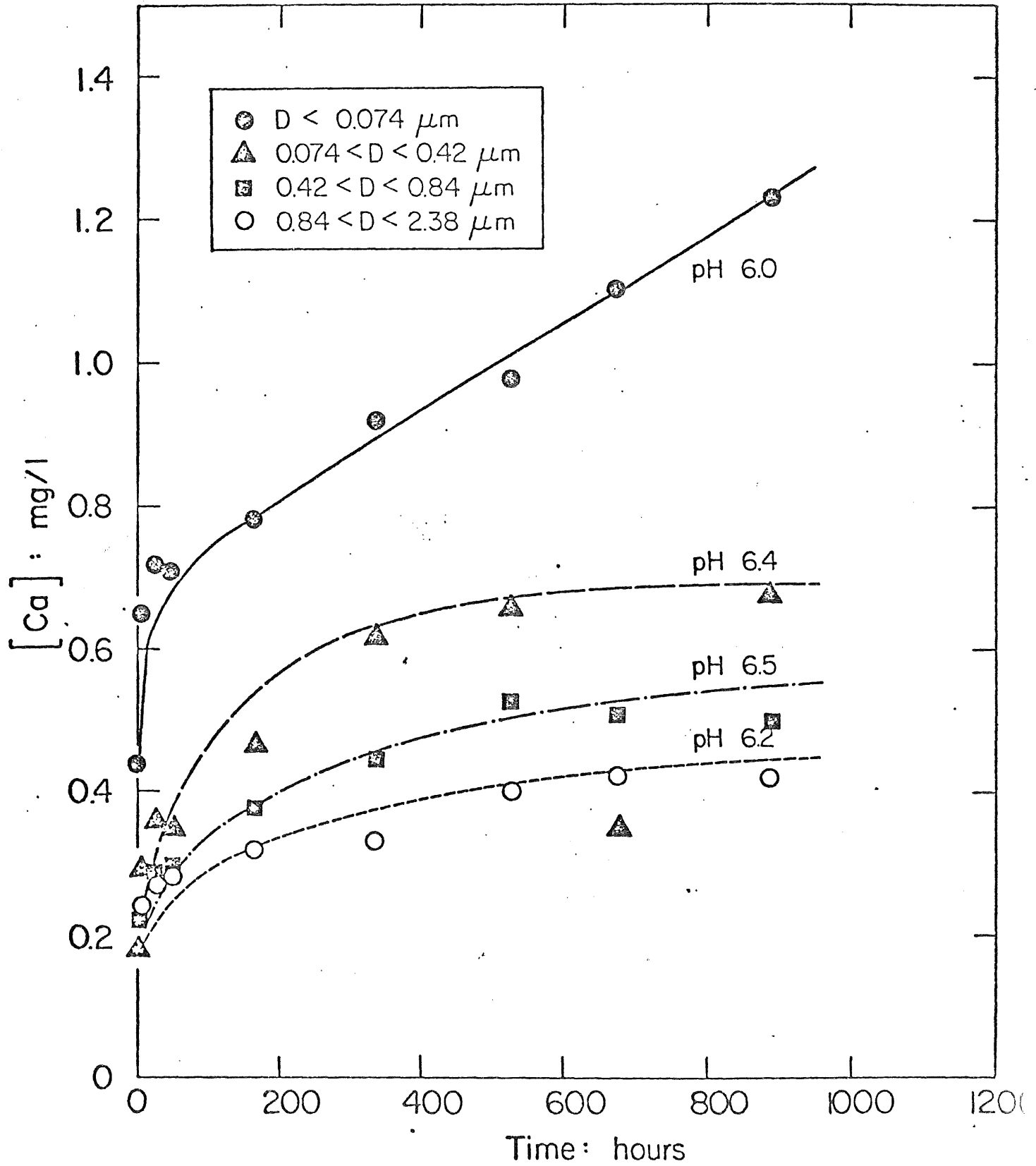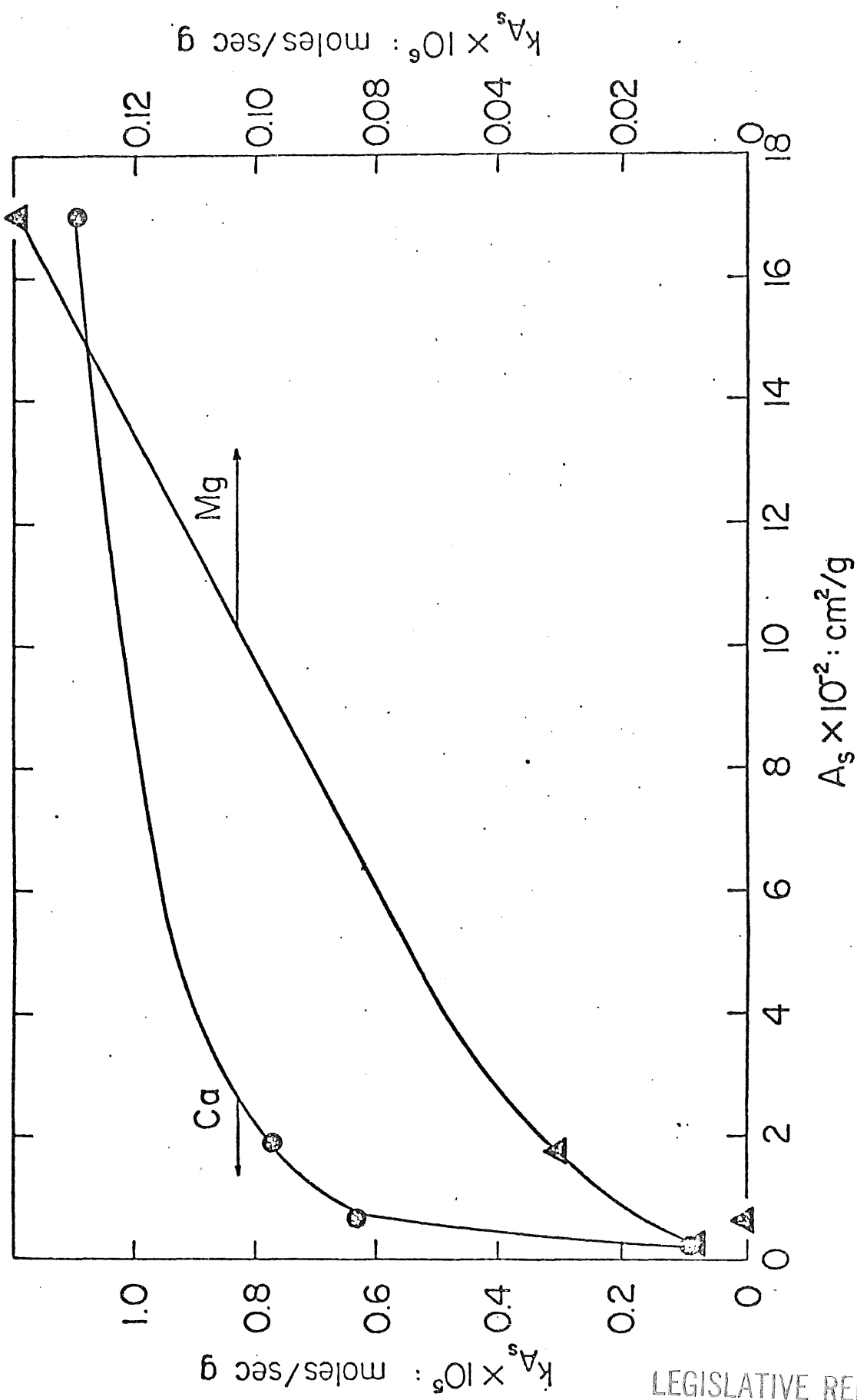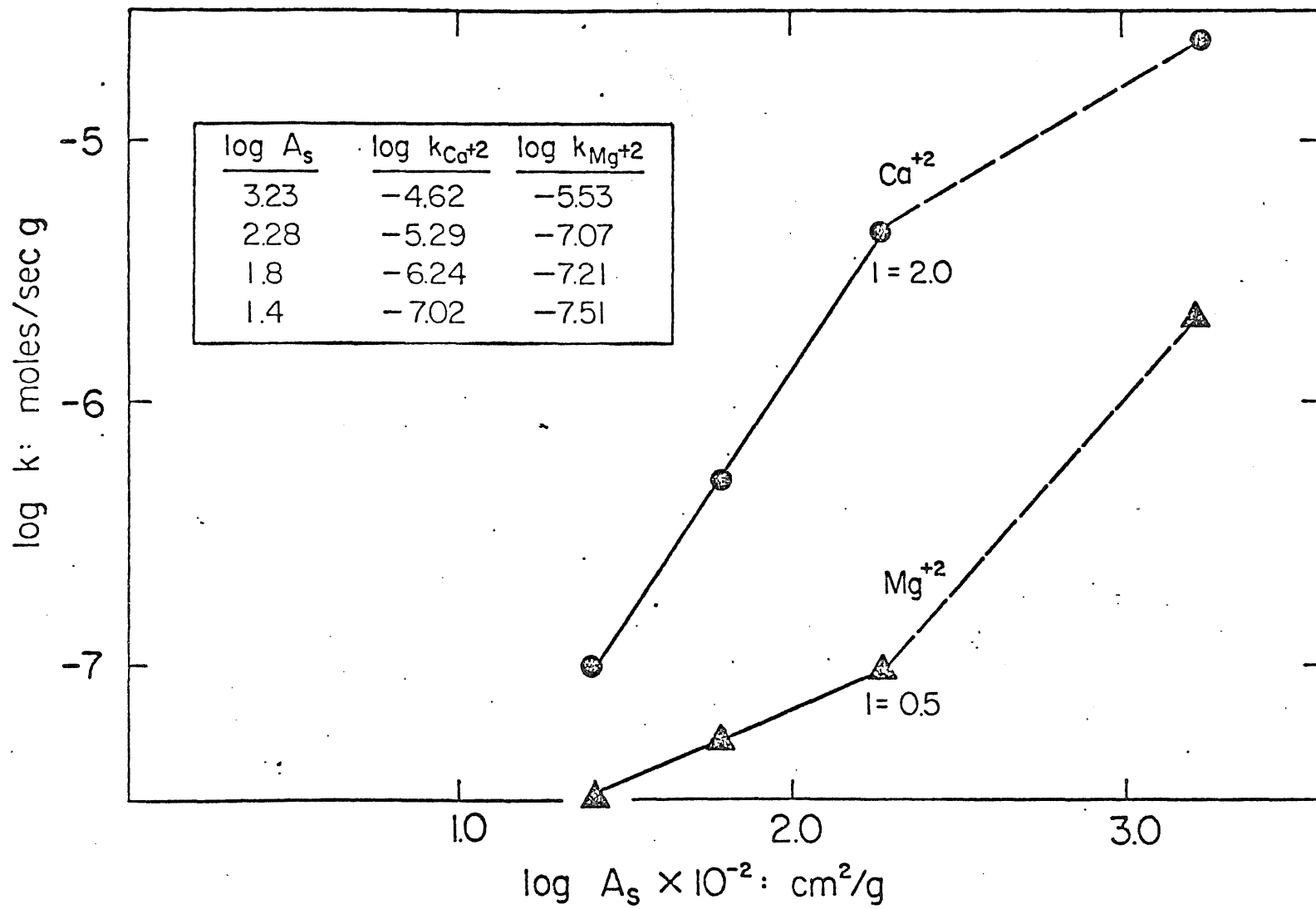
4.4

Effect of pH

The results of previous investigations (Section 1.6) suggest that the net effect of decreasing pH is to increase the extent of alumino-silicate dissolution. In order to determine the effect of solution acidity on silicate dissolution in our studies ($Ca^{+2}$, $Mg^{+2}$ release), 5.71 g.$\ell^{-1}$ of $\leq 74$ µm mineralized gabbro was leached in each of four reactors in which the solution was maintained at pH 5, 6, 7 and 8, respectively, by addition of strong acid or base. Dissolved oxygen was maintained at $\sim$ 9 mg/l and the temperature was 17°C. The results of the pH study are plotted in Figure 4.5 for $Ca^{+2}$ release; similar results were obtained for $Mg^{+2}$ release. The release curves are characterized by an initial rapid release of $Ca^{+2}$ which tends to plateau at $Ca^{+2}$ concentrations between 1.8 and 2.8 mg.$\ell^{-1}$. The quantity of $Ca^{+2}$ and $Mg^{+2}$ appearing in solution (Figure 4.5; Table 3.5) with time increases with decreasing pH. At low pH, less than 10% of the $Ca^{+2}$ released is associated with the particle surface, but as the pH increases to 7 and 8, up to 56% of the total released Ca is sorbed to the particle surface or precipitated in a new solid phase. In contrast, less than 20% of the $Mg^{+2}$ is associated with the solid phase at pH 8. A possible explanation of this behavior is that $Ca^{+2}$ diffusing through the secondary product layer rapidly precipitates out as $Ca(OH)_2$ or $CaCO_3$ at high pH, but remains in solution at low pH. The total quantity of $Ca^{+2}$ released increased with increasing pH while $Mg^{+2}$ exhibited the reverse trend (Table 3.5). Aqueous chemical removal processes apparently control $Ca^{+2}$ observed in solution, while solid dissolution exerts a greater control on $Mg^{+2}$ concentrations.

The rate of $Ca^{+2}$ and $Mg^{+2}$ release to solution increases with increasing pH from pH 6 to 8, and increases below pH 6 (Figure 4.6). Preliminary experi-

ments performed to study the pH effect (Table A    ) showed that $Ca^{+2}$ release rates reached $2.9 \times 10^{-5}$ moles . $sec^{-1}$ . $g^{-1}$ gabbro at pH 4.15, while the $k_{Ca}+2$ achieved at pH 8 was only $0.2 \times 10^{-5}$ moles . $sec^{-1}$ . $g^{-1}$. The increased rate at low pH is likely due to the acid-assisted dissolution of the silicate surface preventing the buildup of a protective layer; therefore, no diffusion limited transport.  Also, low pH inhibits formation of solid carbonates and hydroxides.
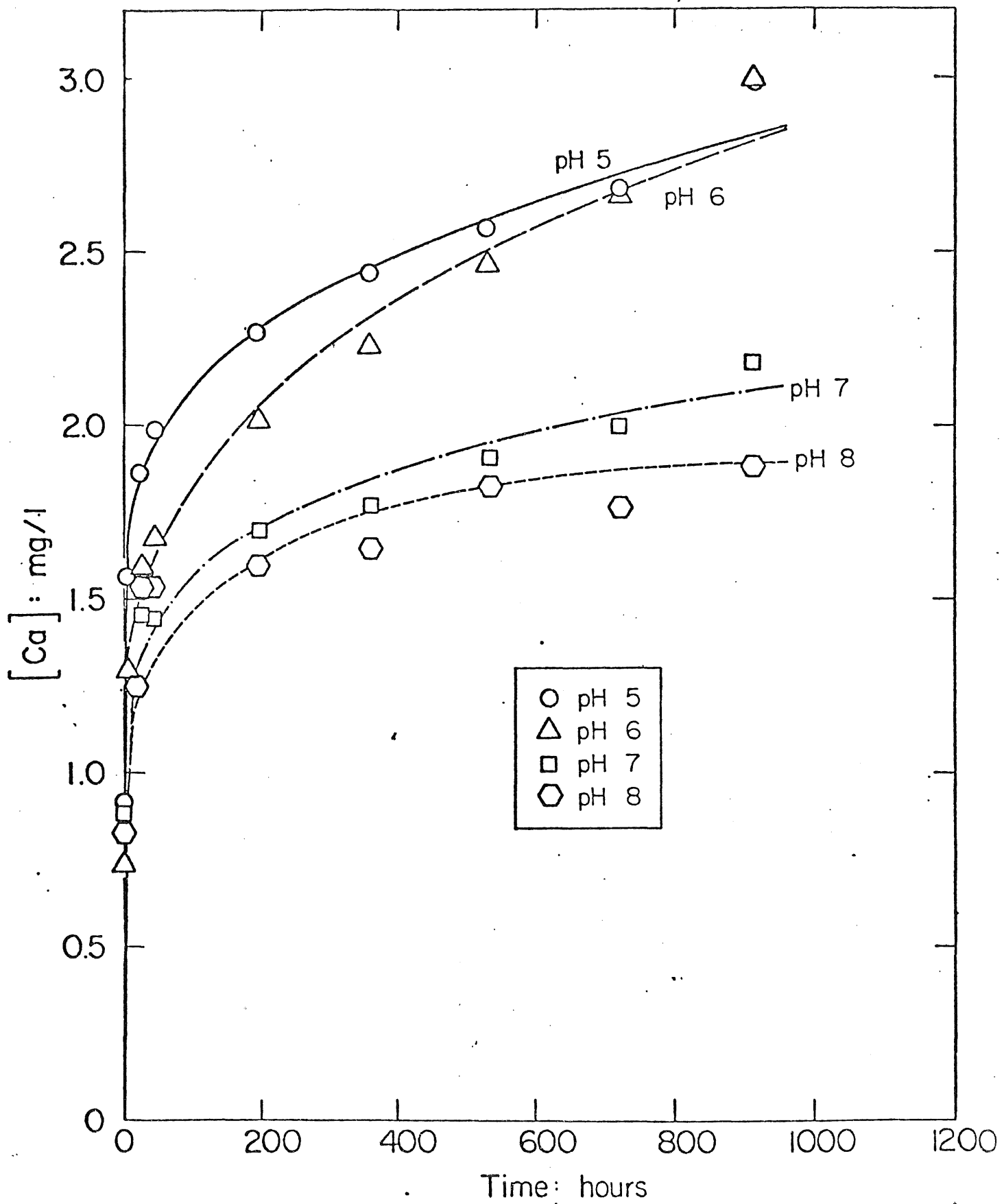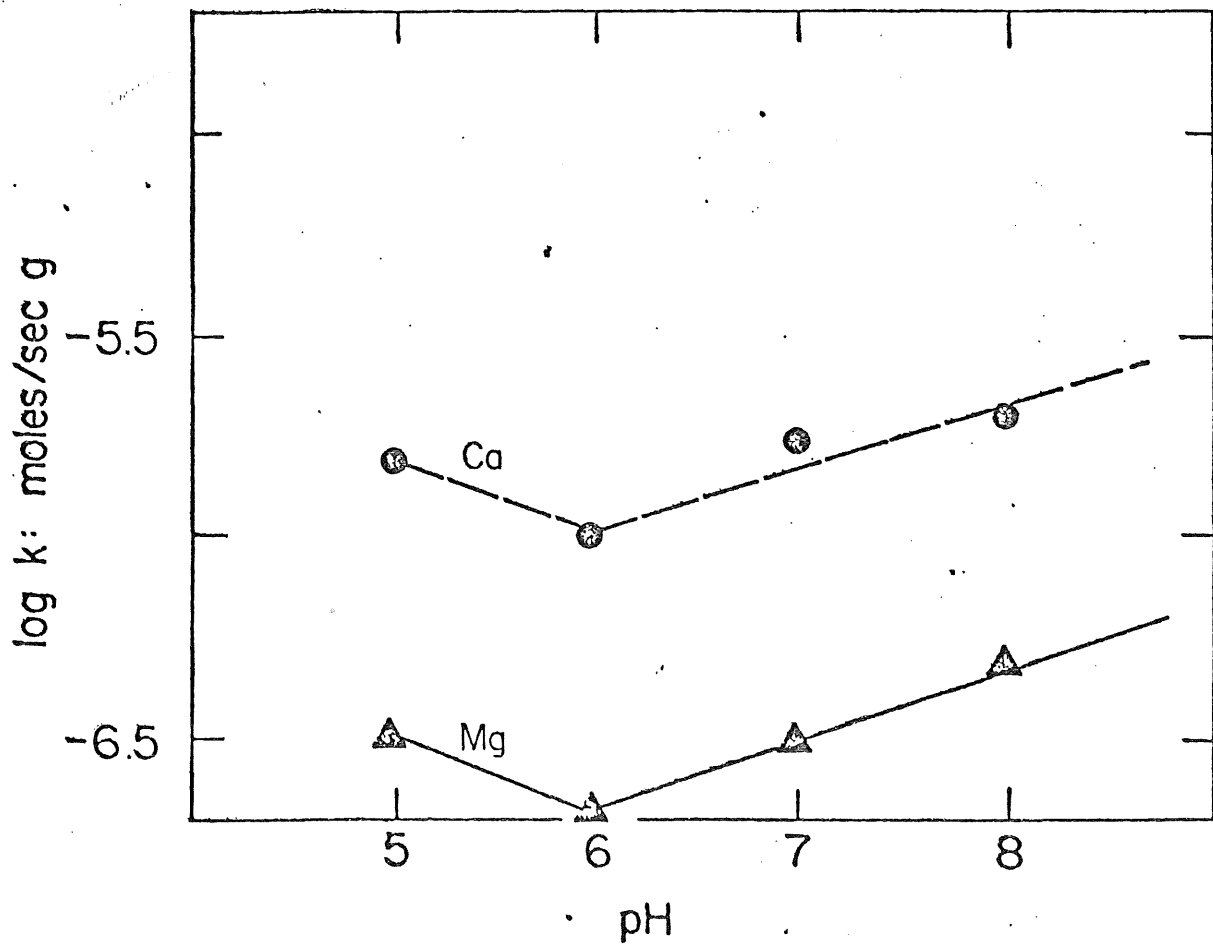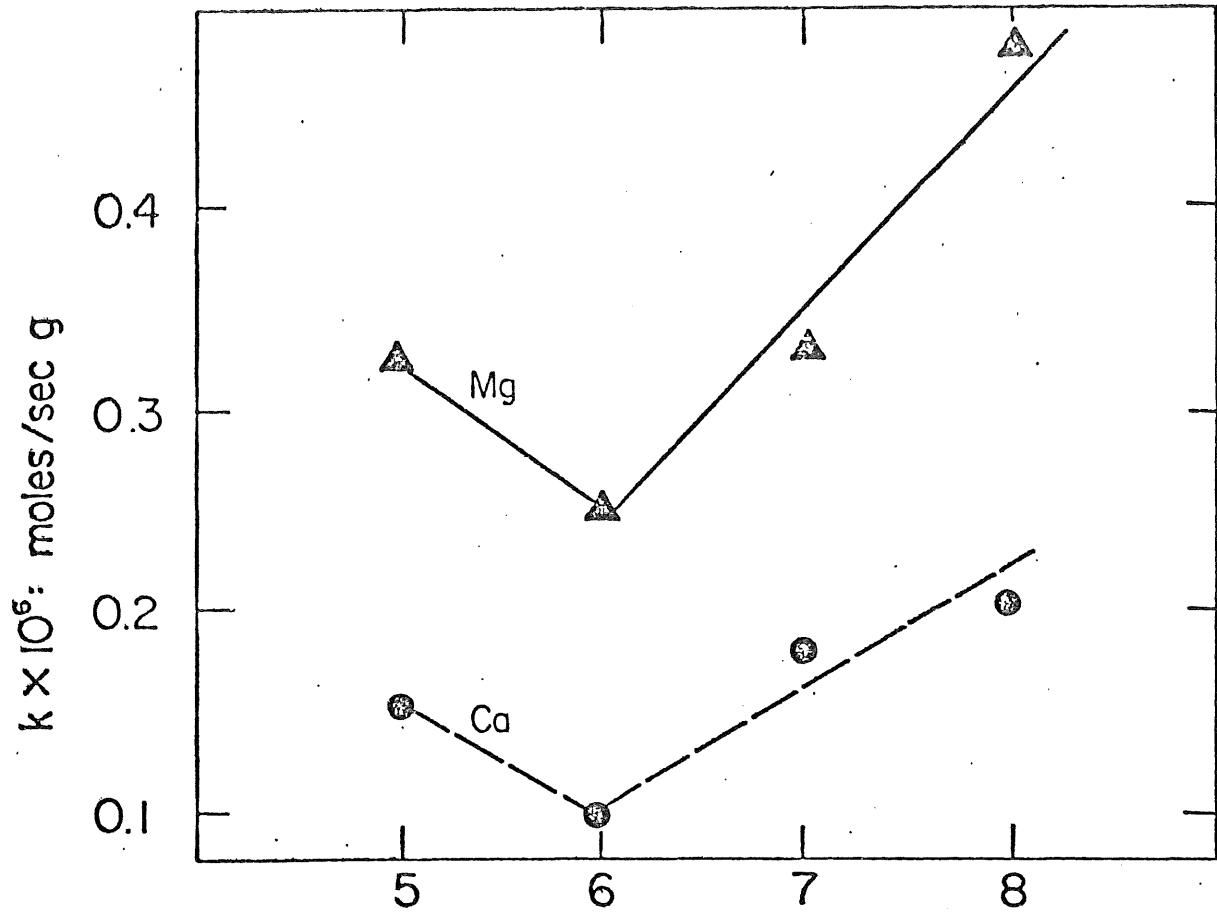
At solution values of pH 5-8, the $k_{Ca}+2$ ranged from $(0.1-0.2) \times 10^{-5}$ moles . $sec^{-1}$ . $g^{-1}$ gabbro and the $k_{Mg}+2$ varied from $0.3-0.5 \times 10^{-6}$ moles . $sec^{-1}$ . $g^{-1}$ gabbro.  The rate of release of $Ca^{+2}$ and $Mg^{+2}$ is relatively independent of pH in the range pH 5-8 in contrast to the $k_{Ni}+2$ values observed (Section 3.5).  To determine the sensititivy of $k_{Mg}+2$ and $k_{Ca}+2$ on pH, a kinetic expression of the type below was developed (Section 3.5):

$$k' = k_H[H^+]^n \qquad\qquad 4.6$$

$$\log k' = \log k_H + n \log [H^+] \qquad\qquad 4.7$$

$$\text{where } k_H = kA_s^\ell[O_2]^m$$

The reaction order, n, was determined to be 2.9 for $Ca^{+2}$ release, and 0.14 for $Mg^{+2}$ release at pH 6-8, using a least-squares fit.  Since $Ca^{+2}$ and $Mg^{+2}$ release rates increase with increasing pH (6 to 8), and $Ni^{+2}$ release rates show the opposite behavior (Section 3.5), it is reasonable to assume that the dissolution kinetics of the silicate minerals have no major effect on metal sulfide dissolution/oxidation.

4.5

Effect of Dissolved Oxygen

The effect of dissolved oxygen on the dissolution of alumino-silicate minerals must of necessity be indirect if observed at all.  In Section 4.4,

the solution pH was found to be relatively unimportant in the dissolution of silicate minerals in the pH range of natural waters. However, the data indicate that depression of the pH below 6 increases the reaction rate by up to a factor of 10 for $Ca^{+2}$ from natural conditions. Increases in solution acidity may result from the increased oxidative dissolution of metal sulfides (Section 3.4). Acidity from this source may increase the release of $Ca^{+2}$ and $Mg^{+2}$ to solution.

To determine the effect of dissolved oxygen on alumino-silicate dissolution in the presence of finely-divided metal sulfide particles, 2.86 $g.\ell^{-1}$ of -200 mesh gabbro were leached in mixed reactors at 17°C under conditions of variable dissolved oxygen concentrations 1-1, 5, 9.3 and 40 $mg.\ell^{-1}$. The dissolved oxygen concentrations achieved by variable mixing of pure $O_2$, compressed air and $N_2$ in the batch reactors. Solution pH was monitored but not controlled so as to prevent sample disturbance.

The release of $Ca^{+2}$ from mineralized gabbro as a function of dissolved oxygen concentration is shown in graphical form in Figure 4.7, and in tabular form in Table 3.4 (and Table A-  ). The results show that the concentration of $Ca^{+2}$ in solution generally increases with increasing dissolved oxygen. However, the $Ca^{+2}$ increase occurred concommitantly with a decrease in solution pH resulting from the oxidation of reduced S species and $Fe^{+2}$. Total $Ca^{+2}$ and $Mg^{+2}$ release (Table 3.4) either remain constant or decrease slightly with increasing dissolved oxygen. As expected, the dissolved oxygen content of the leaching solution has little or no effect on alumino-silicate dissolution, unles solution pH is altered by metal sulfide oxidation.
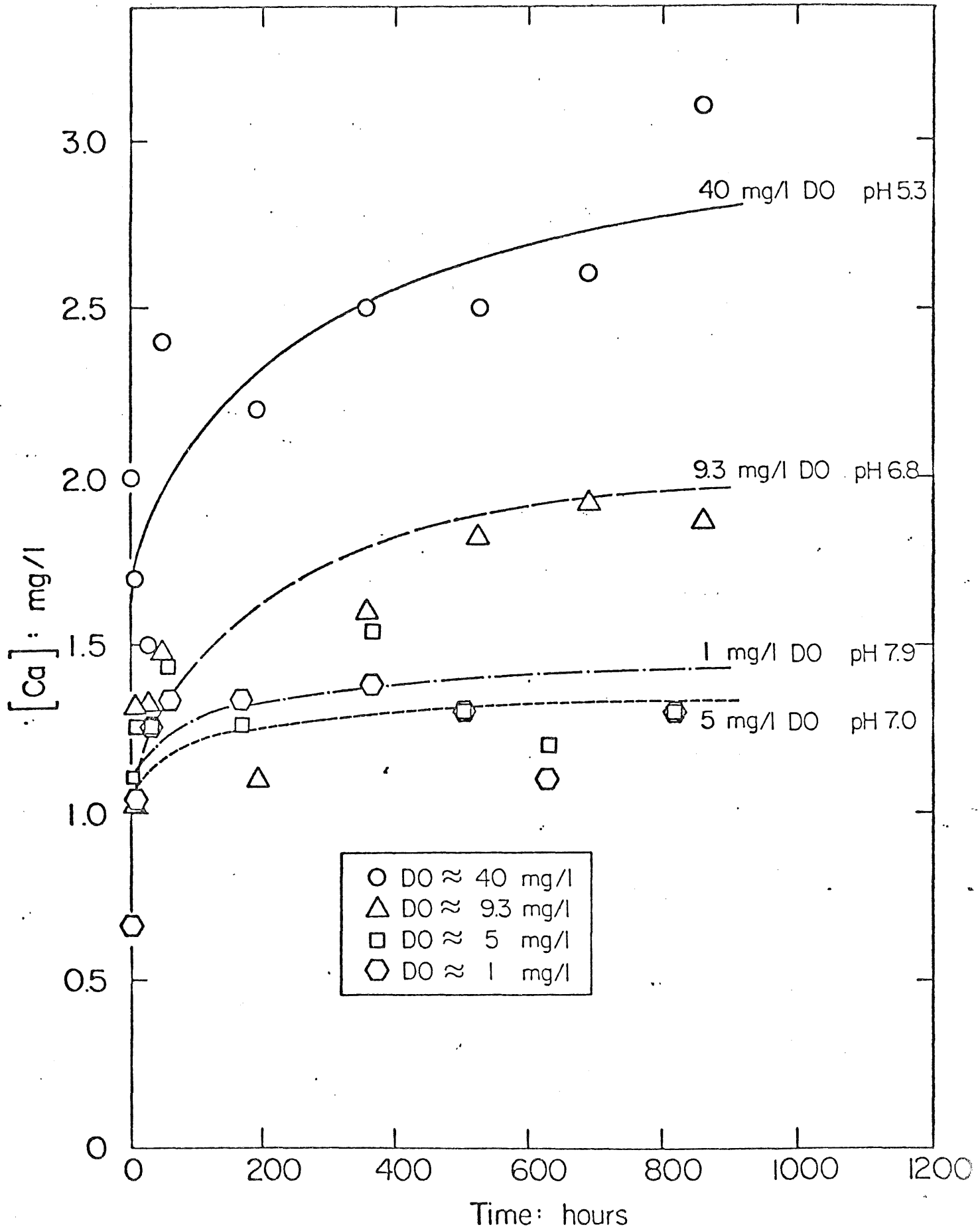
4.6

Effect of Ionic Strength

The general effect of increasing salt content in heterogeneous reactions is to decrease the solubility product of the dissolving solid, thereby increasing its solubility. Equation 3.33 (Section 3.6) illustrates that increasing ionic strength increases solubility, and that the effect of ionic strength is especially important for solids containing multivalent cations. According to the extended Debye-Huckel equation (3.33), the decrease in the solubility product should be proportional to $\sqrt{\mu}$.

To determine the sensitivity of $k_\mu$ to ionic strength, batch reactors containing 5.71 g. $\ell^{-1}$ gabbro were adjusted to 0, 5 x $10^{-3}$M and 5 x $10^{-2}\underline{M}$ NaCl. The reactor solution was maintained at pH 7, 17°C and 9.3 mg.$\ell^{-1}$ D.O.

The results of the ionic strength experiment are plotted as a function of time in Figure 4.8. Silicate dissolution increased slightly with increasing $\mu$ as indicated by the release of $Ca^{+2}$ (Figure 4.8) and $Mg^{+2}$ (Table 3.6) to solution at pH 7. The greatest increase in $Ca^{+2}$ and $Mg^{+2}$ concentration in solution was observed in the reactor having the highest ionic strength. Increased salt content was expected to decrease the initial ion exchange reaction between surface cations and solution $H^+$, but $Na^+$ would probably also be effective in displacing surface $Ca^{+2}$ and $Mg^{+2}$.

The rates of $Ca^{+2}$ ($k_{Ca}+2$) and $Mg^{+2}$ ($k_{Mg}+2$) release increased with increase in ionic strength as shown in Figure 4.9. The following rate constants were observed:

| $\mu$ | $k_{Ca}+2$ | $k_{Mg}+2$ |
|-------|------------|------------|
| 0 | .18 | .033 |
| .005$\underline{M}$ | .84 | .072 |
| .05$\underline{M}$ | .87 | .11 |

$$(\text{moles.sec}^{-1}.g^{-1} \text{ gabbro}) \times 10^{-5}$$
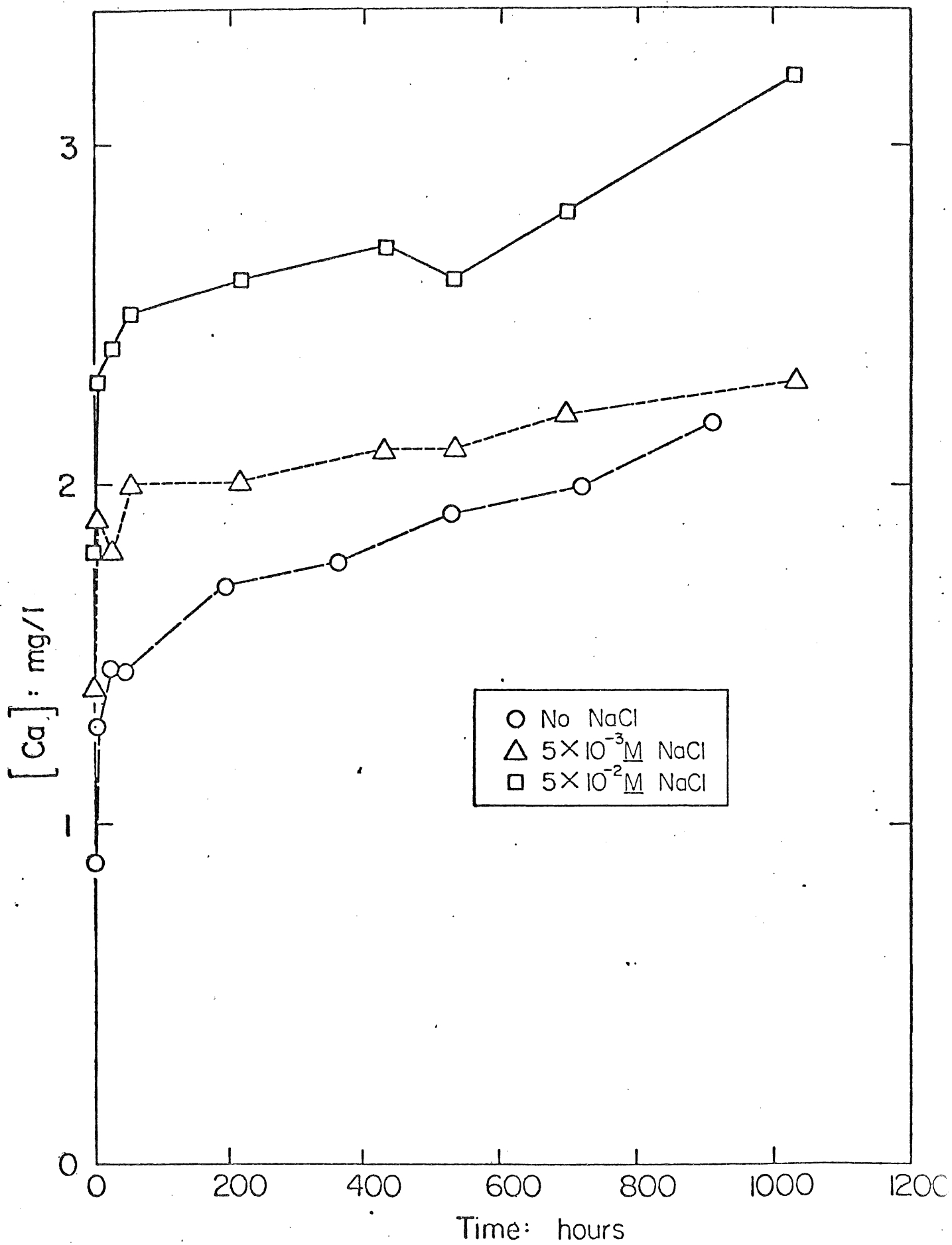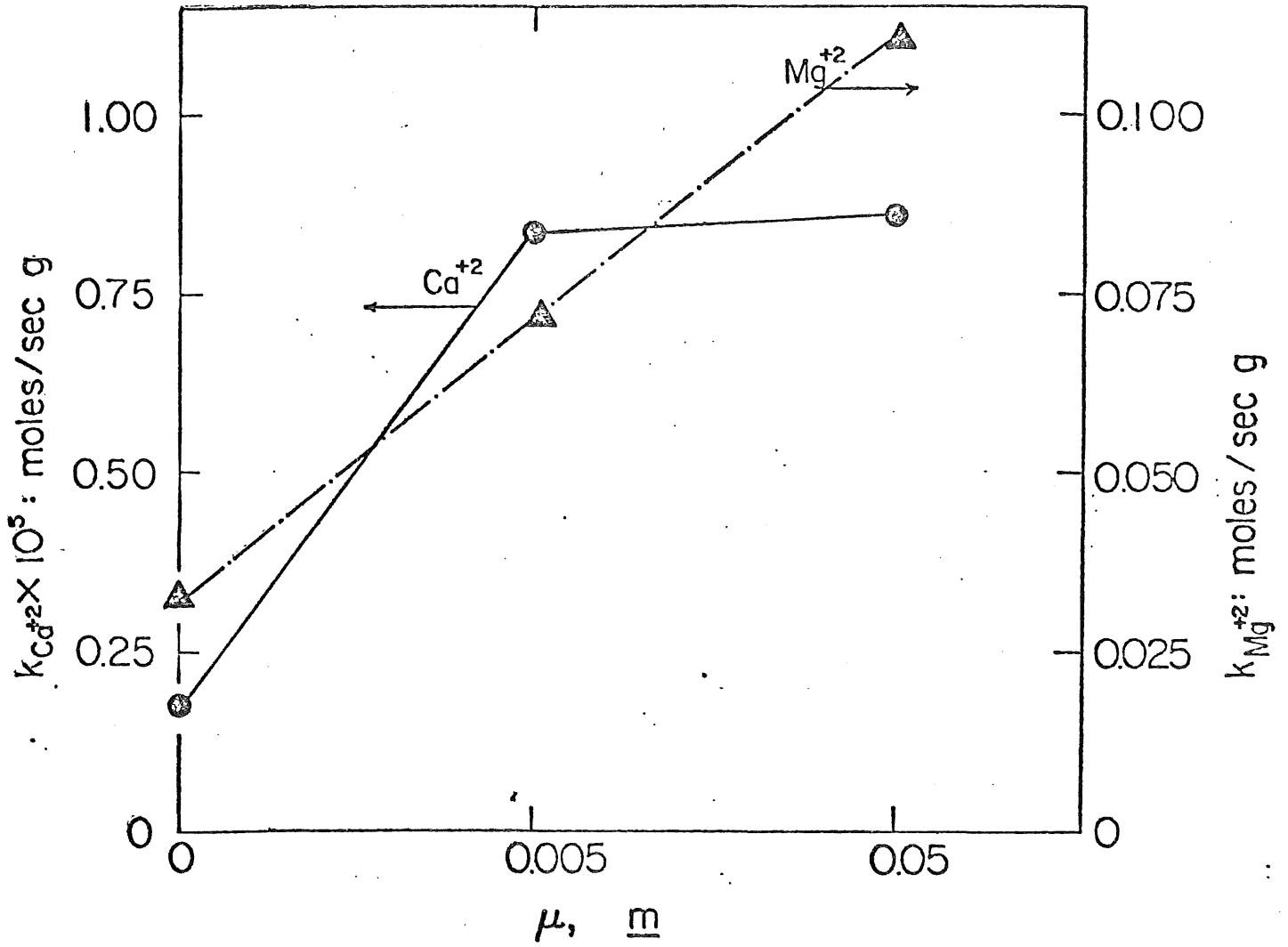
The results indicate that the enhancement in $Ca^{+2}$ release reaches a maximum at 0.005 $\underline{M}$ NaCl and plateaus, whereas $Mg^{+2}$ release increases linearly at least up 59 0.05 $\underline{M}$ NaCl. The increase in $k_{Ca}+2$ at low $\mu$ may be responding to surface-associated cations, while the increase in $k_{Mg}+2$ with increasing $\mu$ may result from increased dissolution of the bulk solid. This interpretation is consistent with that made based on pH variations (Section 4.5).

**4.7**

**Effect of Organic Ligands and Natural Waters**

The effect of synthetic and naturally-occurring organic ligands on the weathering of silicate and mineral sulfides has been reported (21-24). In general, the extent and rate of silicate dissolution is enhanced relative to control conditions. The effect of organic ligands is to form weak to moderately-strong complexes or chelates with structural or surface-associated cations by ligand exchange reactions of the type (Table 1.3):

$$Al_2Si_2O_5(OH)_4 \text{ (s)} + 2Y^- \rightleftharpoons 2 \text{ } AlY^- \text{ (aq)} + 2H_4SiO_4 + H_2O \qquad (4.8)$$
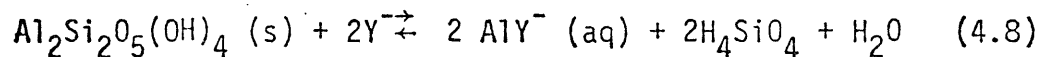
In this example, kaolinite reacts with the organic ligand, $Y^-$, to form a soluble complex with structural Al atoms, thereby degrading the alumino-silicate. Similar reactions can be written for plagioclase minerals whereby Al and surface-associated cations ($Ca^{+2}$, $Mg^{+2}$) are complexed, resulting in an increased rate and extent of mineral dissolution. In experiments performed in this study, the appearance of $Ca^{+2}$ and $Mg^{+2}$ in the reactor solution at a faster rate than observed in the control was used to demonstrate the influence of organic ligands. A further discussion of organic ligand effects on minerals dissolution may be found in Section 3.7.

The effect of organic ligands on silicate dissolution was demonstrated by leaching gabbro under natural conditions by citrate, phthalate and natural

waters consisting of bog and ground water. Citrate and phthalate were chosen to be representative of functionalities thought to exist in natural waters. Citric acid is an aliphatic tri-carboxylic acid ($HO_2CH_2CCOHCO_2H$ $CH_2CO_2H$) having pKa's equal to 3.13, 4.76 and 6.40 at 25°C and zero ionic strength for the successive acid dissociation constants. Under solution conditions used in this experiment (pH 7), greater than 90% of the citric acid is expected to be fully ionized. The reactions pertinent to the binding of $Ca^{+2}$ and $Mg^{+2}$ by citrate are:

$$Ca^{+2} + Y^{\equiv} \rightleftarrows CaY^- \qquad pK = 3.50 \qquad (4.9)$$

$$Ca^{+2} + HY^{\equiv} \rightleftarrows CaHY^\circ \qquad pK = 2.10 \qquad (4.10)$$

$$Mg^{+2} + Y^{\equiv} \rightleftarrows MgY^- \qquad pK = 3.37 \qquad (4.11)$$

$$Mg^{+2} + HY^{\equiv} \rightleftarrows MgHY^\circ \qquad pK = 1.92 \qquad (4.12)$$
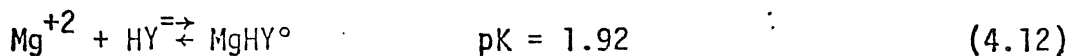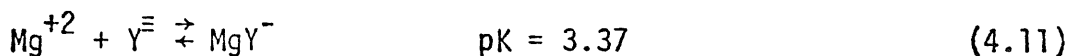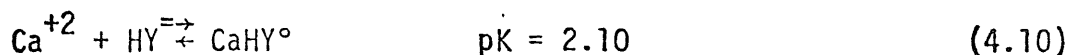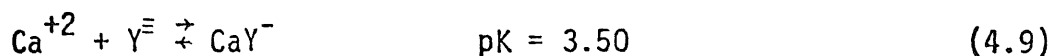
Citric acid is a moderately strong ligand relative to both $Ca^{+2}$ and $Mg^{+2}$, and binds each with about equal strength.

Phthalic acid is an aromatic di-carboxylic acid (benzene, 1-2, dicarboxylic acid) having successive acid dissociation constants of $pK_1 = 2.95$, $pK_2 = 5.10$.

Therefore, phthalic acid is fully de-protonated under the solution conditions used in these experiments. The reaction pertinent to the binding of $Ca^{+2}$ by phthalate is:

$$Ca^{+2} + Y^= \rightleftarrows CaY^\circ \qquad pK = 2.42 \qquad (4.13)$$

The stability constant for the formation of $MgY^\circ$ is not available.

To determine the influence of organic ligands and natural waters on the dissolution rate of silicate minerals, citrate or phthalate was added at concentrations of 0, $1.3 \times 10^{-4}\underline{M}$ to reactors containing 2.86 g.$\ell^{-1}$. The solution was adjusted to pH 7 and maintained throughout the experiment. The control reactor (pH 6.9) contained no ligand, and the pH was not adjusted due

to its proximity to pH 7. In preliminary experiments, amorphous pre-
cipitates were observed which removed trace metals but had lesser effects
on major cations.

Results of these experiments are summarized on Tables 3.7-3.9, A.2,
A.3, A.7 and A.8, and represented graphically in Figures 4.10 and 4.11.
Citrate tended to increase the initial rate and extent of $Ca^{+2}$ release
(Figure 4.9), but concentrations decreased in later stages of the reaction
(after 400 hours). Schalscha, et al. (22) observed this behavior in their
experiments and suggested that it would be explained by a breakdown of
the organic complex, adsorption onto mineral reaction products or other
complicated factors. In this study, precipitation of a new mineral phase
(amorphous metal silicate) may be responsible. Up to 400 hours, the
rate of appearance of $Ca^{+2}$ in solution was enhanced over the control.
The effect of the $1.3 \times 10^{-4}\underline{M}$ ligand concentration was much less than the
effect of the $1.3 \times 10^{-3}\underline{M}$ solution, and did not differ markedly from the
control after 400 hours.

Figure 4.11 shows the release of $Ca^{+2}$ with time in the presence of
increasing concentrations of phthalate. In this case, $Ca^{+2}$ concentrations
were only slightly enhanced over the control up to $\sim$ 100 hours. After 100
hours, increasing concentration of ligand inhibited $Ca^{+2}$ release to solution.
The appearance of a brown precipitate in acidified, filtered samples with-
drawn from the reactors may have caused the apparent concentration decrease.
In any case, phthalate does not apparently enhance silicate dissolution.

The effect of increasing citrate and phthalate concentrations on the
rate of $Ca^{+2}$ and $Mg^{+2}$ release is shown in Figure 4.12. Assuming $Ca^{+2}$ release

as influenced by citrate concentrations can be represented by the equation $k' = k_0[CiT]^n$, then $\log k' = \log k + n \log [CiT]$. As indicated in the lower half of Figure 4.11, a plot of $\log k$ vs $\log [Cit]$ yields a line of slope equal to $\sim 0.3$-$0.4$. This corresponds to an approximate doubling of the observed $k$ as the $[CiT]$ increased by ten times. The $Mg^{+2}$ release rate remained essentially unchanged with increasing $[CiT]$.

The rates of $Ca^{+2}$ release in the presence of citrate ranged from $.77$-$2.1 \times 10^{-5}$ moles . $sec^{-1}$ . $g^{-1}$ while $Mg^{+2}$ rates ranged only from $.33$-$.58 \times 10^{-6}$ moles . $sec^{-1}$ . $g^{-1}$.

To determine the effect of natural waters on the dissolution of silicate minerals, bog and groundwater obtained in the vicinity of the Dunka Pit were used to leach 5.71 g . $\ell^{-1}$ of mineralized gabbro at pH 8. Natural concentrations of $Ca^{+2}$ in bog and groundwater were 7.8 and 18.9 mg .$\ell^{-1}$, respectively. Results of the dissolution experiment are shown in Figure 4.13. Calcium concentrations increased by 3.0 mg . $\ell^{-1}$ in the bog water case over $\sim 1000$ hours, while the $Ca^{+2}$ levels increased by 1.20 mg . $\ell^{-1}$ in the groundwater reactor control experiments showed an$\sim 2.0$ mg . $\ell^{-1}$ increase over the same time period. With this comparison, bog water enhanced the dissolution rate of gabbro by about 50%, while groundwater interactions may have actually removed $Ca^{+2}$. The $Mg^{+2}$ concentration increased by 1.0 mg . $\ell^{-1}$ and 2.90 mg .$\ell^{-1}$, respectively for the groundwater and bog water leach.

The initial reaction on mixing of surface waters with alumino-silicate minerals would be a decrease in the solution concentration due to precipitation/sorption followed by a slow increase as a result of dissolution

by binding structural elements, and maintain higher solution concentrations through complexation. The effect of silicate dissolution on mineral sulfide oxidation may simply be to increase $A_s$ available for leaching.

Legend:
- ○ No Phthallic Acid: 5.71 g gabbro/l
- △ $1.29 \times 10^{-4}$ M Phthallic Acid: 2.86 g gabbro/l
- □ $1.29 \times 10^{-3}$ M Phthallic Acid: 2.86 g gabbro/l

y-axis: [Ca]: mg/l

x-axis: Time: hours
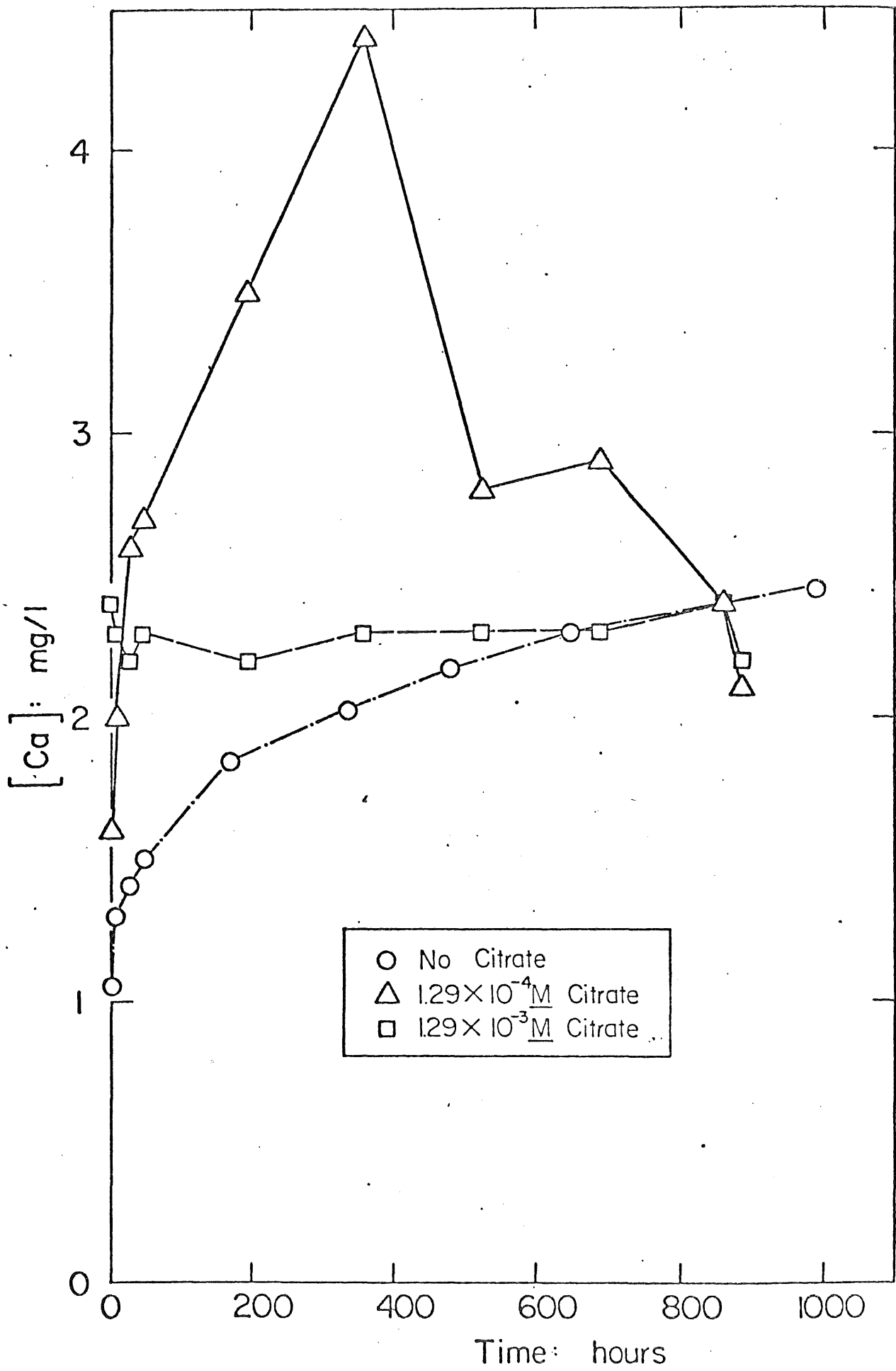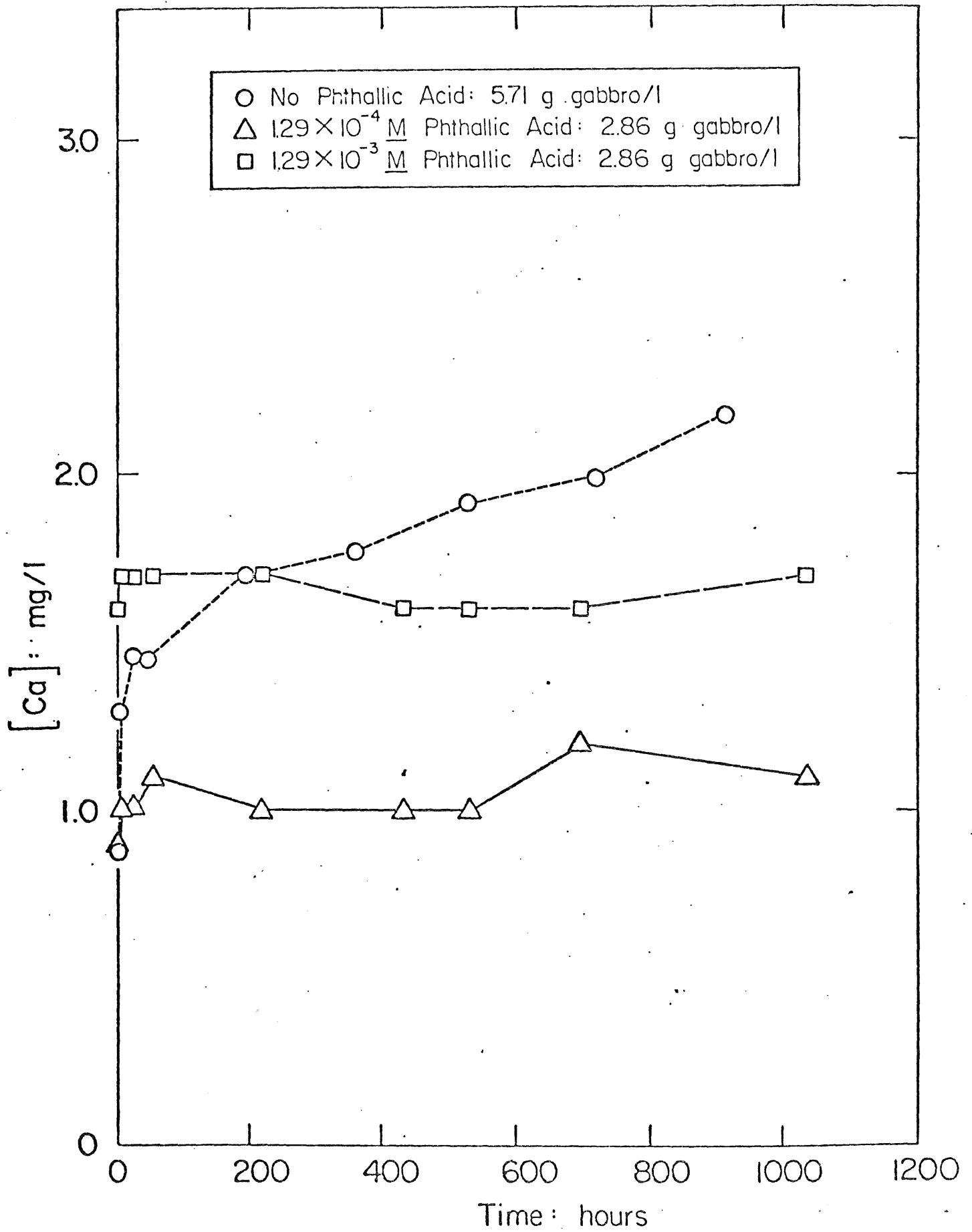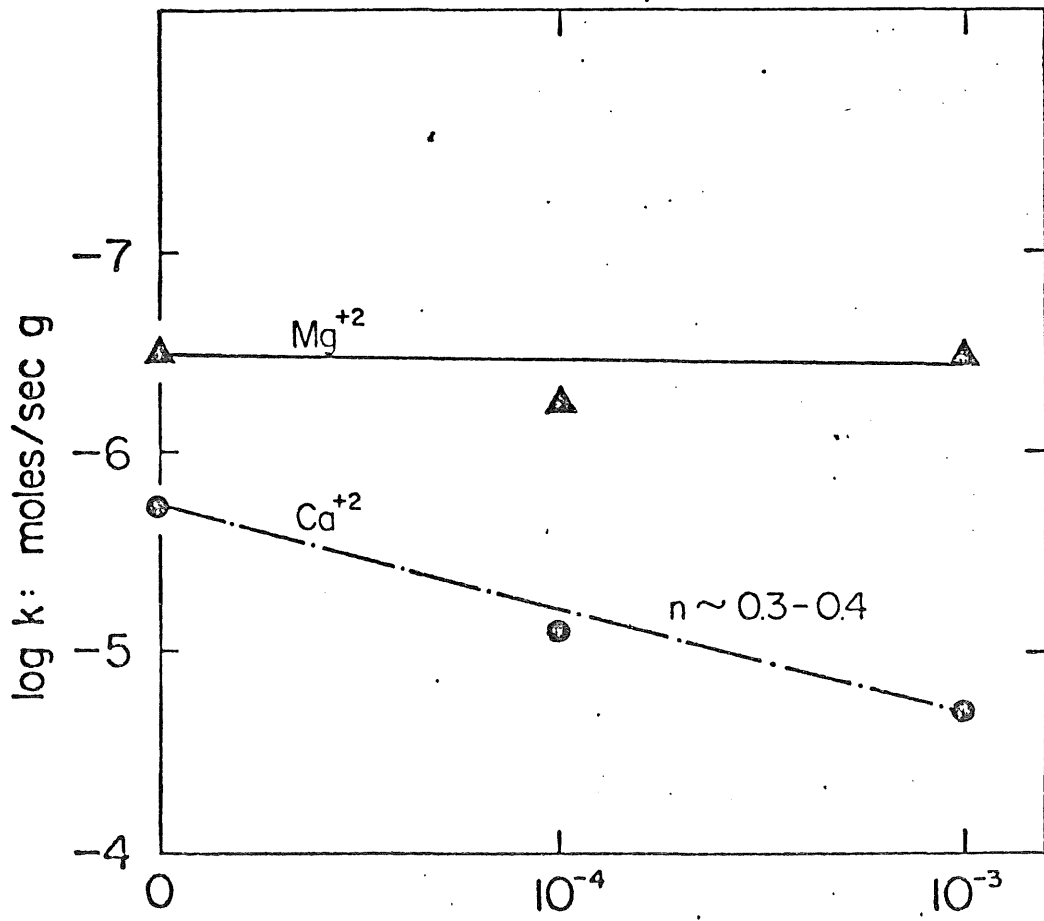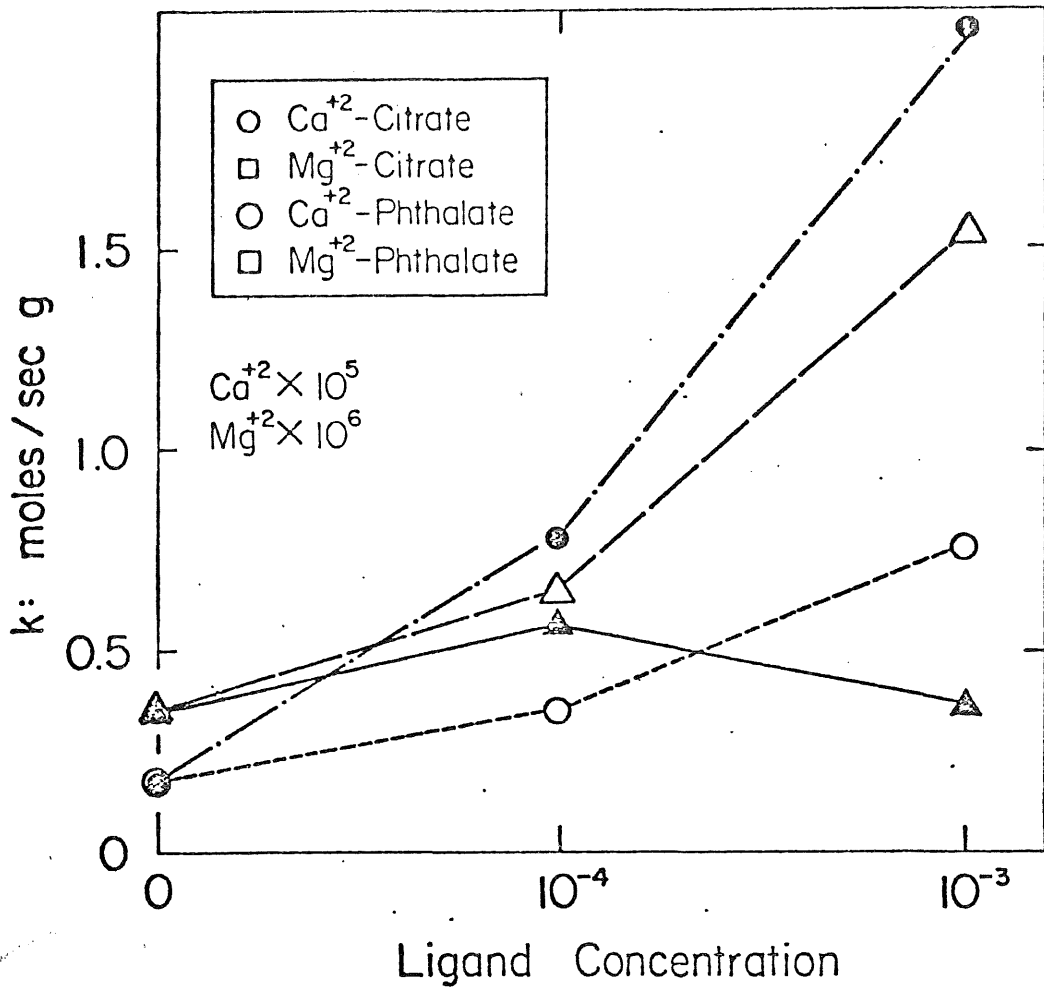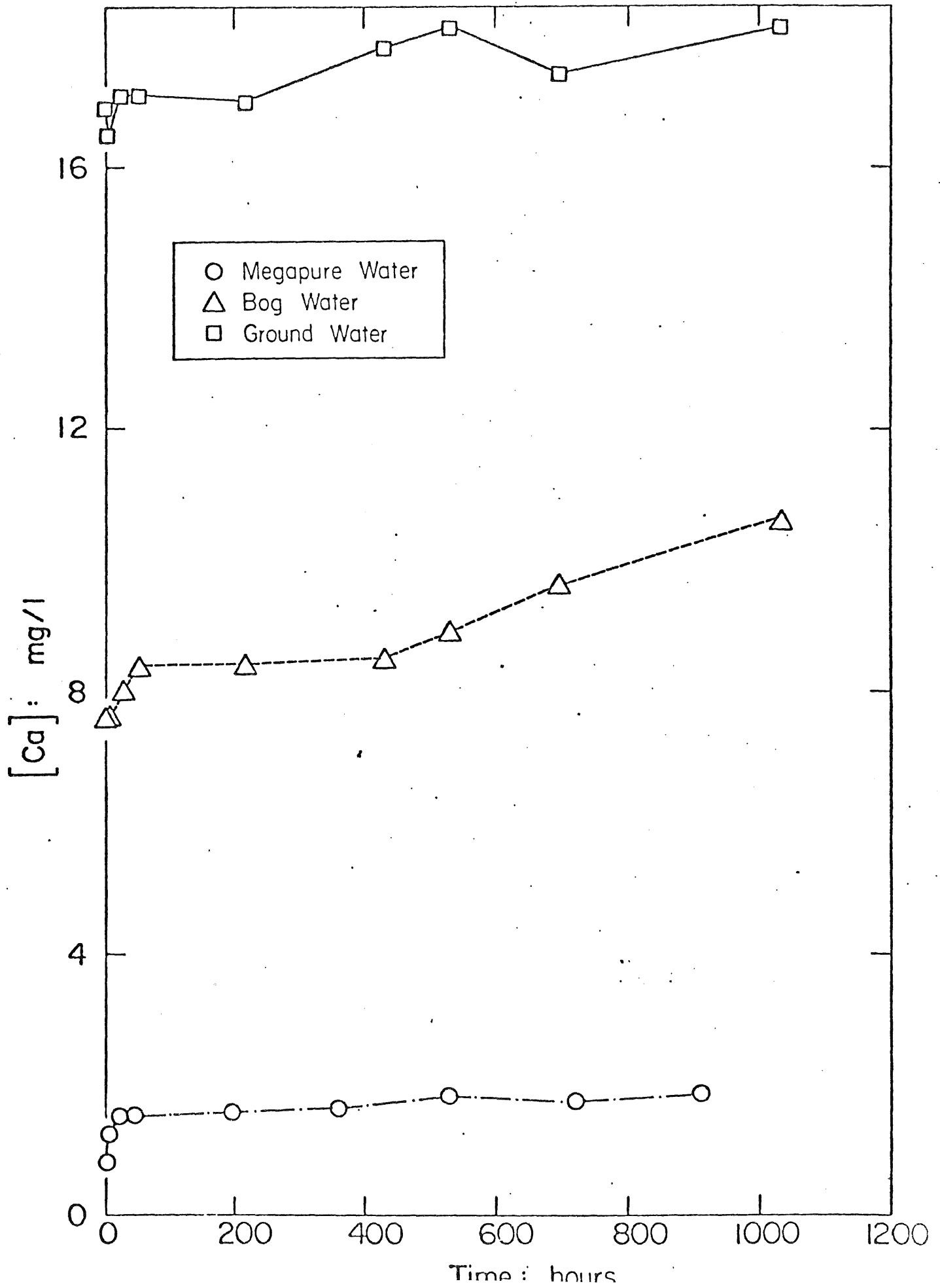
## Chapter 5

### Discussion of Kinetic Results and Mechanisms

### 5.1. Oxidative Dissolution of Metal Sulfides

The kinetic results for the abiotic oxidative dissolution of pentlandite present in the Duluth Gabbro ore can be summarized by the following empirical rate expression:

$$-\frac{d[Fe,Ni)_9S_8]}{dt} = \frac{d[Ni(II)]}{dt} = 2.5kA_s^{0.4}[O_2]^{0.8}[H^+]^{0.2}[CIT]^{0.3} \tag{5.1}$$

When surface area, As, dissolved oxygen, $[O_2]$, pH and organic chelate, $[CIT]$, remains constant, the rate of appearance of Ni is pseudo zero-order (i.e., concentration increases linearly with time).

$$\frac{d[Ni(II)]}{dt} = k^1 \tag{5.2}$$

$$k^1 = 4.5kAs^{0.4}[O_2]^{0.8}[H^+]^{0.2}[CIT]^{0.3} \tag{5.3}$$

Equation 5.3 predicts that magnitude of the observed pseudo zero-order rate constant will increase with an increase in surface area (or a decrease in particle size), with an increase in the dissolved oxygen concentration (over the range 1-10 mg/l which is typical of environmental conditions), with a decrease in pH (an increase in $[H^+]$) and with an increase in the concentration of organic chelates that exhibit specificity for the complexation of Ni(II) or Fe(II).

Similar kinetic dependencies were observed for the rate of release of Cu to solution from the dissolution of chalcopyrite although the reduced solution phase mobility of Cu over a broad pH range prevented the same detailed analysis of Cu dissolution rates. The oxidative dissolution of cubanite and chalcopyrite was significantly enhanced with a decrease in pH and an increase in organic chelate concentration. In fact, the impact of chelation on the release rate of Cu should be predicted to be greater than that of Ni based on fundamental considerations of ligand field stabilization energies (44).

The stability constnat, B, for the formation of analogous complexes of divalent ions follow the general trend $MN^{+2} < Ca^{+2} < Ni^{+2} < Cu^{+2} < Zn^{+2}$ which is called the Irving-Williams order (44). From the concentration time profiles for Cu, it appears that release of copper to solution may be diffusion controlled at higher pH in the absence of strong chelates. This idea is consistent with the observations of other investigators (4, 15, 16) who have observed mixed linear and parabolic release rates for Cu from $CuFeS_2$. Copper has a pronounced tendency to form $Cu_2CO_3(OH)_2$ (malachite) and $Cu(OH)_2$ at the pH and $[HCO_3^-]$ observed during these studies. Formation and deposition of these products on the $CuFeS_2$ surface may provide a barrier to the rapid diffusion of Cu(II) away from the surface and result in a reaction rate which is controlled by mass transport of Cu(II) through the reacted zone. In addition to these non-sulfide products of the oxidative dissolution of $CuFeS_2$, metastable products such as $CuS$ and $Cu_3FeS_4$ may form on the surface.

Dissolution of solid reactants such as $CuFeS_2$ are thought to involve three distinct steps which are firstly; the detachment of ions or molecules which constitute the solid from the crystal lattice, secondly, the transport of the released solutes away from the dissolving crystal face and thirdly, in the case of a chemical reaction at the surface, the transport of this reactant to the crystal surface. For many readily soluble solids such as alkali and alkaline earth halides it has been observed (45) that step 1 is relatively fast and the solution near the surface is saturated. Dissolution of these compounds appears to be diffusion controlled (step 2). Generally, the rate law observed for such systems is

$$\frac{dc}{dt} = \frac{AD}{VS}(C_s - C) \tag{5.4}$$

Where A is the surface area, V is the volume of the solvent, D is the solution phase diffusion coefficient and S, is the "Nernst diffusion layer thickness. (46)". A similar rate law would be predicted for dissusion of a reactant such a $O_2$

through a porous reacted layer on the surface of the dissolving crystal. Diffusion controlled reactions show a unique dependence on temperature and mixing. Increasing the rate of stirring will result in a decrease in S and an increase in the rate of dissolution. The activation energy obtained from the Arrhenius relationship (equation 5.5)

$$d \ln k/dt = Ea/RT^2 \qquad (5.5)$$

$$k = Ze^{-Ea/RT} \qquad (5.6)$$

for a diffusion-controlled reaction is typically <6 kcal/mole whereas a chemically controlled reaction will have activation energies which are generally >8 Kcal/mole (38).

In the future, the rates of dissolution of the sulfide minerals present in the Gabbro ore should be studied as a function of temperature and mixing rate to ascertain the relative importance of mass transport in the rate controlling process.

Even though the rate of oxidative dissolution is predicted to be a function of both the dissolved oxygen concentration and surface area for either a diffusion-controlled or chemically-controlled reaction; the bulk of experimental evidence suggests that the rate of dissolution of pentlandite is controlled by a chemical reaction either on the surface or in solution in close proximity to the surface. A simple hypothetical model for the dissolution of FeS has been presented in equations 3.32 through 3.37. This model assumes that the rate of dissolution is controlled by the solution phase oxidation of $HS^-$ (alternatively, oxidation of $Fe^{+2}$ could be rate controlling). The kinetic expression which results from this model predicts that the rate of dissolution should be a function of $[O_2]$, $[H^+]$, and $[Y^{-2}]$, the organic chelate concentration. Results predicted by this mechanistic model are consistent with the experimental observations of this study and of other investigations (10, 11, 12, 21, 37) although the range of experimental conditions was significantly different.

A similar model, in which the rate of dissolution is controlled by a solution phase reaction, can be presented for $(Fe, Ni)_9S_8$.

$$8H^+ + (Fe,Ni)_9S_8 \rightleftarrows 4.5\ Ni^{+2} + 4.5\ Fe^{+2} + 8HS^- \tag{5.7}$$
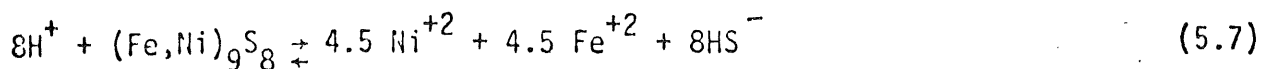
$$K_{so} = [Ni^{+2}]^{4.5}[Fe^{+2}]^{4.5}[HS^-]^8/[H^+]^8 \tag{5.8}$$

To simplify equation 5.8, it is assumed that $[Fe^{+2}] = [Ni^{+2}]$ and that $[Ni^{+2}]^{1.12}$ $[Ni^{-2}]$. Using these assumptions equation 5.8 reduces to

$$K^1_{so} = [Ni^{+2}][HS^-]/[H^+] \tag{5.9}$$

After an equilibrium dissociation of pentlandite the following reactions are postulated to occur in sequence:

$$Ni^{+2} = Y^{-2} \underset{rapid}{\overset{B}{\rightleftarrows}}\ NiY \tag{5.10}$$

$$HS^- + O_2 \underset{slow}{\overset{k}{\rightarrow}} HSO_2^- \tag{5.11}$$

$$HSO_2^- + O_2 \underset{fast}{\rightarrow} HSO_4^- \tag{5.12}$$

Since equation 5.11 is the slow step in the reaction mechanism, the rate of dissolution will be controlled by this step and can be expressed as follows:

$$\frac{-d[(Fe,Ni)_9S_8]}{dt} = k\ [HS^-][O_2] = \frac{1}{4.5}\frac{d\ [Ni(II)]}{dt} \tag{5.13}$$

Substitution of the equilibrium expressions written in equation 5.9 and 5.10 into equation 5.13 yields equation 5.14 after rearrangement.

$$\frac{d[Ni(II)]}{dt} = \frac{4.5\ k\ K_{so}B[Y^{-2}][O_2][H^+]}{[NiY]} \tag{5.14}$$

Equation 5.14 predicts the observed kinetic dependencies within reason. The dependence of the rate on the total concentration of the chelating agent, $Y^{-2}$, will be fractional. The observed kinetic orders for $O_2$ and $H^+$ and 0.8 and 0.2 respectively. 0.8 is close enough to one to suggest a first-order dependence on oxygen, however,

the small fractional dependence is not adequately predicted by this model.

An alternative model that could account for the fractional dependence of both oxygen and hydrogen ion assumes that the rate of the reaction is controlled by a surface reaction between bound HS$^-$ groups and oxygen. Based on the ideas presented by Nelson (12) the model would involve the following sequence of steps: Oxygen must first diffuse to the solid surface and then attach itself to the surface. After attachment of oxygen to the surface electron transfer from sulfur to oxygen must occur. This step would be followed by a molecular rearrangement and bond breaking. It is most likely that a proton assists the bond breaking at the surface. Additional secondary reactions may occur on the solid interface. The final step would involve the diffusion of reaction products into the bulk solution. Assuming the reaction is neither limited by the diffusion involved in the first or last step, the following model for the reaciton of oxygen alone would result. This model considers that a limited number of reactive sites are available on the solid surface.

$$=/-SH + O_2 \underset{k_2}{\overset{k_1}{\rightleftharpoons}} =/-SH \cdot O_2^* \qquad (5.15)$$

$$=/-SH \cdot O_2^* \overset{k_3}{\rightarrow} \text{products} \qquad (5.16)$$
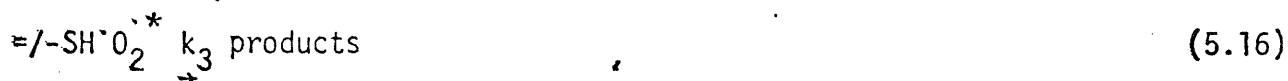
Equation 5.15 represents a rapid pre-rate-determining equilbrium step and equation 5.16 is the rate-determining slow step in the reation sequence. The kinetic expression for the rate of formation of Products, P, is

$$\frac{dP}{dt} = k_3 [=/-SH \cdot O_2^*] \qquad (5.17)$$

Assuming steady-state conditions for the intermediate $=/-SH \cdot O_2^*$ the concentration of this intermediate is given by

$$\frac{d[=/-SH \cdot O_2^*]}{dt} = 0 = k_1 [=/-SH][O_2] - k_2[=/-SH \cdot O_2^*] - k_3[=/-SH \cdot O_2^*] \qquad (5.18)$$

or

$$[\equiv/\text{-}SH\cdot O_2^*] = \frac{k_1 \, [\equiv/\text{-}SH][O_2]}{k_2 + k_3} \qquad (5.19)$$

Substitution of equation 5.20 into equation 5.17 gives

$$\frac{dP}{st} = \frac{k_3 k_1 \, [\equiv/\text{-}SH][O_2]}{k_2 + k_3} \qquad (5.20)$$

However since the concentration of unoccupied reactive sites at any time is unknown, the $[\equiv/\text{-}SH]$ term must be written in terms of the total number of sites available before the reaction begins.

$$[\equiv/\text{-}SH]_t = [\equiv/\text{-}SH] + [\equiv/\text{-}SH\cdot O_2^*] \qquad (5.21)$$

Using equation 5.15, equation 5.20 can be rewritten as

$$[\equiv/\text{-}SH]_t = [\equiv/\text{-}SH]_t/(1 + k_f[O_2]) \qquad (5.23)$$

where kf = $\{k_1/(k_2 + k_3)\}$. Substitution of 5.23 into equation 5.20 yields

$$\frac{k_3 K_f \, [\equiv/\text{-}SH]_t[O_2]}{(1 + k_f[O_2])} \qquad (5.24)$$

The concentration of $[\equiv/\text{-}SH]_t$ can be written as

$$[\equiv/\text{-}SH]_t = \frac{As \cdot N}{V} \qquad (5.25)$$

where Ni is equal to the number of surface sites per unit area, V is the volume of the reactor and As is the total surface area of the sulfide. Substitution of this expression gives

$$\frac{k_3 K_f[O_2]As \; N}{1 + K_f[O_2]V} \qquad (5.26$$

Equation 5.26 can be examined under the boundary condition of $K_f[O_2] \gg 1$, which gives a reaction rate apparently independent of $[O_2]$; and that under the boundary condition of $K_f[O_2] \ll 1$ the reaction will be first-order in $[O_2]$.

The role of pH can be taken into account in the reaction model proposed in equation 5.15 and 5.16 by considering a pre-equilibrium protonation of the metal sulfide surface as follows:

$$=/-SH + H^+ \underset{\leftarrow}{\overset{K_a}{\rightarrow}} =/-SH_2^+ \tag{5.27}$$

$$=/-SH_2^+ + O_2 \underset{\leftarrow}{\overset{k_4}{\rightarrow}} =/-SH_2 \cdot O_2^+ \tag{5.28}$$

$$=/-SH \cdot O_2^+ \overset{k_6}{\rightarrow} products \tag{5.29}$$

Using a similar mathematical development as used in the derivation of equation 5.26 in addition to a mass balance expression for the total reaction sites including protonated and non-protonated sites a new expression can be obtained. This approach is identical to that used by Nelson (12) and yields equation 5.30.

$$\frac{V}{A} = \frac{(k_3 K_1 + k_6 K_2 [H^+] K_a) [O_2] A_s}{1 + K_1 [O_2] + K_a [H^+] + K_a K_2 [H^+][O_2]} \tag{5.30}$$

where $K_1 = k_1/k_2$ and $K_2 = k_4/k_6$. Equations 5.26 and 5.30 are similar mathematically and conceptually to monosubstrate and bisubstrate Michaelis-Mention enzyme kinetics, respectively. Equation 5.30 predicts fractional orders in both the hydrogen concentration and dissolved oxygen concentration.

In all likelihood the rate of dissolution is a function of all three mechanistic pathways. That is: diffusion, solution phase and surface phase reactions may occur simultaneously to give the overall rate of oxidation. Additional experimental work is needed to determine the primary mechanistic pathways and specific rate constants involved.

## 5.2. Dissolution of Alumino-Silicate Minerals

The incongruent dissolution of alumino-silicate minerals containing up to 4.0% sulfur and 1.5% combined Cu, Ni as sulfides within interstitial spaces was investigated in well-mixed batch reactors at 20°C and atmospheric pressure. The kinetic results for the abiotic dissolution of plagioclase (PL) present in Duluth Gabbro can be summarized by the following empirical rate expressions:

$$\frac{-d[PL]}{dt} = \frac{d[Ca^{+2}]}{dt} = k_1 A_s^{2.0} [H^+]^{2.9} [CIT]^{0.3} \qquad (5.31)$$

and

$$\frac{-d[PL]}{dt} = \frac{d[Mg^{+2}]}{dt} = k_2 A_s^{0.5} [H^+]^{.14} \qquad (5.32)$$

where $A_s$ = surface area, CIT = citrate and $H^+$ = hydrogen ion. Unlike the case of pentlandite dissolution described by equations (5.1-5.3), silicate mineral dissolution is not dependent on the dissolved oxygen $(O_2)$ concentration in aqueous solution. However, pH solution may change as a result of oxidative dissolution of metal sulfides which will alter the rate and extent of silicate dissolution. Several qualitative differences were observed in the release characteristics of $Ca^{+2}$ and $Mg^{+2}$ to solution indicating that they are bound differently in the gabbro rock. Firstly, the reaction orders observed for $Ca^{+2}$ release as a function of $A_s$ (2.0) and $H^+$ (2.9) were significantly greater than the corresponding orders for $Mg^{+2}$ release (As, 0.5; $H^+$, .14). Secondly, the release of $Mg^{+2}$ to solution was not dependent on citrate concentration whereas $Ca^{+2}$ release was fractionally dependent. This behavior was observed even though stability constants for the $Ca^{+2}$-citrate and $Mg^{+2}$-citrate complexes are similar. Thirdly, the rate of $Ca^{+2}$ release under all experimental conditions exceeded $Mg^{+2}$ release rates by up to $10^2$.

Given this information, it is apparent that $Ca^{+2}$ and $Mg^{+2}$ are bound in different mineral forms. The principal $Ca^{+2}$-bearing mineral is plagioclase which represents 47 to 64% of the rock by weight. Principal $Mg^{+2}$ minerals are olivine, clinopyroxene and biotite. In each of the above named cases, $Ca^{+2}$ is the cation associated with the silicate mineral maintaining neutrality, while $Mg^{+2}$ is a structural component of the mineral lattice. Therefore, the respective associations of $Ca^{+2}$ and $Mg^{+2}$ in Duluth Gabbro are borne out by the observed release behavior to solution.

A summary of the $Ca^{+2}$ and $Mg^{+2}$ kinetic constants are given below for parametric variations of As, pH, u, $O_2$, CIT, PHTA:

|  | $k_{Ca}+2$ ($\times 10^5$ moles.sec$^{-1}$.g$^{-1}$) | $k_{Mg}+2$ ($\times 10^6$ moles.sec$^{-1}$.g$^{-1}$) |
|---|---|---|
| As | .009-1.1 | .008-0.9 |
| pH | .1 - .2 | .26-.58 |
| u | .43-.52 | .72-1.1 |
| $O_2$ | .4 - .9 | .35- .8 |
| CITRATE | .8 -2.1 | .6 - 1.3 |
| PHTHALATE | .3 - .7 | .6 - 1.6 |

Under natural environmental conditions, the $Ca^{+2}$ release rate is in the range of 0.1-1 mole.g$^{-1}$.sec$^{-1}$, while the $Mg^{+2}$ release rate is $\sim$ 0.21-1.5 mole .sec$^{-1}$.g$^{-1}$. The slower release rates observed for $Mg^{+2}$ release as compared to $Ca^{+2}$ are a result of smaller concentrations in the bulk solid and occurrence in different mineral phases. The principal controls on the buildup of $Ca^{+2}$ and $Mg^{+2}$ in solution are pH and binding ligands. The occurrence of natural organic ligands in water contacting plagioclase minerals will increase the rate and extent of weathering (dissolution). The organic ligand may prevent the buildup of the secondary product layer, thereby eliminating solute diffusion through the layer as a rate-limiting step. Decreasing solution pH to less than 5 may cause similar effects.

The shapes of the $Ca^{+2}$ and $Mg^{+2}$ release curves with time are consistent

with the mechanism of aluminosilicate minerals proposed by Busenberg and Clemency (34). However, the complexity of the Gabbro rock leached in batch reactors precludes the proposed mechanism from being fully substantiated. According to Busenberg and Clemency (34), the dissolution of aluminosilicate minerals can be explained by a four-stage kinetic process in which the initial step is the  exchange of solution protons for surface cations followed by the concurrent release of structural cations and silicic acid. In the second stage lasting $\sim$ 50 hours, silicic acid reacts with newly-formed amorphous $Al(OH)_3$ at the solid surface to form a slightly-soluble product layer consisting of microcrystalline gibbsite or halloysite (hydrated form of kaolinite). The third stage is parabolic, lasts up to 19 days and represents a diffusion-limited transport step. The fourth stage, lasting beyond 21 days, exhibits linear kinetics in which the rate of formation of the secondary product layer equals the rate at which the layer is destroyed by dissolution or fragmentation (32). Cation release curves were similar to those previously observed (34) and likely represent similar processes. Although parabolic kinetics are suspected after $\sim$ 50 hours in our studies, insufficient data points were obtained to verify this hypothesis.

The results of parametric studies of the dissolution of aluminosilicate minerals indicate that weathering increases with increasing particle surface area, acidity, pe, solution ionic strength and presence of organic ligands.

# References

1. Eger, P., Lapakko, K., "Leaching Metal Transport and Metal Pathways in the Field," Final Report submitted to the Environmental Quality Council from the Cu-Ni Regional Study (1979).

2. Hoffmann, M.R., Yost, E.C., Rastetter, D.R., Eisenreich, S.J., "Characterization of Soluble and Collordol Phase Organo-metallic Complexes by Ultrafiltration: A Mass Balance Approach," submitted to Enriron. Sci. Tech. (1979).

3. Murr, L.E., Tarma, A.E., Brierly, J.A., "Metallurgical Applications of Leaching and Related Microbiological Phenomena," Academic Press, New York, (1978).

4. Wadsworth, M.E., "Advances in the Leaching of Sulfide Minerals," Min. Sci. Eng., 4, 36 (1972).

5. Roman, R.J., Benner, B.R., "The Dissolution of Copper Concentrates," Min. Sci. Eng., 5, 3 (1973).

6. Dutrizae, J.E., MacDonald, R.J.C., "Ferric Ion as a Leaching Medium," Min. Sci. Eng., 6, 59 (1974).

7. Eisenreich, S.J., Hoffmann, M.R., Iwasaki, I., Bydalek, T.J., "Metal Sulfide Leaching Potential in the Duluth Gabbro Complex," Report submitted to the Cu-Ni Regional Study of the Minnesota State Planning Agency, 130 pages (1976).

8. Singer, P.C., Stumm, W., "Acid Mine Drainage: The Rate Determining Step," Science, 167, 1121 (1970).

9. Peters, E., "Thermodynamic and Kinetic Factors in the Leaching of Sulfide Minerals from Ore Deposits and Dumps," AIME Short Course on Bio-Extractive Mining, Denver, Colorado (1970).

10. Locher, L.D., deBruyn, P.L., "The Kinetics of Dissolution of II-VI Semiconductor Compounds in Non-oxidizing Acids," J. Electrochem. Soc., 116, 1659 (1969).

11. Pankow, J.F., "The Dissolution Rates and Mechanisms of Tetragonal Ferrous Sulfide in Anoxic Aqueous Systems," Ph.D. Thesis, California Institute of Technology, 148 pages (1978).

12. Nelson, M., "The Oxidation Dissolution of Ferrous Monosulfides and the Behavior of Associated Trace Metals," Ph.D. Thesis, Stanford University, Palo Alto, CA (1977).

13. Stumm, W., Lee, G., "Oxygenation of Ferrous Iron," Ind. Eng. Chem., 53, 143, (1961).

14. Chen, K.Y., Morris, J.C., "Kinetics of the Oxidationof Aqueous Sulfide by $O_2$, Environ. Sci. Tech., 6, 529 (1972).

15. Madsen, B.W., Wadsworth, M.E., Graves, R.D., "Application of a Mixed Kinetics Model to the Leaching of Low Grade Copper Sulfide Ores," Trans. Soc. Min. Eng. A.I.M.E., 258, 69 (1975).

16. Dutrizer, J.E., MacDonald, R.J.C. and Ingraham, T.R., "The Kinetics of Dissolution of Cubanite in Aqueous Ferric Sulphate Solutions," Metall. Trans., 1, 3083 (1970).

17. Dutrizar, J.E., MacDonald, R.J.C., "Percolation Leaching of Pentlandite Ore, Can. Min. Met. Bull., 64, 108 (1974).

18. Sato, M., "Oxidation of Sulfur Orebodies II. Oxidation Mechanism of Sulfide Minerals at 25°C," Econ. Geol., 55, 1202 (1960).

19. Bryner, L.C., Anerson, R., "Microorganisms in Leaching Sulfide Minerals," Ind. Eng. Chem., 49, 1721 (1957).

20. Ichikuni, M., "The Dissolution of Sulfide Minerals in Various Media III. Factors Intervening in the Dissolution of Chalcopyrite," Bull. Chem. Soc. Japan, 33, 1159 (1960).

21. Baher, W.E., "The Role of Humic Acids from Tasmanian Podzolu Soils in Mineral Degradation and Metal Mobilization," Geochem. Cosmochem. Acta, 37, 269 (1973).

22. Schalscha, E.B., Appelt, H., Schatz, A. "Chelation as a Weathering Mechanism I. Effect of Complexing Agents on the Sobulization of Iron from Minerals and Granodiorite," Geochem. Cosmochim. Acta.

23. Rashid, M.A., "Role of Quinone Groups in Solubility and Complexing of Metals in Sediments and Soils," Chem. Geol., 9, 241 (1972).

24. Gardner, L.R., "Organic versus Inorganic Trace Metal Complexes in Sulfidic Marine Waters," Geochim. Cosmochim. Acta, 38, 1297 (1974).

25. Gruner, J.W., "The Oregin of Sedimentary Iron Formations: The Biwabik Formation of the Mesabi Range," Econ. Geol., 17, 407 (1922).

26. Stumm. W., Morgau, J.J., "Aquatic Chemistry," Wiley-Interscience, New York (1970).

27. Garrels, R.M., Howard, P., "Reactions of Feldspar and Mica with Water at Low Temperature and Pressure," Clays Clay Mineral, 6, 68-88 (1957).

28. Wollast, R., "Kinetics of the Alteration of K-Feldspar in Buffered Solutions at Low Temperature, Geochim. Cosmochim. Acta, 31, 635-648 (1967).

29. Helgeson, H., "Kinetics of Mass Transfer Among Silicates and Aqueous Solutions," Geochim. Cosmochim. Acta, 35, 421-469 (1971).

30. Helgeson, H., "Kinetics of Mass Transfer Among Silicates and Aqueous Solutions: Correction and Clarification", Geochim. Cosmochim. Acta, 36, 1067-1070 (1972).

31. Luce, R.W., Bartlett, R.W., Parks, G.A., "Dissolution Kinetics of Magnesium Silicates," Geochim. Cosmochim. Acta, 36, 35-50 (1972).

32. Paces, T., "Steady-State Kinetics and Equilibrium Between Ground Water and Granitic Rock," Geochim. Cosmochim. Acta, 37, 2641-2663 (1973).

33. Petcovic, R., "Rate Control in Feldspar Dissolution-II. The Protective Effect of Precipitates," Geochim. Cosmochim. Acta, 40, 1509-1521 (1976).

34. Busenberg, E., Clemency, C.V., "The Dissolution Kinetics of Feldspars at $25^{0}$C and 1 Atm $CO_2$ Partial Pressure," Geochim. Comochim. Acta, 40, 41-49 (1976).

35. Busenberg, E., "The Products of the Interaction of Feldspars with Aqueous Solutions at $25^{0}$C," Geochim. Cosmochim. Acta, 42, 1679-1686 (1978).

36. Dayal, R., "Kinetics of Silica Sorption and Clay Dissolution Reactions at 1 and 670 Atm.", Geochim. Cosmochim. Acta, 41, 135-141 (1977).

37. "Standard Methods: For the Examination of Water and Wastewater," 14th Edition, APHA-AWWA-WPCF, Amer. Public Health Assoc., Washington, D.C., (1975).

38. Environmental Protection Agency, "Methods for Chemical Analysis of Water and Wastes," 298 pp., 1976.

39. Frost, A.A., Pearson, R.G., "Kinetics and Mechanism," Wiley & Sons, Inc., New York (1961).

40. Hoffmann, M.R., Lim, B.C.H., "Kinetics and Mechanism of the Oxidation of Sulfide by Oxygen: Catalysis by Homogeneous Metal Phthalocyamine Complexes, In Press, Environ. Sci. Tech. (1979).

41. Morel, F.M., Morgan, J.J., Environ. Sci. Tech., 6, 58 (1972).

42. Theis, T.L., Singer, P.C., "The Stabilization of Ferrous Iron by Organic Compounds in Natural Waters," in Trace Metals and Metal-Organic Interactions in Natural Waters, Ann Arbor Science, Ann Arbor, MI (1973).

43. Chen, K.Y., Morris, J.C., J. Sanit. Eng. Div., ASCE, 98, 215 (1972).

44. Colton, F.A., Wilkinson, G., "Advanced inorganic Chemistry," Wiley-Interscience, New York, p. 596 (1972).

45. Barton, A. Wilde, N., Trans. Farad. Soc., 67, 3590 (1971).

46. Nerust, W., Z. Physik. Chem., 47, 52 (1904).
47. Torma, A.E., Sakaguchi, H., "Relation between the Solubility Product and the Rate of Metal Sulfide Oxidation by Throbacillus ferrooxiduns," J. Ferment. Technol., 56, 173 (1978).
48. Glasstone, S., Lardler, K.J., Eyring. H., "The Theory of Rate Processes," McGraw-Hill, New York (1941).

## Table A.1
### Experiment 2

REACTOR 1:   2 g/l unmineralized-200 mesh gabbro, air diffusion

| TIME (Hrs) | pH | SO$_4$ (mg/l) | Ni (µg/l) | Cu (µg/l) | Fe (µg/l) | Ca (mg/l) | Mg (mg/l) | Si (mg/l) |
|---|---|---|---|---|---|---|---|---|
| 0.75 | 3.66 | 2.8 | 100.4 | 178.2 | 4240 | 2.36 | 0.35 | 6.43 |
| 3.25 | 3.82 | 3.0 | 111.2 | 156.2 | 5550 | 2.46 | 0.53 | 1.10 |
| 6.00 | 3.89 | 2.9 | 115.3 | 174.9 | 5910 | 2.21 | 0.57 | 1.10 |
| 26.75 | 4.00 | 2.6 | 130.8 | 232.1 | 6780 | 2.34 | 0.66 | 1.29 |
| 49.50 | 4.20 | 3.6 | 144.8 | 254.1 | 7140 | 2.45 | 0.80 | 1.81 |
| 146.0 | 4.41 | 3.6 | 210.0 | 307.3 | 7580 | 2.52 | 0.98 | 1.83 |
| 319.3 | 4.42 | 3.6 | 326.6 | 378.0 | 7520 | 2.60 | 1.0 | 1.84 |
| 507 | 4.51 | 3.4 | 460.0 | 436.5 | 7980 | 2.74 | 1.01 | 1.92 |
| 748 | 4.48 | 4.8 | 564.0 | 526.6 | 8000 | 2.88 | 1.13 | 2.22 |
| 1-AD-2 | | 0 | 5.5 | 17.2 | 440 | 0.30 | 0.07 | 0.98 |

REACTOR 2:   1.0 g/l unmineralized-200 mesh gabbro, air diffusion

| TIME (Hrs) | pH | SO$_4$ (mg/l) | Ni (µg/l) | Cu (µg/l) | Fe (µg/l) | Ca (mg/l) | Mg (mg/l) | Si (mg/l) |
|---|---|---|---|---|---|---|---|---|
| 0.75 | 7.10 | 2.6 | 16.6 | 2.2 | 15.7 | 3.71 | 0.34 | 0.86 |
| 3.25 | 7.19 | 2.5 | 16.0 | ND | 16.9 | 3.9 | 0.7 | 1.00 |
| 6.0 | 7.18 | 2.5 | 31.4 | 0.3 | 13.3 | 4.23 | 1.02 | 24.56 |
| 26.75 | 7.21 | 2.5 | 102.2 | ND | 8.5 | 4.56 | 1.45 | 1.53 |
| 49.50 | 7.41 | 3.6 | 154.4 | ND | 22.2 | 4.83 | 1.10 | 1.89 |
| 146.0 | 7.39 | 3.3 | 298.8 | 0.6 | 16.6 | 5.26 | 1.21 | 2.54 |
| 319.3 | 7.11 | 9.9 | 373.0 | 1.0 | 16.8 | 5.73 | 1.15 | 3.36 |
| 507 | 7.12 | 12.9 | 410.8 | 2.0 | 17.8 | 5.86 | 1.40 | 4.15 |
| 748 | 6.90 | 13.7 | 317.4 | ND | 16.5 | 6.14 | 1.83 | 3.71 |
| 2-AD-2 | | 3.8 | 242.5 | 105.2 | 1650 | | | 1.32 |

REACTOR 3:   50 g/l unmineralized-200 mesh gabbro, air diffusion

| TIME (Hrs) | pH | SO$_4$ (mg/l) | Ni (µg/l) | Cu (µg/l) | Fe (µg/l) | Ca (mg/l) | Mg (mg/l) | Si (mg/l) |
|---|---|---|---|---|---|---|---|---|
| 0.75 | 8.19 | 3.0 | 7.5 | 0.8 | 12.4 | 4.53 | 0.71 | 1.62 |
| 3.25 | 7.88 | 3.7 | 4.6 | 0.1 | 6.9 | 6.42 | 1.00 | 0.83 |
| 6.0 | 7.92 | 4.4 | 8.1 | ND | 6.2 | 8.75 | 1.31 | 1.22 |
| 26.75 | 7.89 | 5.2 | 89.5 | 3.7 | 45.6 | 12.87 | 2.20 | 2.97 |
| 49.50 | 8.01 | 7.0 | 95.7 | 0.1 | 9.5 | 13.69 | 2.40 | 2.91 |
| 146.0 | 8.02 | 10.5 | 107.1 | 0.7 | 11.4 | 14.23 | 3.10 | 3.77 |
| 319.3 | 7.81 | 20.4 | 110.8 | 0.6 | 22.3 | 15.33 | 3.85 | 3.76 |
| 507.0 | 7.49 | 53.3 | 145.6 | ND | 19.7 | 17.45 | 4.60 | 4.23 |
| 748 | 7.55 | 110 | 127.0 | 1.9 | 14.5 | 18.23 | 5.10 | 4.71 |
| 3-AD-2 | | 3.8 | 707.7 | 1009 | 5660 | 12.45 | 1.66 | 0.45 |

REACTOR 4:  100 g/l unmineralized-200 mesh gabbro, air diffusion

| TIME (Hrs) | pH | SO$_4$ (mg/l) | Ni (µg/l) | Cu (µg/l) | Fe (µg/l) | Ca (mg/l) | Mg (mg/l) | Si (mg/l) |
|---|---|---|---|---|---|---|---|---|
| 0.75 | 8.80 | 6.4 | 12.3 | 6.1 | 11.6 | 4.45 | 1.05 | 1.27 |
| 3.25 | 8.50 | 6.0 | 1.4 | ND | 44.2 | 5.17 | 1.23 | 1.52 |
| 6.00 | 8.41 | 7.6 | 2.3 | ND | 6.4 | 6.50 | 1.60 | 1.47 |
| 26.75 | 8.12 | 10.3 | 47.1 | 0.8 | 8.3 | 13.35 | 4.00 | 2.42 |
| 49.50 | 8.22 | 11.8 | 66.2 | 1.2 | 11.0 | 15.63 | 4.65 | 2.72 |
| 146.00 | 8.21 | 16.0 | 77.8 | 1.2 | 11.0 | 16.79 | 5.00 | 3.87 |
| 319.30 | 8.04 | 59.5 | 113.5 | 1.3 | 10.3 | 22.75 | 6.40 | 4.44 |
| 507.00 | 8.02 | 128.0 | 196.1 | ND | 9.6 | 31.13 | 7.50 | 4.28 |
| 748.00 | 7.87 | 148.0 | 145.5 | ND | 14.3 | 28.38 | 8.40 | 4.75 |
| 4-AD-2 | | 3.7 | 2253.8 | 5850.0 | 13,272.0 | | | 14.66 |

REACTOR 5:  2 g/l unmineralized-200 mesh gabbro, N$_2$ diffusion

| TIME (Hrs) | pH | SO$_4$ (mg/l) | Ni (µg/l) | Cu (µg/l) | Fe (µg/l) | Ca (mg/l) | Mg (mg/l) | Si (mg/l) |
|---|---|---|---|---|---|---|---|---|
| 0.75 | 4.27 | 2.9 | 56.5 | 2.0 | 5010 | | 0.47 | 2.38 |
| 3.25 | 4.79 | 3.0 | 51.1 | 7.9 | 6580 | | 0.49 | 0.96 |
| 6.00 | 5.00 | 3.0 | 56.8 | 9.7 | 6920 | | 0.78 | 0.96 |
| 26.75 | 5.32 | 2.5 | 71.8 | 10.8 | 7330 | 2.05 | 0.78 | 1.22 |
| 49.50 | 5.69 | 3.6 | 69.8 | 2.1 | 7250 | | 0.74 | 1.33 |
| 146.00 | 5.72 | 3.6 | 101.8 | 1.7 | 7240 | | 0.77 | 1.89 |
| 319.30 | 5.18 | 3.7 | 230.6 | 41.8 | 6880 | | 0.80 | 1.67 |
| 507.00 | 5.12 | 3.5 | 330.4 | 46.1 | 6910 | 2.05 | 0.83 | 1.38 |
| 748.00 | 5.04 | 3.8 | 342.4 | 49.1 | 7210 | | 0.92 | 2.30 |
| 5-AD-2 | | 0 | 9.8 | 19.2 | 760 | 0.30 | 0.12 | 0.44 |

REACTOR 6:  50 g/l unmineralized-200 mesh gabbro, N$_2$ diffusion

| TIME (Hrs) | pH | SO$_4$ (mg/l) | Ni (µg/l) | Cu (µg/l) | Fe (µg/l) | Ca (mg/l) | Mg (mg/l) | Si (mg/l) |
|---|---|---|---|---|---|---|---|---|
| 0.75 | 7.21 | 3.6 | 10.1 | ND | 22.4 | 9.97 | 2.00 | 1.21 |
| 3.25 | 7.51 | 2.7 | 4.5 | ND | 37.3 | 11.20 | 2.02 | 1.36 |
| 6.00 | 7.51 | 4.6 | 5.8 | ND | 42.9 | 11.93 | 2.55 | 1.24 |
| 26.75 | 7.61 | 4.9 | 3.6 | ND | 41.4 | 11.63 | 3.05 | 1.23 |
| 49.50 | 7.93 | 6.0 | 3.7 | ND | 45.7 | 11.10 | 3.40 | 2.61 |
| 146.00 | 8.12 | 6.7 | 3.6 | ND | 48.2 | 11.73 | 4.05 | 3.09 |
| 319.30 | 7.85 | 10.1 | 17.1 | 1.6 | 39.1 | 13.03 | 4.80 | 3.34 |
| 507.00 | 7.51 | 25.1 | 15.2 | ND | 31.1 | 13.75 | 5.30 | 3.02 |
| 748.00 | 7.43 | 29.1 | 11.5 | ND | 33.4 | 13.60 | 5.05 | 3.13 |
| 6-AD-2 | | 3.5 | 501.8 | 635.0 | 5150.0 | 10.40 | 1.76 | .90 |

## Table A.2
## Experiment 3

REACTOR 1:  2.86 g/l unmineralized-200 mesh gabbro, air diffusion

| TIME (Hrs) | pH | SO$_4$ (mg/l) | Ni (μg/l) | Cu (μg/l) | Fe (mg/l) | Ca (mg/l) | Mg (mg/l) |
|---|---|---|---|---|---|---|---|
| 0.5 | 6.89 | 0 | 2.6 | 1.7 | 0.022 | 1.05 | 0.140 |
| 6.0 | 6.86 | 0 | 10.3 | 1.1 | 0.009 | 1.30 | 0.260 |
| 24.5 | 6.80 | 2.9 | 39.7 | 1.5 | <0.005 | 1.43 | 0.341 |
| 48.0 | 6.94 | 0 | 88.9 | 1.7 | 0.020 | 1.50 | 0.386 |
| 168.5 | 6.86 | 0 | 285.0 | 1.5 | <0.005 | 1.85 | 0.465 |
| 335.0 | 6.80 | 3.2 | 460.0 | 4.1 | 0.026 | 2.05 | 0.574 |
| 480.0 | 6.90 | 3.6 | 590.0 | 1.2 | <0.005 | 2.17 | 0.614 |
| 651.0 | 6.86 | 2.5 | 562.0 | 1.8 | <0.006 | 2.30 | 0.652 |
| 987.5 | 6.90 | 5.3 | 586.0 | 4.6 | <0.005 | 2.46 | 0.732 |
| 1-AD-3 | | | 117.0 | 66.1 | 0.640 | 2.50 | 0.128 |

REACTOR 2:  2.86 g/l unmineralized-200 mesh gabbro; air diffusion; add 1.6 ml 1N HClO$_4$

| TIME (Hrs) | pH | SO$_4$ (mg/l) | Ni (μg/l) | Cu (μg/l) | Fe (mg/l) | Ca (mg/l) | Mg (mg/l) |
|---|---|---|---|---|---|---|---|
| 0.5 | 4.09 | 3.2 | 42.9 | 74.6 | 3.96 | 2.28 | 0.605 |
| 6.0 | 4.52 | 3.3 | 66.0 | 92.7 | 6.06 | 2.34 | 0.708 |
| 24.5 | 4.72 | 3.2 | 94.6 | 101.0 | 6.60 | 2.46 | 0.805 |
| 48.0 | 4.80 | 3.1 | 156.0 | 109.0 | 6.63 | 2.28 | 0.793 |
| 168.5 | 4.76 | 3.1 | 392.0 | 153.0 | 6.41 | 2.39 | 0.968 |
| 335.0 | 4.73 | 4.0 | 548.0 | 182.0 | 6.39 | 2.61 | 1.020 |
| 480.0 | 4.71 | 3.6 | 720.0 | 205.0 | 6.25 | 2.57 | 1.040 |
| 651.0 | 4.67 | 3.5 | 824.0 | 240.0 | 6.71 | 2.81 | 1.150 |
| 987.5 | 4.59 | 7.0 | 1040.0 | 270.0 | 5.92 | 2.94 | 1.220 |
| 2-AD-3 | | 0 | ND | 10.4 | 0.51 | 0.24 | 0.011 |
| B-AD-3 | | 0 | | | | | |

REACTOR 3:  2.86 g/l unmineralized-200 mesh gabbro; air diffusion; add 3.2 ml 1 N HClO

| TIME (Hrs) | pH | SO$_4$ (mg/l) | Ni (μg/l) | Cu (μg/l) | Fe (mg/l) | Ca (mg/l) | Mg (mg/l) |
|---|---|---|---|---|---|---|---|
| 0.5 | 3.57 | 3.2 | 50.9 | 87.2 | 7.02 | 4.14 | 0.713 |
| 6.0 | 3.76 | 3.3 | 80.6 | 149.0 | 9.38 | 4.30 | 0.899 |
| 24.5 | 3.92 | 3.3 | 99.5 | 187.0 | 10.70 | 4.46 | 1.170 |
| 48.0 | 4.06 | 4.1 | 136.0 | 205.0 | 11.70 | 4.38 | 1.350 |
| 168.5 | 4.30 | 3.2 | 268.0 | 227.0 | 12.50 | 4.98 | 1.600 |
| 335.0 | 4.40 | 3.9 | 440.0 | 265.0 | 12.50 | 5.25 | 1.660 |
| 480.0 | 4.44 | 4.0 | 562.0 | 289.0 | 13.00 | 5.30 | 1.700 |
| 651.0 | 4.45 | 4.7 | 679.0 | 317.0 | 13.00 | 5.33 | 1.780 |
| 987.5 | 4.43 | 6.2 | 715.0 | 310.0 | 12.20 | 5.95 | 1.820 |
| 3-AD-3 | | 0 | 0.4 | 11.6 | 0.51 | 0.20 | 0.033 |

## Table A.2
### Experiment 3

REACTOR 4:  2.86 g/l unmineralized-200 mesh gabbro; air diffusion;
add 4.8 ml 1 $\underline{N}$ HClO$_4$

| TIME (Hrs) | pH | SO$_4$ (mg/l) | Ni (µg/l) | Cu (µg/l) | Fe (mg/l) | Ca (mg/l) | Ma (mg/l) |
|---|---|---|---|---|---|---|---|
| 0.5 | 3.25 | 3.3 | 57.2 | 61.4 | 7.67 | 5.63 | 0.803 |
| 6.0 | 3.41 | 3.4 | 82.3 | 121.0 | 12.00 | 6.21 | 1.120 |
| 24.5 | 3.53 | 3.5 | 101.0 | 161.0 | 13.90 | 6.84 | 1.470 |
| 48.0 | 3.63 | 4.1 | 116.0 | 174.0 | 15.90 | 7.17 | 1.760 |
| 168.5 | 3.87 | 4.1 | 222.0 | 198.0 | 17.70 | 7.56 | 2.380 |
| 335.0 | 3.99 | 4.1 | 380.0 | 226.0 | 18.30 | 8.12 | 2.780 |
| 480.0 | 4.05 | 3.8 | 494.0 | 258.0 | 19.40 | 8.36 | 2.910 |
| 651.0 | 4.10 | 5.2 | 662.0 | 291.0 | 20.50 | 8.70 | 3.240 |
| 987.5 | 4.15 | 7.2 | 708.0 | 274.0 | 21.20 | 9.42 | 3.580 |
| 4-AD-3 | | 0 | 1.9 | 12.2 | 0.74 | 0.26 | 0.060 |


REACTOR 5:  2.86 g/l unmineralized-200 mesh gabbro; air diffusion;
citrate addition; 1.29 * 10$^{-4}$ $\underline{M}$

| TIME (Hrs) | pH | SO$_4$ (mg/l) | Ni (µg/l) | Cu (µg/l) | Fe (mg/l) | Ca (mg/l) | Ma (mg/l) |
|---|---|---|---|---|---|---|---|
| 0.5 | 7.24 | 0 | 13.2 | 9.8 | 9.064 | 2.61 | 0.258 |
| 6.0 | 7.01 | 0 | 30.6 | 16.3 | 1.580 | 2.68 | 0.356 |
| 24.5 | 7.23 | 2.7 | 68.6 | 32.4 | 1.980 | 3.08 | 0.480 |
| 48.0 | 7.30 | 3.6 | 130.0 | 45.5 | 2.770 | 3.15 | 0.540 |
| 168.5 | 7.64 | 2.9 | 99.5 | 1.8 | 0.143 | 3.84 | 0.627 |
| 335.0 | 7.66 | 2.5 | 110.0 | 2.4 | 0.041 | 4.06 | 0.644 |
| 480.0 | 7.63 | 2.7 | 110.0 | 1.8 | 0.034 | 4.21 | 0.704 |
| 651.0 | 7.58 | 2.9 | 122.0 | 2.0 | 0.028 | 4.43 | 0.692 |
| 987.5 | 7.55 | 5.3 | 114.0 | 1.7 | 0.024 | 4.72 | 0.720 |
| 5-AD-3 | | 0 | 219.0 | 107.5 | 0.940 | 3.88 | 0.121 |


REACTOR 6:  2.86 g/l unmineralized-200 mesh gabbro; air diffusion;
citrate addition; 1.29 * 10$^{-3}$ $\underline{M}$

| TIME (Hrs) | pH | SO$_4$ (mg/l) | Ni (µg/l) | Cu (µg/l) | Fe (mg/l) | Ca (mg/l) | Ma (mg/l) |
|---|---|---|---|---|---|---|---|
| 0.5 | 7.95 | 3.0 | 17.5 | 19.7 | 0.95 | 2.94 | 0.258 |
| 6.0 | 7.61 | 3.0 | 40.0 | 44.6 | 3.79 | 3.08 | 0.430 |
| 24.5 | 7.63 | 3.7 | 137.0 | 88.5 | 6.51 | 3.26 | 0.711 |
| 48.0 | 7.74 | 4.3 | 277.0 | 118.0 | 7.46 | 3.44 | 0.892 |
| 168.5 | 8.25 | 3.8 | 737.0 | 162.0 | 8.28 | 3.52 | 1.060 |
| 335.0 | 8.33 | 4.2 | 1010.0 | 175.0 | 8.13 | 3.59 | 1.080 |
| 480.0 | 8.38 | 3.8 | 1070.0 | 181.0 | 8.00 | 3.75 | 1.050 |
| 651.0 | 8.38 | 4.0 | 1050.0 | 213.0 | 6.80 | 3.95 | 1.070 |
| 987.5 | 8.49 | 3.4 | 1250.0 | 226.0 | 6.66 | 4.17 | 1.140 |
| 6-AD-3 | | 0 | 117.0 | 54.0 | 1.71 | 3.63 | 0.322 |

## Table A.3
## Experiment 4

### REACTOR 1:  2.86 g/l -200 mesh mineralized gabbro

| TIME (Hrs) | pH | SO4 (PPM) | Ni (PPB) | Cu (PPB) | Fe (PPB) | Ca (PPM) | Mg (PPM) |
|---|---|---|---|---|---|---|---|
| 0.5 | 6.72 | 4.6 | 7.8 | 0 | 6.45 | 0.44 | 0.080 |
| 5.5 | 6.80 | 4.6 | 17.2 | 0.3 | 0.74 | 0.65 | 0.132 |
| 25.0 | 6.75 | 4.5 | 42.0 | 0.1 | <5.00 | 0.72 | 0.178 |
| 48.0 | 6.57 | 4.5 | 69.5 | 0.2 | 0.62 | 0.71 | 0.188 |
| 163.5 | 6.65 | 5.1 | 194.0 | 0.6 | 9.02 | 0.78 | 0.258 |
| 336.0 | 6.50 | 5.5 | 460.0 | 1.4 | 8.09 | 0.92 | 0.326 |
| 526.0 | 6.02 | 7.4 | 839.0 | 8.8 | <5.00 | 0.98 | 0.450 |
| 672.0 | 5.75 | 9.0 | 1070.0 | 34.8 | 10.90 | 1.10 | 0.443 |
| 891.0 | 5.44 | 9.8 | 1510.0 | 92.5 | 65.00 | 1.23 | 0.532 |
| 1-AD-4 | | 3.9 | 19.9 | 18.6 | 95.60 | 0.32 | 0.046 |

### REACTOR 2:  2.86 g/l $^{+}$200- $^{-}$40 mesh mineralized gabbro

| TIME (Hrs) | pH | SO4 (PPM) | Ni (PPB) | Cu (PPB) | Fe (PPB) | Ca (PPM) | Mg (PPM) |
|---|---|---|---|---|---|---|---|
| 0.5 | 6.03 | 4.0 | 3.4 | 0.3 | 2.5 | 0.18 | 0.016 |
| 5.5 | 6.28 | 3.9 | 7.2 | 0.6 | 17.7 | 0.29 | 0.064 |
| 25.0 | 6.44 | 3.9 | 11.1 | 1.0 | 12.5 | 0.36 | 0.070 |
| 48.0 | 6.43 | 3.8 | 18.7 | 0.1 | 2.7 | 0.35 | 0.092 |
| 163.5 | 6.64 | 4.2 | 62.4 | 1.5 | 22.8 | 0.47 | 0.120 |
| 336.0 | 6.55 | 4.1 | 122.0 | 0.1 | 0.8 | 0.62 | 0.123 |
| 526.0 | 6.38 | 4.3 | 221.0 | 0.6 | 1.7 | 0.66 | 0.174 |
| 672.0 | 6.35 | 4.5 | 293.0 | 2.6 | <5.0 | 0.35 | 0.162 |
| 891.0 | 6.33 | 4.6 | 384.0 | 4.8 | 1.6 | 0.68 | 0.190 |
| 2-AD-4 | | | | | | | |

### REACTOR 3:  2.86 g/l $^{+}$40- $^{-}$20 mesh mineralized gabbro

| TIME (Hrs) | pH | SO4 (PPM) | Ni (PPB) | Cu (PPB) | Fe (PPB) | Ca (PPM) | Mg (PPM) |
|---|---|---|---|---|---|---|---|
| 0.5 | 5.84 | 4.0 | 1.6 | 0.4 | 5.2 | 0.23 | 0.004 |
| 5.5 | 6.10 | 3.9 | 4.7 | 0.4 | 8.0 | 0.22 | 0.012 |
| 25.0 | 6.25 | 3.8 | 11.6 | 0.3 | 10.8 | 0.29 | 0.054 |
| 48.0 | 6.31 | 4.0 | 16.5 | 0.3 | 11.8 | 0.30 | 0.072 |
| 163.5 | 6.46 | 4.1 | 45.7 | 0 | 1.8 | 0.38 | 0.082 |
| 336.0 | 6.50 | 4.1 | 92.7 | 0 | 9.5 | 0.45 | 0.093 |
| 526.0 | 6.44 | 4.0 | 153.0 | 1.0 | 32.1 | 0.53 | 0.130 |
| 672.0 | 6.49 | 4.2 | 175.0 | 0.8 | <5.0 | 0.51 | 0.152 |
| 891.0 | 6.59 | 4.1 | 203.0 | 0.4 | <5.0 | 0.50 | 0.145 |
| 3-AD-4 | | 4.0 | 13.4 | 6.8 | 45.4 | 0.27 | 0.009 |

## Table A.3

### Experiment 4

REACTOR 4:   +20- -8 mesh mineralized gabbro

| TIME (Hrs) | pH | SO₄ (PPM) | Ni (PPB) | Cu (PPB) | Fe (PPB) | Ca (PPM) | Mg (PPM) |
|---|---|---|---|---|---|---|---|
| 0.5 | 5.72 | 4.0 | 2.1 | 0.2 | 4.1 | 0.22 | 0.025 |
| 5.5 | 5.93 | 3.4 | 6.6 | 1.2 | 15.2 | 0.24 | 0.026 |
| 25.0 | 5.98 | 3.3 | 10.1 | 0.7 | 27.5 | 0.27 | 0.035 |
| 48.0 | 6.03 | 3.4 | 13.3 | 0.5 | 25.2 | 0.28 | 0.041 |
| 163.5 | 6.13 | 3.3 | 33.2 | 0 | 15.0 | 0.32 | 0.047 |
| 336.0 | 6.22 | 3.4 | 60.0 | 0.6 | 2.4 | 0.33 | 0.055 |
| 526.0 | 6.25 | 3.5 | 79.6 | 0.7 | 38.0 | 0.40 | 0.093 |
| 672.0 | 6.30 | 3.5 | 86.3 | 0.4 | 4.1 | 0.42 | 0.075 |
| 891.0 | 6.52 | 3.5 | 130 | 0.7 | 5.5 | 0.42 | 0.082 |
| 4-AD-4 | | 3.4 | 7.0 | 3.2 | 59.4 | 0.22 | 0.026 |

REACTOR 5:   2.86 g/l -200 mesh unmineralized gabbro, [CIT]=$1.29 \times 10^{-4}$ $\underline{M}$

| TIME (Hrs) | pH | SO₄ (PPM) | Ni (PPB) | Cu (PPB) | Fe (PPB) | Ca (PPM) | Mg (PPM) |
|---|---|---|---|---|---|---|---|
| 0.5 | 7.24 | 5.0 | 34.2 | 16.6 | 602 | 0.66 | 0.240 |
| 6.5 | 7.30 | 4.0 | 48.3 | 21.2 | 2150 | 0.84 | 0.358 |
| 24.0 | 7.28 | 3.6 | 127 | 35.7 | 3050 | 0.86 | 0.493 |
| 49.5 | 7.42 | 3.6 | 144 | 28.9 | 2200 | 0.80 | 0.542 |
| 142.0 | 7.58 | 3.6 | 64.8 | 1.0 | 169 | 0.72 | 0.543 |
| 358.0 | 7.66 | 4.2 | 68.4 | 0.9 | 11.3 | 0.86 | 0.598 |
| 531.0 | 7.72 | 4.5 | 54.1 | 0.4 | 5.5 | 0.92 | 0.601 |
| 721.0 | 7.69 | 4.9 | 48.5 | 0.7 | <5 | 1.01 | 0.656 |
| 867.0 | 7.77 | 5.1 | 56.5 | 1.3 | <5 | 0.98 | 0.704 |
| 1088 | 7.86 | 3.6 | | | | | |
| 5-AD-4 | | | 28.5 | 36.8 | 18.1 | 0.50 | 0.030 |

REACTOR 6:   2.86 g/l -200 mesh unmineralized gabbro [CIT]=$1.29 \times 10^{-3}$ $\underline{M}$

| TIME (Hrs) | pH | SO₄ (PPM) | Ni (PPB) | Cu (PPB) | Fe (PPB) | Ca (PPM) | Mg (PPM) |
|---|---|---|---|---|---|---|---|
| 0.5 | 7.04 | 0.8 | 30.6 | 31.7 | 2300 | 1.04 | 0.408 |
| 6.5 | 7.39 | 0.8 | 65.8 | 52.5 | 5250 | 1.04 | 0.594 |
| 24.0 | 7.47 | 1.0 | 193 | 90.3 | 8200 | 1.14 | 0.832 |
| 49.5 | 7.77 | 1.0 | 353 | 106 | 9550 | 1.10 | 1.01 |
| 142.0 | 8.40 | 2.2 | 484 | 76.2 | 7250 | 0.90 | 0.882 |
| 358.0 | 8.60 | 3.4 | 6.5 | 7.1 | 181.3 | 0.82 | 0.766 |
| 531.0 | 8.61 | 2.9 | 5.3 | 9.6 | 32.5 | 0.84 | 0.810 |
| 721.0 | 8.63 | 2.8 | 5.2 | 9.9 | 9.5 | 0.84 | 0.821 |
| 867.0 | 8.68 | 4.4 | 5.1 | 9.3 | 55.4 | 0.90 | 0.826 |
| 1088 | 8.71 | | | | | | |
| 6-AD-4 | | 1.4 | 42.7 | 72.8 | 451.0 | 0.84 | 0.15 |

## Table A.4

## Experiment 5

### REACTOR 1: 2.86 g/1 mineralized-200 mesh gabbro, nitrogen diffusion

| TIME (Hrs) | pH | SO$_4$ (mg/1) | Ni (µg/1) | Cu (µg/1) | Fe (µg/1) | Ca (mg/1) | Mg (mg/1) |
|---|---|---|---|---|---|---|---|
| 0.75 | 7.98 | 2.8 | 0 | 0.3 | 20.5 | 0.66 | 0.15 |
| 5.5 | 7.33 | 2.8 | 3.4 | 1.1 | 51.2 | 1.04 | 0.28 |
| 25.5 | 7.56 | 2.8 | 3.8 | 0.8 | 12.5 | 1.26 | 0.34 |
| 53 | 7.87 | 2.8 | 16.5 | 0.4 | 1.8 | 1.32 | 0.40 |
| 168 | 8.40 | 3.0 | 7.9 | 0.7 | 6.8 | 1.32 | 0.45 |
| 363 | 7.05 | 4.4 | 24.6 | 2.0 | 8.8 | 1.38 | 0.51 |
| 502 | 7.91 | 4.9 | 30 | 2.5 | 15.4 | 1.3 | 0.5 |
| 628 | 7.79 | 6.4 | 32 | 3.0 | 13.3 | 1.1 | 0.5 |
| 817 | 7.56 | 8.2 | 22 | 1.6 | 9.7 | 1.3 | 0.5 |
| 1-AD | | | 33 | 53.7 | 280 | 1.6 | 0.3 |

### REACTOR 2: 2.86 g/1, mineralized-200 mesh gabbro, N$_2$ & air diffusion

| TIME (hrs) | pH | SO$_4$ (mg/1) | Ni (µg/1) | Cu (µg/1) | Fe (µg/1) | Ca (mg/1) | Mg (mg/1) |
|---|---|---|---|---|---|---|---|
| 0.75 | 7.25 | 4.3 | 8.1 | 4.3 | 34.1 | 1.10 | 0.18 |
| 5.5 | 7.06 | 4.3 | 15.2 | 0.8 | 6.8 | 1.26 | 0.26 |
| 25.5 | 7.10 | 4.3 | 27.0 | 2.1 | 8.4 | 1.26 | 0.34 |
| 53 | 7.18 | 4.4 | 43.7 | 0 | 0.3 | 1.43 | 0.37 |
| 168 | 7.08 | 4.6 | 110.9 | 3.6 | 2.1 | 1.26 | 0.45 |
| 363 | 6.48 | 5.1 | 199.6 | 4.1 | 0.4 | 1.54 | 0.51 |
| 502 | 6.88 | 4.6 | 268 | 18.2 | 20.6 | 1.3 | 0.5 |
| 628 | 6.95 | 5.0 | 50 | 5.1 | 10.8 | 1.2 | 0.5 |
| 817 | 6.94 | 5.1 | 26 | 2.4 | 3.7 | 1.3 | 0.6 |
| 2-AD | | | 28 | 54.4 | 200 | 0.9 | 0.1 |

### REACTOR 3: 2.86g/1 mineralized-200 mesh gabbro, air diffusion

| TIME (Hrs) | pH | SO$_4$ (mg/1) | Ni (µg/1) | Cu (µg/1) | Fe (µg/1) | Ca (mg/1) | Mg (mg/1) |
|---|---|---|---|---|---|---|---|
| 0.75 | 6.58 | 3.4 | 27.0 | 1.6 | 12.4 | 1.04 | 0.16 |
| 5 | 6.86 | 3.3 | 42.7 | 3.1 | 11.7 | 1.32 | 0.22 |
| 24 | 6.80 | 3.5 | 61.3 | 2.2 | 2.4 | 1.32 | 0.24 |
| 46 | 6.76 | 3.5 | 92.4 | 2.1 | 1.4 | 1.48 | 0.25 |
| 192 | 6.45 | 4.0 | 237.4 | 2.1 | 0.4 | 1.1 | 0.32 |
| 356 | 6.33 | 4.6 | 351 | 4.2 | 2.0 | 1.60 | 0.37 |
| 523 | 5.95 | 5.3 | 454 | 13.2 | 6.4 | 1.82 | 0.42 |
| 690 | 5.97 | 6.8 | 595 | 27.6 | 8.7 | 1.92 | 0.46 |
| 860 | 5.54 | 7.9 | 721 | 48.5 | 10.1 | 1.87 | 0.50 |
| 886 | | | 724 | 50.8 | 12.2 | 2.09 | 0.57 |
| 3-AD-5 | - | - | 53.4 | 54.8 | 151.2 | 1.21 | 0.08 |

## Table A.4
## Experiment 5

### REACTOR 4: 2.86 g/l mineralized -200 mesh gabbro, $O_2$ diffusion

| TIME (Hrs) | pH | $SO_4$ (mg/l) | Ni (µg/l) | Cu (µg/l) | Fe (µg/l) | Ca (mg/l) | Mg (mg/l) |
|---|---|---|---|---|---|---|---|
| 0.75 | 6.82 | 3.1 | 23.7 | 2.4 | 19.7 | 2.0 | 0.18 |
| 5 | 7.51 | 3.1 | 34.2 | 0.9 | 3.9 | 1.7 | 0.19 |
| 24 | 7.25 | 3.1 | 71.8 | 1.2 | 4.1 | 1.5 | 0.24 |
| 46 | 7.41 | 3.3 | 80.0 | 3.4 | 5.6 | 2.4 | 0.25 |
| 192 | 6.94 | 3.7 | 157 | 1.6 | 2.8 | 2.2 | 0.31 |
| 356 | 6.04 | 5.3 | 226 | 19.1 | 4.4 | 2.5 | 0.40 |
| 523 | 5.20 | 7.5 | 381 | 226 | 870 | 2.5 | 0.70 |
| 690 | 5.00 | 10.6 | 540 | 347 | 240 | 2.6 | 0.64 |
| 860 | 4.71 | 15.7 | 774 | 558 | 850 | 3.1 | 0.72 |
| 886 | | | 785 | 596 | 1110 | 3.4 | 0.75 |
| 4-AD-5 | | | 21.3 | 41.6 | 187.2 | 1.3 | 0.10 |

### REACTOR 5: 2.86 g/l unmineralized -200 mesh gabbro, $1.29 * 10^{-4}$ $\underline{M}$ citrate, adjust to pH 7

| TIME (Hrs) | $SO_4$ (mg/l) | Ni (µg/l) | Cu (µg/l) | Fe (µg/l) | Ca (mg/l) | Mg (mg/l) |
|---|---|---|---|---|---|---|
| 0.75 | 3.4 | 20 | 16.2 | 440 | 1.6 | 0.28 |
| 5 | 3.6 | 56 | 33.0 | 1120 | 2.0 | 0.51 |
| 24 | 3.5 | 122 | 36.3 | 2980 | 2.6 | 0.63 |
| 46 | 3.4 | 163 | 52.8 | 3350 | 2.7 | 0.70 |
| 192 | 3.7 | 348 | 92.6 | 2550 | 3.5 | 0.87 |
| 356 | 3.5 | 455 | 136 | 1030 | 4.4 | 0.90 |
| 523 | 3.8 | 456 | 140 | 470 | 2.8 | 0.95 |
| 690 | 3.8 | 362 | 79.8 | 107 | 2.9 | 0.95 |
| 860 | 4.8 | 307 | 20.7 | 64 | 2.4 | 0.96 |
| 886 | | 276 | 5.6 | 85 | 2.1 | 1.04 |
| 5-AD-5 | | 234 | 111.3 | 730 | 3.8 | 0.29 |

### REACTOR 6: 2.86 g/l unmineralized -200 mesh gabbro, $1.29 * 10^{-3}\underline{M}$ citrate adjust to pH 7

| TIME (Hrs) | $SO_4$ (mg/l) | Ni (µg/l) | Cu (µg/l) | Fe (µg/l) | Ca (mg/l) | Mg (mg/l) |
|---|---|---|---|---|---|---|
| 0.75 | 3.8 | 34.0 | 31 | 1980 | 2.4 | 0.46 |
| 5 | 4.0 | 68.0 | 62 | 5000 | 2.3 | 0.72 |
| 24 | 5.1 | 123 | 105 | 8320 | 2.2 | 1.12 |
| 46 | 4.0 | 195 | 113 | 10,080 | 2.3 | 1.42 |
| 192 | 5.5 | 563 | 130 | 15,410 | 2.2 | 2.44 |
| 356 | 8.8 | 810 | 144 | 19,210 | 2.3 | 2.98 |
| 523 | 13.0 | 1020 | 140 | 24,100 | 2.3 | 3.09 |
| 690 | 15.1 | 1090 | 133 | 25,800 | 2.3 | 3.11 |
| 860 | 16.2 | 1170 | 191 | 28,800 | 2.4 | 3.51 |
| 886 | | 1260 | 158 | 28,800 | 2.2 | 3.37 |
| 6-AD-5 | | 16.9 | 32.9 | 870 | 2.4 | 0.43 |

## Table A.5
## Experiment 6

REACTOR 1:  5.7 g $\ell^{-1}$ -200 mesh mineralized gabbro, pH 5

| TIME (Hrs) | pH | Ni ($\mu$g/1) | $SO_4$ (mg/1) | Cu ($\mu$g/1) | Fe (mg/1) | Ca (mg/1) | Mg (mg/1) |
|---|---|---|---|---|---|---|---|
| 0.5 | | 13 | 3.4 | 2.0 | 350 | .91 | .27 |
| 5.5 | | 19 | 3.3 | 7.9 | 820 | 1.57 | .43 |
| 24 | | 52 | 3.3 | 6.6 | 340 | 1.87 | .58 |
| 44 | | 73 | 3.3 | 8.0 | 450 | 1.99 | .69 |
| 196 | | 180 | 3.8 | 78.7 | 1020 | 2.27 | 1.03 |
| 360 | | 450 | 6.9 | 131 | 530 | 2.44 | 1.16 |
| 530 | | 700 | 11.2 | 242 | 860 | 2.57 | 1.26 |
| 720 | | 930 | 16.4 | 233 | 700 | 2.68 | 1.36 |
| 912 | | 1170 | 23.7 | 297 | 620 | 2.99 | 1.50 |
| 3-AD-6 | | 27 | | 66.9 | 380 | 0.24 | .06 |

REACTOR 2:  5.71 g$\ell^{-1}$ -200 mesh mineralized gabbro, pH 6

| TIME (Hrs) | pH | Ni ($\mu$g/1) | $SO_4$ (mg/1) | Cu ($\mu$g/1) | Fe (mg/1) | Ca (mg/1) | Mg (mg/1) |
|---|---|---|---|---|---|---|---|
| 0.5 | | 6 | 3.2 | 0.2 | 140 | .74 | .22 |
| 5.5 | | 15 | 3.3 | 0.6 | 230 | 1.30 | .37 |
| 24 | | 35 | 3.2 | 0.5 | 20 | 1.60 | .53 |
| 44 | | 57 | 3.5 | 0.2 | 12 | 1.68 | .60 |
| 196 | | 160 | 4.4 | 12.9 | 19 | 2.05 | .87 |
| 360 | | 480 | 6.8 | 19.1 | 13 | 2.23 | .99 |
| 530 | | 770 | 8.1 | 30.9 | 18 | 2.47 | 1.10 |
| 720 | | 1050 | 10.9 | 25.6 | 9 | 2.66 | 1.23 |
| 912 | | 1430 | 12.7 | 77.5 | 22 | 3.00 | 1.36 |
| 4-AD-6 | | 950 | | 129 | 370 | 1.18 | 0.10 |

REACTOR 3:  5.71 g$^{-1}$ -200 mesh mineralized gabbro, pH 7

| TIME (Hrs) | pH | Ni ($\mu$g/1) | $SO_4$ (mg/1) | Cu ($\mu$g/1) | Fe (mg/1) | Ca (mg/1) | Mg (mg/1) |
|---|---|---|---|---|---|---|---|
| 0.5 | | 7 | 3.6 | 0.4 | 43 | .88 | .23 |
| 5.5 | | 9 | 3.5 | 1.1 | 20 | 1.29 | .32 |
| 24 | | 26 | 3.5 | 0.3 | 5 | 1.46 | .42 |
| 44 | | 36 | 3.5 | 0.1 | 5 | 1.45 | .50 |
| 196 | | 100 | 4.5 | 6.6 | 13 | 1.70 | .71 |
| 360 | | 250 | 6.6 | 3.1 | 9 | 1.77 | .77 |
| 530 | | 400 | 8.1 | 5.3 | 8 | 1.91 | .85 |
| 720 | | 450 | 9.8 | 4.3 | 8 | 1.99 | .93 |
| 912 | | 490 | 11.3 | 34.5 | 210 | 2.18 | 1.04 |
| 1-AD-6 | | 130 | | 410 | 690 | 3.04 | .20 |

## Table A.5

### Experiment 6

REACTOR 4:  5.7 g$\ell^{-1}$ -200 mesh mineralized gabbro, pH 8

| TIME (Hrs) | pH | Ni (μg/l) | So$_4^{-2}$ (mg/l) | Cu (μg/l) | Fe (mg/l) | Ca (mg/l) | Mg (mg/l) |
|---|---|---|---|---|---|---|---|
| 0.5 | 4 | 3.5 | 0.6 | 27 | .83 | .23 | |
| 5.5 | 6 | 3.6 | 1.3 | 11 | 1.25 | .34 | |
| 24 | 19 | 3.3 | 1.0 | 21 | 1.52 | .48 | |
| 44 | 30 | 3.3 | 0.7 | 14 | 1.52 | .51 | |
| 196 | 52 | 4.3 | 7.2 | 35 | 1.60 | .61 | |
| 360 | 48 | 6.4 | 4.8 | 51 | 1.65 | .68 | |
| 530 | 38 | 7.5 | 4.5 | 103 | 1.83 | .79 | |
| 720 | 36 | 8.1 | 6.0 | 69 | 1.77 | .77 | |
| 912 | 36 | 10.7 | 3.5 | 14 | 1.88 | .80 | |
| 2-AD-6 | 87 | | 306 | 520 | 2.40 | .19 | |

Table A.6

Experiment 7

REACTOR 1:  5.71 g$\ell^{-1}$ -200 mesh mineralized gabbro, bog water

| TIME (Hrs) | pH | So$^{-2}$ ($\mu$g/1) | Ni (mg/1) | Cu ($\mu$g/1) | Fe ($\mu$g/1) | Ca (mg/1) | Mg (mg/1) |
|---|---|---|---|---|---|---|---|
| 0.75 | 8.03 | 4.5 | 14 | 4 | 620 | 7.6 | 8.4 |
| 5 | 8.09 | 5.1 | 15 | 3 | 440 | 7.6 | 8.4 |
| 27 | 8.11 | 4.7 | 22 | 7 | 570 | 8.0 | 8.7 |
| 52 | 8.02 | 4.6 | 22 | 13 | 570 | 8.4 | 8.3 |
| 218 | 7.99 | 5.3 | 30 | 15 | 460 | 8.4 | 8.8 |
| 431 | 8.08 | 6.4 | 39 | 17 | 490 | 8.5 | 9.3 |
| 531 | 8.10 | 6.7 | 43 | 22 | 310 | 8.9 | 9.6 |
| 698 | 8.14 | 7.2 | 44 | 23 | 320 | 9.6 | 9.9 |
| 1034 | 8.12 | 9.9 | 46 | 36 | 250 | 10.6 | 11.3 |
| 1-AD-7 | | | 69 | 220 | 1550 | 3.8 | 0.73 |
| T=0 | | 3.9 | 0 | 3 | 160 | 7.8 | 8.9 |

REACTOR 2:  5.71 g$\ell^{-1}$ -200 mesh mineralized gabbro, ground water

| TIME (Hrs) | pH | So$^{-2}$ ( g/1) | Ni (mg/1) | Cu ($\mu$g/1) | Fe ($\mu$g/1) | Ca (mg/1) | Mg (mg/1) |
|---|---|---|---|---|---|---|---|
| 0.75 | 8.03 | 6.7 | 9 | 2 | 17 | 16.9 | 9.8 |
| 5 | 8.11 | 7.1 | 7 | 3 | 27 | 16.5 | 9.9 |
| 27 | 8.13 | 7.7 | 14 | 3 | 33 | 17.1 | 9.1 |
| 52 | 8.04 | 7.9 | 20 | 5 | 42 | 17.1 | 9.9 |
| 218 | 8.01 | 7.9 | 27 | 4 | 26 | 17.0 | 9.8 |
| 431 | 8.11 | 8.9 | 27 | 3 | 26 | 17.8 | 10.2 |
| 531 | 8.14 | 9.5 | 29 | 4 | 21 | 18.1 | 10.3 |
| 698 | 8.16 | 12.0 | 37 | 7 | 32 | 17.4 | 10.0 |
| 1034 | 8.03 | 11.6 | 36 | 5 | 38 | 18.1 | 10.8 |
| 2-AD-7 | | | 30 | 110 | 680 | 1.9 | 0.29 |
| T=0 | | 6.4 | 4 | 4 | 37 | 18.9 | 10.2 |

REACTOR 3:  5.71 g$\ell^{-1}$ -200 mesh mineralized gabbro,  =5*10$^{-3}$

| TIME (Hrs) | pH | So$^{-2}$ ($\mu$g/1) | Ni (mg/1) | Cu ($\mu$g/1) | Fe ( g/1) | Ca (mg/1) | Mg (mg/1) |
|---|---|---|---|---|---|---|---|
| 0.75 | | 2.9 | 2 | 0.9 | 92 | 1.4 | 0.36 |
| 5 | | 2.7 | 19 | 2 | 18 | 1.9 | 0.46 |
| 27 | | 2.9 | 51 | 0.8 | 12 | 1.8 | 0.56 |
| 52 | | 3.3 | 71 | 3 | 27 | 2.0 | 0.60 |
| 218 | | 5.0 | 220 | 2 | 19 | 2.0 | 0.75 |
| 431 | | 7.1 | 330 | 3 | 6 | 2.1 | 0.90 |
| 531 | | 7.5 | 460 | 4 | 6 | 2.1 | 0.87 |
| 698 | | 9.6 | 590 | 5 | 15 | 2.2 | 1.01 |
| 1034 | | 13.3 | 640 | 7 | 12 | 2.3 | 1.13 |
| 3-AD-7 | | | 120 | 96 | 450 | 1.2 | 0.093 |

# Table A.6

## Experiment 7

REACTOR 4:  5.71 g$\ell^{-1}$ -200 mesh mineralized gabbro, $\mu=5*10^{-2}$

| TIME (Hrs) | pH | So$^{-2}$ ($\mu$g/l) | Ni (mg/l) | Cu ($\mu$g/l) | Fe ($\mu$g/l) | Ca (mg/l) | Mg (mg/l) |
|---|---|---|---|---|---|---|---|
| 0.75 | | 3.1 | 22 | 6 | 250 | 1.8 | 0.36 |
| 5 | | 2.8 | 32 | 6 | 130 | 2.3 | 0.76 |
| 27 | | 3.1 | 70 | 2 | 8 | 2.4 | 0.71 |
| 52 | | 3.4 | 97 | 2 | 7 | 2.5 | 0.80 |
| 218 | | 4.6 | 275 | 0.3 | 9 | 2.6 | 0.85 |
| 431 | | 7.7 | 520 | 2 | 4 | 2.7 | 0.98 |
| 531 | | 9.1 | 670 | 2 | 23 | 2.6 | 1.05 |
| 698 | | 10.8 | 860 | 2 | 13 | 2.8 | 1.03 |
| 1034 | | 16.1 | 1200 | 4 | 4 | 3.2 | 1.20 |
| 4-AD-7 | | | 74 | 180 | 650 | 0.8 | 0.066 |

REACTOR 5:  5.71 g$\ell^{-1}$ -200 mesh mineralized gabbro, $1.29*10^{-4}$ phthallic acid

| TIME (Hrs) | ph | So$^{-2}$ ($\mu$g/l) | Ni (mg/l) | Cu ($\mu$g/l) | Fe ($\mu$g/l) | Ca (mg/l) | Mg (mg/l) |
|---|---|---|---|---|---|---|---|
| 0.75 | | 2.8 | 6 | 0.6 | 45 | 0.9 | 0.21 |
| 5 | | 3.0 | 9 | 1.3 | 41 | 1.0 | 0.30 |
| 27 | | 3.0 | 14 | 0.1 | 13 | 1.0 | 0.30 |
| 52 | | 2.8 | 23 | 0.6 | 16 | 1.1 | 0130 |
| 218 | | 3.0 | 63 | 0.7 | 45 | 1.0 | 0.38 |
| 431 | | 3.3 | 100 | 0 | 44 | 1.0 | 0.38 |
| 531 | | 3.4 | 130 | 0:9 | 51 | 1.0 | 0.36 |
| 698 | | 3.9 | 180 | 3 | 48 | 1.2 | 0.50 |
| 1034 | | 5.3 | 210 | 3 | 44 | 1.1 | 0.6 |
| 5-AD-7 | | | 58 | 7 | 210 | 0.8 | 0.045 |

REACTOR 6:  5.71 g$\ell^{-1}$ -200 mesh mineralized gabbro, $1.29*10^{-3}$ phthallic acid

| TIME (Hrs) | pH | So$^{-2}$ ($\mu$g/l) | Ni (mg/l) | Cu ($\mu$g/l) | Fe ($\mu$g/l) | Ca (mg/l) | Mg (mg/l) |
|---|---|---|---|---|---|---|---|
| 0.75 | | 3.2 | 11 | 0 | 84 | 1.6 | 0.38 |
| 5 | | 2.7 | 13 | 0 | 41 | 1.7 | 0.34 |
| 27 | | 3.1 | 13 | o | 74 | 1.7 | 0.32 |
| 52 | | 2.8 | 16 | 0.4 | 31 | 1.7 | 0.38 |
| 218 | | 3.3 | 34 | 0.6 | 74 | 1.7 | 0.40 |
| 431 | | 3.0 | 55 | 0 | 52 | 1.6 | 0.46 |
| 531 | | 3.5 | 64 | 0 | 55 | 1.6 | 0.46 |
| 698 | | 3.2 | 78 | 2 | 62 | 1.6 | 0.48 |
| 1034 | | 3.4 | 110 | 7 | 120 | 1.7 | 0.52 |
| 6-AD-7 | | 3.9 | 49 | 35 | 180 | 0.5 | 0.09 |
| BOg H$_2$0 | | 6.4 | 0 | 3 | 164 | 7.8 | 8.9 |
| GRND H$_2$0 | | | 4 | 4 | 37 | 18.9 | 10.2 |

## Table A.7

### Experiment 8

#### REACTOR 1:  50 g$\ell^{-1}$ tailings, pH 4

| TIME (Hrs) | pH=4 | Ni (μg/1) | So$^{-2}$ (mg/1) | Cu (μg/1) | Fe (μg/1) | Ca (mg/1) | Mg (mg/1) |
|---|---|---|---|---|---|---|---|
| 1 | | 22 | 2.7 | 0 | 78 | 13.9 | 0.9 |
| 27 | | 77 | 2.7 | 5.6 | 2,450 | 23.4 | 2.8 |
| 218 | | 440 | 4.1 | 170 | 16,300 | 23.5 | 7.1 |
| 432* | | 550 | 6.4 | 320 | 33,200 | 25.6 | 12.4 |
| 532 | | 650 | 8.1 | 260 | 38,100 | 26.8 | 14.2 |
| 0.5 | | 23 | 3.0 | 24 | 1,870 | 0.8 | 0.4 |
| 22 | | 550 | 3.1 | 40 | 3,770 | 1.6 | 1.4 |
| 190 | | 840 | 3.8 | 44 | 9,130 | 2.9 | 2.9 |

#### REACTOR 2:  50 g$\ell^{-1}$ tailings, pH 6

| TIME (Hrs) | PH=4 | Ni (μg/1) | So$^{-2}$ (mg/1) | Cu (μg/1) | Fe (μg/1) | Ca (mg/1) | Mg (mg/1) |
|---|---|---|---|---|---|---|---|
| 1 | | 5 | 2.9 | 0 | 97 | 11.2 | 0.7 |
| 27 | | 11 | 2.7 | 0 | 28 | 17.8 | 1.0 |
| 218 | | 92 | 3.2 | 0.6 | 93 | 18.1 | 2.3 |
| 432 | | 140 | 3.5 | 0 | 75 | 18.8 | 3.1 |
| 532* | | 160 | 3.7 | 0.4 | 66 | 19.3 | 3.4 |
| 95 | | 5 | 2.8 | 0.1 | 34 | 0.8 | 0.1 |
| 22 | | 41 | 3.0 | 4.1 | 60 | 2.6 | 0.4 |
| 190 | | 100 | 2.8 | 3.7 | 48 | 3.1 | 0.7 |

#### REACTOR 3:  50 g$\ell^{-1}$ tailings, natural pH

| TIME (Hrs) | PH | Ni (μg/1) | So$^{-2}$ (mg/1) | Cu (μg/1) | Fe (μg/1) | Ca (mg/1) | Mg (mg/1) |
|---|---|---|---|---|---|---|---|
| 1 | 9.10 | 3 | 3.2 | 1 | 76 | 7.7 | 0.3 |
| 27 | 8.02 | 1 | 2.9 | 2 | 25 | 13.9 | 0.6 |
| 218 | 8.08 | 1 | 3.1 | 1 | 25 | 14.0 | 0.9 |
| 432 | 8.01 | 7 | 3.7 | 2 | 63 | 14.2 | 1.1 |
| 532* | 8.12 | 2 | 4.0 | 2 | 22 | 14.7 | 1.2 |
| 0.5 | 6.88 | 9 | 3.1 | 4 | 76 | 1.3 | 0.1 |
| 22 | 7.50 | 11 | 3.1 | 5 | 260 | 5.1 | 1.2 |
| 190 | 7.94 | 7 | 3.7 | 2 | 49 | 4.4 | 2.3 |

*Solids removed for 5 day drying period

## Table A.7

### Experiment 8

REACTOR 4: 50 g$\ell^{-1}$ tailings, bog water

| TIME (Hrs) | PH | Ni (µg/l) | So$^{-2}$ (mg/l) | Cu (µg/l) | Fe (µg/l) | Ca (mg/l) | Mg (mg/l) |
|---|---|---|---|---|---|---|---|
| 1 | 8.16 | 5 | 3.8 | 9 | 180 | 9.3 | 6.5 |
| 27 | 8.17 | 5 | 3.8 | 9 | 180 | 9.4 | 5.7 |
| 218 | 8.26 | 16 | 4.2 | 10 | 130 | 11.0 | 6.4 |
| 432 | 8.16 | 15 | 5.3 | 14 | 92 | 11.5 | 7.3 |
| 532* | 8.34 | 15 | 7.7 | 17 | 78 | 14.9 | 10.1 |
| 95 | 8.15 | 7 | 3.6 | 11 | 350 | 7.8 | 7.5 |
| 22 | 8.24 | 7 | 3.9 | 10 | 240 | 8.8 | 7.8 |
| 190 | 8.37 | 13 | 4.4 | 9 | 82 | 9.1 | 8.9 |
| T=0 | | 0 | 3.9 | 3 | 160 | 7.8 | 8.9 |

REACTOR 5: 50 g$\ell^{-1}$ tailings, ground water

| TIME (Hrs) | PH | Ni (µg/l) | So$^{-2}$ (mg/l) | Cu (µg/l) | Fe (µg/l) | Ca (mg/l) | Mg (mg/l) |
|---|---|---|---|---|---|---|---|
| 1 | 8.15 | 5 | 7.8 | 6 | 91 | 17.5 | 8.1 |
| 27 | 8.20 | 3 | 7.2 | 5 | 30 | 17.0 | 7.7 |
| 218 | 8.24 | 4 | 7.4 | 29 | 80 | 17.3 | 8.5 |
| 432 | 8.18 | 4 | 9.7 | 32 | 29 | 18.2 | 9.0 |
| 532* | 8.26 | 4 | 9.4 | 19 | 14 | 18.1 | 9.9 |
| 0.5 | 8.17 | 4 | 6.0 | 14 | 88 | 16.3 | 10.2 |
| 22 | 8.25 | 6 | 7.0 | 14 | 37 | 17.6 | 10.2 |
| 190 | 8.52 | 13 | 21.5 | 12 | 520 | 23.8 | 25.9 |
| T=0 | | 4 | 6.4 | 4 | 37 | 18.9 | 10.2 |

*Solids removed for 5 day drying period

## Table A.8

Calcium and Magnesium Kinetics:  Summary of Data

$$[C] = kt^n$$

$k = moles, sec^{-1} (g\ gabbro)^{-1}$

$t = time$

$n = dimensionless$

| Reactor | Ca | | | Mg | | |
|---|---|---|---|---|---|---|
| | $k \times 10^5$ | $r^2$ | $n$ | $k \times 10^6$ | $r^2$ | $n$ |
| 2-1 | 2.39 | .555 | .021 | 2.94 | .959 | .140 |
| 2-2 | .51 | .987 | .073 | .009 | .701 | .531 |
| 2-3 | .058 | .931 | .191 | .061 | .995 | .286 |
| 2-4 | .0095 | .968 | .300 | .031 | .957 | .322 |
| 2-5 | - | - | - | 5.5 | .727 | .083 |
| 2-6 | .38 | .766 | .038 | .44 | .971 | .154 |
| 3-1 | .36 | .966 | .114 | .44 | .995 | .210 |
| 3-2 | 1.54 | .619 | .028 | 4.16 | .957 | .091 |
| 3-3 | 2.43 | .834 | .045 | 3.78 | .983 | .131 |
| 3-4 | 2.90 | .966 | .065 | 2.26 | .986 | .204 |
| 3-5 | 1.09 | .916 | .084 | 1.35 | .980 | .139 |
| 3-6 | 1.79 | .903 | .043 | .94 | .932 | .198 |
| 4-1 | 1.11 | .931 | .119 | .16 | .965 | .247 |
| 4-2 | .77 | .974 | .180 | .033 | .936 | .299 |
| 4-3 | .63 | .885 | .129 | .0019 | .945 | .481 |
| 4-4 | .0089 | .901 | .091 | .0075 | .865 | .178 |
| 4-5 | .43 | .586 | .042 | 1.40 | .947 | .132 |
| 4-6 | 1.32 | .533 | -.037 | 3.88 | .583 | .082 |
| 5-1 | .39 | .618 | .076 | .71 | .936 | .163 |
| 5-2 | .88 | .248 | .026 | .77 | .986 | .159 |
| 5-3 | .47 | .931 | .085 | .59 | .927 | .162 |
| 5-4 | .76 | .559 | .077 | .35 | .832 | .216 |
| 5-5 | .77 | .536 | .088 | 1.32 | .953 | .163 |
| 5-6 | 2.05 | .019 | -.002 | .58 | .992 | .300 |
| 6-1 | .16 | .965 | .139 | .33 | .996 | .230 |
| 6-2 | .099 | .980 | .167 | .26 | .997 | .239 |
| 6-3 | .18 | .970 | .106 | .33 | .986 | .203 |
| 6-4 | .20 | .917 | .095 | .49 | .991 | .166 |
| 7-1 | 2.37 | .700 | .036 | 44.7 | .575 | .031 |
| 7-2 | 6.66 | .614 | .010 | 63.3 | .292 | .010 |
| 7-3 | .43 | .842 | .054 | .72 | .964 | .154 |
| 7-4 | .52 | .870 | .059 | 1.13 | .855 | .131 |
| 7-5 | .34 | .432 | .022 | .64 | .792 | .111 |
| 7-6 | .73 | .008 | -.001 | 1.56 | .589 | .051 |
| 8-1a | .34 | .900 | .096 | .019 | .981 | .434 |
| 8-1b | .008 | .987 | .213 | .027 | 1.000 | .333 |
| 8-2a | .31 | .882 | .081 | .060 | .920 | .258 |
| 8-2b | .007 | .940 | .238 | .007 | .993 | .332 |
| 8-3a | .19 | .841 | .096 | .042 | .996 | .215 |
| 8-3b | .014 | .800 | .223 | .002 | .972 | .543 |
| 8-4a | .27 | .599 | .056 | 3.35 | .286 | .045 |
| 8-4b | .32 | .975 | .027 | 4.97 | .803 | .027 |
| 8-5a | .82 | .255 | .056 | 5.14 | .489 | .028 |
| 8-5b | .72 | .205 | .019 | 2.57 | .604 | .139 |

Note:  Consult Table 3.10 for Reactor and Experiment conditions

## Table A.8
### Mineral Analysis of Gabbro

| Mineral | Formula | Weighted Mean Percent Unmineralized | Mineralized |
|---|---|---|---|
| Plagioclase | $NaAlSi_3O_8-CaAl_2Si_2O_8$ | 64 | 47 |
| Sericite | $K_2Al_4Si_6Al_2O_{22}(OH,F)_4$ | 1.6 | 0.069 |
| Olivine | $(Fe,Mg)_2SiO_4$ | 14 | 11 |
| Clinopyroxene | $Ca(Fe,Mg)Si_2O_6$ | 7.6 | 26 |
| Monocrystalline Amphibole | $(Na,K)_{0-1}(Ca,Mg,Fe^{+2},Fe^{+3},Al)_7 \cdot (Si_{6-8}Al_{2-0})O_{22}(OH,F,Cl)_2$ non-acicular morphology | 0.054 | - |
| Fibrous Amphibole | Same as Above; fibrous or acicular morphology | 0.005 | - |
| Chlorite | $(mg,Fe,Al)_{12}(Si,Al)_8O_{20}(OH)_{16}$ | 1.7 | 0.40 |
| Serpentine | $Mg_3Si_2O_5(OH)_4$ | 0.016 | 0.014 |
| Iodingsite | Serpentine + iron oxide phase | 0.017 | 0.053 |
| Talc | $Mg_6Si_8O_{20}(OH)_4$ | - | - |
| Biotite | $K_2(Mg,Fe^{2+})_{6-4}(Fe^{3+},Al,Ti)_{0-2} \cdot (Si_{6-5}Al_{2-3})O_{20}(OH,F)_4$ | 3.3 | 5.0 |
| Smectite | $(1/2\ Ca,Na)_{0.7}(Al,Mg,Fe)_4(Si,Al)_8 \cdot O_{20}(OH)_4 \cdot NH_2O$ | - | - |
| Celadonite | $KMgFe^{3+}Si_4O_{10}(OH)_2$ | 0.014 | - |
| Orthopyroxene | $(Fe,Mg)_2Si_2O_6$ | 2.8 | 2.3 |

## Mineral Analysis of Gabbro

| Mineral | Formula | Weighted Mean Percent Unmineralized | Mineralized |
|---|---|---|---|
| Opaque Minerals (Following Six) | | | |
| Chalcopyrite-Cubanite | $CuFeS_2-CuFe_2S_3$ | 0.13 | 7.9 |
| Pentlandite | $(Fe,Ni)_9S_8$ | 0.032 | 1.3 |
| Pyrrhotite | $Fe_7S_8-FeS$ | 0.0403 | 0.34 |
| Ilmenite | $FeTiO_3$ | 4.0 | 3.1 |
| Magnetite | $Fe_3O_4$ | | 3.1 |
| Graphite | C | - | 0.025 |
| Spinel | $MgAl_2O_4$ | - | - |
| Myrmekitic Intergrowths | Generally between plagioclase 7 olivine | - | - |
| Apatite | $Ca_5(PO_4)_3(OH,F,Cl)$ | 0.18 | 0.074 |
| Epidote | $CaFe^{3+}Al_2Si_3O_{12}(OH)$ | 0.17 | - |
| Allanite | $(Ca,Ce)_2(Fe^{2+},Fe^{3+}) \cdot Al_2Si_3O_{12}OH$ | - | - |
| Calcite | $CaCO_3$ | 0.026 | 0.006 |
| Quartz | $SiO_2$ | - | - |
| Cordierite | $Al_3(Mg,Fe^{+2})_2Si_5AlO_{18}$ | - | - |
| | $\Sigma=$ | 104.6 | 107.7 |

## Table A.9

### Elemental Analyses:  All Values in Weight Percent

| | Mineralized | | | Unmineralized | | |
|---|---|---|---|---|---|---|
| Element | NAA | Acid Digestion | Acid Digestion[1] | NAA | Acid Digestion | Acid Digestion |
| Ag | 0.00046 | | | <0.00014 | | |
| Al | 4.55 | | | 8.04 | | |
| As | 0.00073 | | | 0.00008 | | |
| Au | 0.000003 | | | 0.000004 | | |
| Ba | 0.036 | | | 0.034 | | |
| Ca | 4.69 | 2.27 | | 7.08 | 2.55 | |
| Cd | <0.00065 | | | <0.00029 | 0 | |
| Co | 0.039 | | | 0.082 | 0.01 | |
| Cr | 0.011 | | | 0.014 | | |
| Cu | 1.18 | 1.41 | 0.85 | 9,156 | 0.245 | 0.28 |
| Fe | 20.18 | 17.2 | 15.17 | 13.14 | 10.4 | 11.13 |
| Hg | 0.0009 | | | <0.00001 | | |
| Mg | 3.12 | 1.92 | | 2.000 | 2.05 | |
| Mn | 0.134 | | | 0.138 | 0.265 | |
| Na | 1.76 | | | 2.050 | | |
| Ni | 0.624 | 0.355 | 0.23 | 0.138 | 0.0954 | 0.10 |
| S | | | 3.92 | | | 1.1 |
| Sb | <0.00007 | | | <0.00005 | | |
| Sc | | | | <0.00017 | | |
| Se | 0.00062 | | | | | |
| Sn | <0.048 | | | <0.050 | | |
| Sr | <0.057 | | | 0.062 | | |
| Ti | 1.32 | | | | | |
| V | 0.012 | | | 0.018 | | |
| W | 0.00014 | | | <0.00016 | | |
| Zn | 0.012 | | | <0.00088 | | |

[1] Mineral Resource Research Center, University of Minnesota